Tréhu, A.M., Bohrmann, G., Rack, F.R., Torres, M.E., et al., 2003
Proceedings of the Ocean Drilling Program, Initial Reports Volume 204

9. Site 1250[1]

Shipboard Scientific Party[2]

INTRODUCTION

Site 1250 (proposed Site HR4a) was drilled in ~792 m of water ~100 m west of the southern summit of Hydrate Ridge and ~100 m east of the carbonate chemoherm known as the Pinnacle (see Fig. **F1,** p. 51, in the "Leg 204 Summary" chapter). The Pinnacle is the only carbonate mound on southern Hydrate Ridge, whereas at northern Hydrate Ridge several major chemoherms are known (Torres et al., 2002; Teichert et al., in press). It has near-vertical flanks, rising ~40 m above the seafloor. The carbon source for formation of the Pinnacle is known to be biogenic methane from the very low $\delta^{13}C$ values (Teichert et al., in press). $^{230}Th/^{234}U$ data indicate that it formed during the last 11.4 k.y. (Teichert et al., in press). It is located within a high-reflectivity patch mapped by a deep-towed side-scan sonar survey (Johnson et al., in press), which is interpreted to indicate scattered carbonates close to the seafloor and/or shallow gas hydrates (see Fig. **F7,** p. 57, in the "Leg 204 Summary" chapter). The precruise three-dimensional (3-D) seismic-reflection survey data show that seismic Horizon A (~150 meters below seafloor [mbsf] at Site 1250) meets the bottom-simulating reflector (BSR) (~114 mbsf at Site 1250) just below the Pinnacle (see Fig. **F7,** p. 57, in the "Leg 204 Summary" chapter).

The primary objective at Site 1250 was to sample the sediments, aqueous fluids, gases, and gas hydrate under the high-backscatter seafloor flanking the Pinnacle. The sediments at Site 1250 were expected to be strongly affected by the upward fluid migration that has resulted in the formation of the Pinnacle chemoherm. In this context, understanding the role of Horizon A as a conduit for fluid flow and its interaction with the BSR was of special interest.

Six holes were drilled at Site 1250 (Fig. **F1**). Recording of the logging-while-drilling (LWD) resistivity-at-the-bit (RAB) tool failed during the first run in Hole 1250A as a result of depleted batteries; therefore, the

F1. Bathymetric map, p. 31.

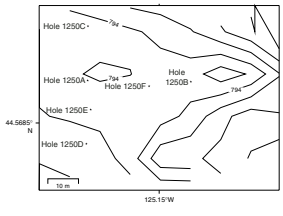

[1]Examples of how to reference the whole or part of this volume.
[2]Shipboard Scientific Party addresses.

Ms 204IR-109

LWD operation was repeated in Hole 1250B. Holes 1250C and 1250D were cored using the advanced piston corer (APC) and extended core barrel (XCB) to 145 mbsf. Holes 1250C and 1250D are each composed of 19 cores, with average core recoveries of 82% of the total penetration (see Table T1, p. 71, in the "Leg 204 Summary" chapter). Hole 1250E, which was dedicated to biogeochemical sampling, comprises two cores, with 92% core recovery. Because of relatively high levels of higher hydrocarbons encountered near Horizon A at Site 1248, we decided not to penetrate Horizon A until a better understanding of possible hazards associated with this horizon had been obtained from drilling through it further downdip. After coring through Horizon A at Sites 1245 and 1247, we returned to Site 1250 to core Hole 1250F from 100 to 180 mbsf.

OPERATIONS

Six holes were drilled at Site 1250 (Table T1), under good weather conditions. Wind speed was 0–11 kt, gusting to 16 kt; seas were 0–4 ft; swell was 4–8 ft and the prevailing sea-surface current was from the north at ~0.5 kt. Holes 1245A and 1250B were drilled without coring on 21–22 July 2002 to obtain the initial LWD data for this site. We returned to this site on 2–4 August to core Holes 1250B through 1250E and again on 24–27 August to core Hole 1250F (Table T1).

T1. Coring summary, p. 77.

Hole 1250A was spudded at 1830 hr on 21 July to obtain the initial LWD data for this site (see "Downhole Tools and Pressure Coring," p. 19). Drilling proceeded at reduced rates of penetration (ROPs) of 15 m/hr and 15 strokes per minute (spm) circulation to moderate formation washout below seafloor. No real-time measurement-while-drilling (MWD) or nuclear magnetic resonance (NMR) data were recorded over this interval. The penetration rate was increased to 25 m/hr at a bit depth of 30 mbsf to a total depth (TD) of 210 mbsf, and real-time MWD and NMR data were acquired. The LWD tools were pulled to the rig floor at 1415 hr on 22 July for a total bit run of ~21 hr, at which time we noted that recording of the RAB tool had failed because of depleted batteries; the LWD operation was repeated in Hole 1250B.

Hole 1250B was spudded at 1400 hr on 23 July, after waiting for the *Sonne* to finish instrument deployment at this site. Drilling proceeded at a moderate ROP of 25 m/hr and 15 spm circulation to 20 mbsf. No real-time MWD or NMR data were recorded over this interval. The ROP was increased to 50 m/hr and maintained to a TD of 180 mbsf. The pipe was pulled up from the bottom of the hole (BOH) to ~160 mbsf without rotating to evaluate the effect of drilling motion on the NMR log (see "Downhole Tools and Pressure Coring," p. 19). The tools were recovered at the rig floor at 0600 hr on 23 July.

Holes 1250C and 1250D were APC/XCB cored down to 148 and 147 mbsf, respectively, with average core recoveries of 82% of the total penetration. Because of the high levels of higher hydrocarbons encountered near Horizon A at Site 1248, we decided to terminate drilling in Holes 1250C and 1250C at depths shallower than 150 mbsf. Further penetration was delayed until a better understanding of potential hazards associated with drilling through this horizon were evaluated by drilling further downdip.

Special tools were used for temperature measurements in Hole 1250C, including five APCT tool and two DVTPP runs. Temperature

measurements in Hole 1250D included four APCT tool and two DVTPP runs (Table T15).

The PCS was deployed two times in Hole 1250C and three times in Hole 1250D (Table T16). Two deployments of HYACINTH tools were made, one with the FPC in Hole 1249C and one with the HRC in Hole 1249D. A good core was recovered with the FPC, but full retraction into the autoclave was prevented as a result of inadvertent line tension during the coring operation. The HRC, on the other hand, recovered a short core at full in situ pressure, which was then transferred under full pressure and logged in the Vertical Multi Sensor Core Logger (V-MSCL) before being depressurized. Unfortunately, the Drill String Acceleration (DSA) tool was still plagued by technical difficulties and failed to provide any useful downhole data (see **"Downhole Tools and Pressure Coring,"** p. 19)

Hole 1250E, which comprises two cores with 92% core recovery, was drilled to 16 mbsf for special biogeochemistry sampling. No special tools were run in this hole, but Whirl-Paks and perfluorocarbon tracer (PFT) were used for each of these cores (see Table T3, p. 73, in the "Leg 204 Summary" chapter).

Hole 1250F was APC/XCB cored from 100 to 182 mbsf on 24–27 August to extend the depth of sampling after coring Horizon A at Sites 1245 and 1247. The PCS was deployed three times in Hole 1250F (Table T16). There were no deployments of the HYACINTH tools, nor were temperature measurements conducted in this hole.

Wireline logging was performed in Hole 1250F using separate runs of the triple combination (triple combo) (Temperature/Acceleration/Pressure [TAP] tool/Dual Induction Tool [DIT]/Hostile Environment Litho-Density Tool [HLDT]/Accelerator Porosity Sonde [APS]/Hostile Environment Gamma Ray Sonde [HNGS]/Inline Checkshot Tool [QSST]) and the Formation MicroScanner (FMS)-sonic (FMS/Dipole Sonic Imager [DSI]/Scintillation Gamma Ray Tool [SGT]) tool strings down to 180 mbsf (see **"Downhole Logging,"** p. 22). Vertical and offset vertical seismic profiles (VSPs) were acquired with the *JOIDES Resolution* and the *Ewing* (located at an offset of ~700 m) alternating shots. This was followed by walkaway VSPs shot by the *Ewing* to downhole seismometers clamped at 91, 138, and 172 mbsf.

LITHOSTRATIGRAPHY

We drilled six holes, four of which (Holes 1250C–1250F) were cored at Site 1250, located at the southern summit of Hydrate Ridge on the carbonate apron known as the Pinnacle identified as an authigenic carbonate mound on the seafloor (Bohrmann et al., 2002). It is characterized by high acoustic backscatter on side-scan sonar imagery (Johnson et al., in press) (see Figs. F1, p. 51, and F7, p. 57, both in the "Leg 204 Summary" chapter). Hole 1250C was cored to 145 mbsf, with good recovery (~82%). Hole 1250D was cored to 145 mbsf. Hole 1250E was only cored to 16 mbsf but provided additional data for the top part of the sedimentary sequence. Hole 1250F was cored from 103 to 180 mbsf, extending 35 m deeper than Hole 1250C.

Three lithostratigraphic units (Units I–III) (Figs. F2, F3) were defined on the basis of visual core description, smear slide and thin section analyses, and other parameters such as calcium carbonate content (expressed as weight percent $CaCO_3$), total organic carbon (TOC), and mineralogy from X-ray diffraction (XRD). Using these criteria, correla-

F2. Lithostratigraphic summary, Hole 1250D, p. 32.

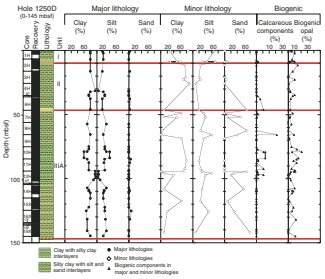

F3. Lithostratigraphic summary, Hole 1250F, p. 33.

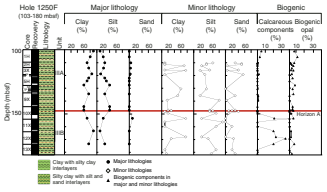

tion between the four holes cored at Site 1250 was made. We also compare our results with the 3-D multichannel seismic reflection data, downhole LWD data (resistivity and density), and physical property measurements (magnetic susceptibility [MS]) to better constrain the lithostratigraphic units (Fig. F4). Correlation of the lithostratigraphic units defined here with the other Leg 204 sites is summarized in Figure F10, p. 60, in the "Leg 204 Summary" chapter.

Lithostratigraphic Units

Lithostratigraphic Unit I

Intervals: Cores 204-1250C-1H through 2H; 204-1250D-1H through Section 2H-3; and Core 204-1250E-1H through Section 2H-3
Depths: Hole 1250C: 0.00–9.50 mbsf; Hole 1250D: 0.00–9.50 mbsf; and Hole 1250E: 0.00–9.50 mbsf
Age: mid Pleistocene–Holocene

Lithostratigraphic Unit I is composed mainly of dark greenish gray (5GY 4/1) diatom-bearing clay to diatom-rich silty clay near its base (Fig. F2). Although the recovery in this lithostratigraphic unit was poor and substantial sampling of gas hydrate occurred on the catwalk prior to description, a clay sequence containing two distinct volcanic glass–rich layers was observed in both Holes 1250C and 1250D. Smear slide estimates indicate the dominant lithology of lithostratigraphic Unit I contains ~70% clay, ~20% silt, and ~10% sand (Fig. F5). Biogenic opal (mainly diatoms) composes ~5% of the total sedimentary components of lithostratigraphic Unit I (Fig. F2). Calcareous components (calcareous nannofossils and foraminifers) are rare, except near the base of lithostratigraphic Unit I in Hole 1250D, where they reach up to 3%. Rare bioturbation is recorded only in the lower part of lithostratigraphic Unit I, above the volcanic glass horizons in Holes 1250C and 1250D (Fig. F6). The middle and lower part of this unit contain sparse sulfide precipitates, giving the core a mottled appearance in places.

Authigenic carbonate precipitates are present as small lenses at depths of 0.53 and 0.74 mbsf in Section 204-1250D-1H-1. Smear slide observations suggest that these lenses are composed of 80% calcite needles. XRD analysis of Sample 204-1250D-1H-1, 72–76 cm, also suggests a high calcite content based on the d(104) peak height (Fig. F7). Calcium carbonate content ranges from 2 to 5 wt% throughout lithostratigraphic Unit I and does not show the presence of the carbonate precipitate layers because the sample spacing was too large.

Two volcanic glass–rich silty clay and silt layers (5–6 cm thick), interbedded with a diatom-rich silty clay layer, are present in the lowest part of lithostratigraphic Unit I (intervals 204-1250D-2H-4, 47–69 cm, and 2H-4, 110–130 cm) (Fig. F6). These layers were not observed in Hole 1250C because of poor recovery. The color of the volcanic glass–rich silty clay layers grades from 10Y 6/1 to 10Y 5/1 with variations in glass content from 40% to 80% of the total sedimentary components (Fig. F6). The boundary between lithostratigraphic Units I and II (9.5 mbsf) was placed at the base of the lower volcanic glass–rich layer (Fig. F2).

F4. Seismic reflection profile and LWD data, p. 34.

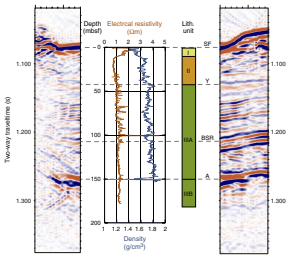

F5. Distribution of grain-size classes, p. 35.

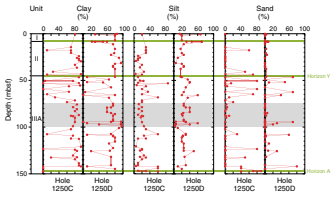

F6. Volcanic glass couplet, p. 36.

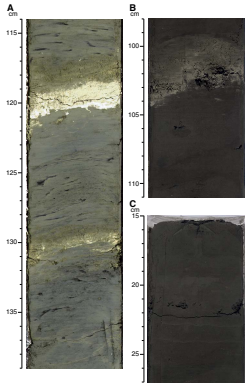

F7. XRD record of a carbonate-rich area, p. 37.

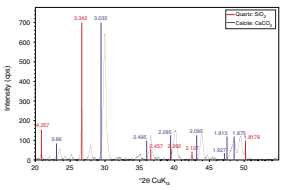

Lithostratigraphic Unit II

Intervals: Cores 204-1250C-2H through 6H-1; Core 204-1250D-2H through Section 6H-2; and Core 204-1250E-2H
Depths: Hole 1250C: 9.50–43.75 mbsf; Hole 1250D: 9.50–39.50 mbsf; and Hole 1250E: 9.50–16.00 mbsf
Age: middle–late Pleistocene

Lithologic characteristics of lithostratigraphic Unit II are based on the sequences recovered in Holes 1250C and 1250D, as Hole 1250E recovered only the uppermost 4.5 m of this lithostratigraphic unit. Lithostratigraphic Unit II is a sequence of diatom-bearing to diatom-rich silty clay to layers interbedded with thin silt and fine sand, which we interpret as turbidites. The frequency of turbidites varies between holes at Site 1250, with sand layers present from 9.5 to 13.5 mbsf in Holes 1250C and 1250E and from 15.5 to ~43.0 mbsf in Hole 1250D.

In comparison to lithostratigraphic Unit I, the abundance of biogenic opal in lithostratigraphic Unit II increased from ~5% to ~15% of the sedimentary components in Hole 1250C and from ~3% to ~20% of the sedimentary components in Hole 1250D. The abundance of calcareous nannofossils and foraminifers also increased slightly, reaching up to ~3% in the lower part of lithostratigraphic Unit II in both holes (Fig. **F2**). Bioturbation varies in intensity but is present throughout lithostratigraphic Unit II, and sulfide patches or mottles were observed throughout the recovered sequence. Iron sulfide nodules or lenses are present in the upper part of Holes 1250C and 1250D.

Authigenic carbonate is present as ~3- to 8-cm-thick layers in Sections 204-1250C-4H-3 and 4H-4. Only one carbonate-bearing clay lens was observed in Section 204-1250D-3H-CC. Smear slide observations indicate these precipitates are dominantly composed of 60%–80% calcite needles.

Lithostratigraphic Unit III

Intervals: Sections 204-1250C-6H-2 through 19X-CC; 204-1250D-6H-3 through 19X-CC; and 204-1250F-1H-1 through 13H-CC.
Depths: Hole 1250C: 43.75–145.00 mbsf; Hole 1250D: 39.50–145.00; and Hole 1250F: 100.00–180.00 mbsf
Age: early–middle Pleistocene

Lithostratigraphic Unit III consists of diatom-bearing to diatom-rich silty clay to nannofossil-rich clay interbedded with abundant layers of silt to fine sand (Figs. **F2, F3, F5**). A fine-grained thick debris flow deposit, dominated by calcareous biogenic components, disrupts the cycle of turbidites toward the middle of the lithostratigraphic unit (Fig. **F8**). Seismic Horizon A, a regional stratigraphic marker mainly composed of volcanic glass–rich sands, was also identified within lithostratigraphic Unit III (Figs. **F4, F5, F8**) (see Fig. **F6,** p. 56, in the "Leg 204 Summary" chapter). Core recovery in lithostratigraphic Unit III was high, which provided a good stratigraphic correlation between the three deep holes at Site 1250. The boundary of lithostratigraphic Unit III is located at ~45 mbsf and is defined by (1) the onset of high-frequency turbidite sequences, (2) an increase in the grain size of minor lithologies, and (3) an increase in biogenic, especially calcareous, components (Figs. **F2, F3**). The boundary between lithostratigraphic Units II and III (Fig. **F2, F3, F4**) correlates with seismic Horizon Y, a regional unconformity also identi-

F8. Distribution of biogenic components, p. 38.

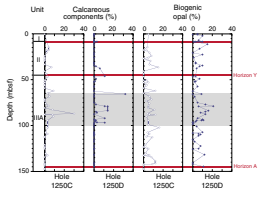

fied at Sites 1245 and 1247–1249 (see Figs. F5, p. 55, F7, p. 57, F10, p. 60, all in the "Leg 204 Summary" chapter). The lower boundary of lithostratigraphic Unit III is present at the base of Holes 1250C and 1250D, which both reached similar TDs, as well as in Hole 1250F, which reached to 180 mbsf. Based on the variations in abundance of biogenic calcareous components, lithostratigraphic Unit III was divided into two subunits (Subunits IIIA and IIIB).

Lithostratigraphic Subunit IIIA

Lithostratigraphic Subunit IIIA (Hole 1250C: 43.75–145 mbsf; Hole 1250D: 39.5–145 mbsf; and Hole 1250F: 103–153.5 mbsf) consists of dark greenish gray (5GY 4/1) diatom-bearing to diatom-rich clay and silty clay interbedded with thin (2–4 mm to 1 cm), closely spaced (centimeter) graded sandy silt and silt turbidites. The turbidites have an average frequency of one turbidite per meter. Near the top of lithostratigraphic Subunit IIIA (from 44 to 50 mbsf), coarser-grained, higher-frequency (50 cm), and thicker (up to 20 cm thick) single graded sands are observed (Fig. F9). This interval (Sections 204-1250C-6H-2 through 6H-4) corresponds to the location of Horizon Y on the 3-D seismic data. This interval is associated with a density increase recorded in the LWD data and a large positive excursion of the whole-core MS (see "Magnetic Susceptibility," p. 18, in "Physical Properties"). Opaque grains, mostly sulfides in irregular and framboidal forms, are common in lithostratigraphic Subunit IIIA. They compose between 5% and 10% of the sediment, locally reaching from 25% to 40% (opaque-rich sandy silt) in Cores 204-1250C-12H and 204-1250D-11H through 12H (92.1–97.2 mbsf). Bioturbation, often highlighted by iron sulfide precipitates, is moderate to abundant. Biogenic components (calcareous and siliceous) are common in Subunit IIA, ranging between 5% and 10% (rarely, 20%–30%) (Fig. F8). The lower boundary of lithostratigraphic Unit IIIA is defined by an increase in the abundance of calcareous nannofossils below Horizon A in Section 204-1250F-11X (~153.5 mbsf) (Fig. F3).

Smear slide analyses indicate that the major lithology of lithostratigraphic Subunit IIIA is primarily composed of sediment, with 80% clay, 20% silt, and <1% sand. The texture of the minor lithology is dominated by sand and silt, which, on average, composes 34% and 32% of the sediments, respectively (Fig. F2). The major nonbiogenic components of this lithostratigraphic subunit are clay minerals, feldspar, quartz, and opaque minerals.

In both Holes 1250C and 1250D, we recovered a sedimentary sequence characterized by soft-sediment deformation features, convoluted bedding, and mud clasts that we interpret to be a debris flow deposit (see Sections 204-1250C-11H-2 to 12H-4 [86.5–100 mbsf] and 204-1250D-10H-2 to 11H-6 [75–96 mbsf]) (Figs. F10, F5). Mud clasts, ranging from 1 to 5 cm in diameter, are embedded in a clay-rich convoluted matrix (Fig. F10). Clasts are rich in glauconite (up to 40% in Sample 204-1250C-10H-1, 25 cm [73.25 mbsf]), sulfides, and volcanic glass (20% glass), which is present as a lens or thin clast (Sample 204-1250D-12H-1, 53 cm [94.5 mbsf]). Biogenic components (both calcareous and siliceous) are abundant throughout the debris flow interval (Fig. F8). In particular, nannofossils compose up to 30% of the sedimentary components observed in Sample 204-1250C-11H-4, 55–56 cm (87 mbsf).

Several light-colored volcanic glass–rich layers were observed between 146.5 and 149.5 mbsf (intervals 204-1250C-19X-7, 7–28 cm, and 64–68 cm, and Sections 204-1250D-10H-3 to 10H-5) defining the base of lithostratigraphic Subunit IIIA (Fig. F11) and seismic Horizon A. The

F9. Turbidite sequences located around Horizon Y, p. 39.

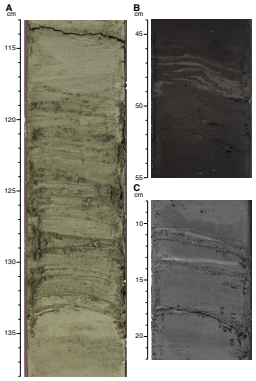

F10. Debris flow deposit, p. 40.

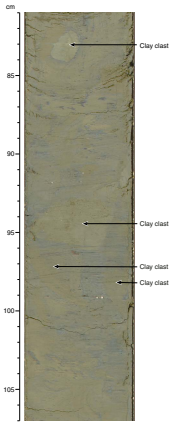

F11. Volcanic glass–rich layers, p. 41.

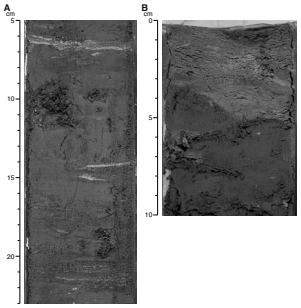

glass-rich sequences are mostly composed of thick layers (up to 10 cm-thick) of volcanic glass–rich clayey to sandy silt (10%–30% glass) that grade to volcanic ash deposits a few centimeters thick containing ~60% glass (Figs. **F11, F12**). A high-resolution color reflectance (b*, from blue to yellow) and MS (spacing = 1 cm, count time = 10 s) study was conducted over the glass-rich and ash intervals. This study showed a negative correlation between the high b* values and the low MS values. Three thick layers of ash, located at 147.5, 148.15, and 149.5 mbsf, respectively, in Hole 1250F, are clearly identified in both the MS and reflectance data (Fig. **F13**). The uppermost interval (located between 146.6 and 147.2 mbsf in Holes 1250C and 1250F) is characterized by thinly interbedded glass-rich silty sand and ash layers (0.5 cm thick) (Fig. **F11A**). This is expressed as small positive amplitude anomalies in the reflectance data and negative excursions in the MS data (Figs. **F11A, F13**). The glass-rich layers also correlate with a low density anomaly in the LWD data and with the bright Horizon A seismic reflector on the 3-D seismic data (Fig. **F4**) (see Fig. **F6,** p. 56, in the "Leg 204 Summary" chapter).

F12. Distribution of volcanic glass, p. 42.

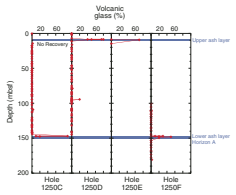

F13. Color reflectance and MS, p. 43.

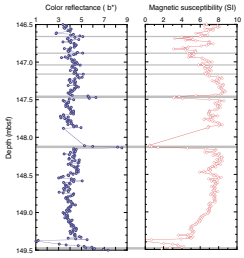

Lithostratigraphic Subunit IIIB

Lithostratigraphic Subunit IIIB is only present in Hole 1250F, from 149.5 to 180 mbsf, and consists of dark greenish gray to greenish gray nannofossil-rich clay and silty clay. (Fig. **F3**). Smear slide analyses indicate that sediment is primarily composed of 80% clay, 20% silt, and <1% sand. The major lithology is interbedded with thin (2–5 mm thick) sandy silt layers. Dark gray (N3) glauconite-rich sandy silt is present in Sections 204-1250F-13X-2 to 13X-6. Sulfide precipitates are rare. Calcareous biogenic components are abundant throughout this lithostratigraphic subunit. Macroscopic foraminifers compose up to 15% of the sedimentary components and nannofossils up to 30% in Sample 204-1250F-11X-1, 31 cm (Fig. **F3**).

Sedimentary Evidence for Gas Hydrate

Seventeen gas hydrate samples (7 samples from Hole 1250C and 10 samples from Hole 1250D) were taken at Site 1250 between 0 and 95 mbsf. Soupy and mousselike textures related to the presence of gas hydrate (Fig. **F14**) were observed in the sediments of Site 1250, although these textures are present less frequently than at the neighboring Site 1249.

F14. Mousselike and soupy textures, p. 44.

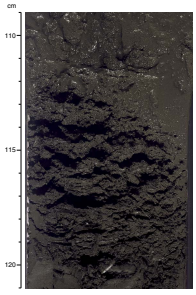

Eleven gas hydrate samples were recovered from 0 to 5 mbsf in lithostratigraphic Unit I in Sections 204-1250C-1H-1 through 2H-CC, 204-1250D-1H-1 to 1H-CC, and 204-1250E-2H-1, and evidence of gas hydrate at the top of the stratigraphic sequence was indicated prior to coring by a large resistivity peak in the LWD data (Fig. **F4**). Few soupy and mousselike textures were observed, however, and these were mainly limited to interval 204-1250C-1H-1, 49–115 cm. The lack of soupy and mousselike textures in the sediment may be explained by the sampling procedures for gas hydrate on the catwalk, which removes 5–10 cm of sediment on either side of each gas hydrate sample taken. The sediments immediately bordering and hosting the gas hydrate are the sediments in which soupy and mousselike textures are expected to form upon dissociation of the gas hydrate. Gas hydrate sampling as whole rounds prior to core description also limits the identification of all soupy and mousselike textures.

Only one gas hydrate sample was taken from lithostratigraphic Unit II, at a depth of 27.5 mbsf (Core 204-1250C-3H). Mousselike textures were observed in Core 204-1250D-5H at a depth of 35.5 mbsf, although no gas hydrate was recovered.

Four gas hydrate samples were recovered from the top of lithostratigraphic Subunit IIIA between 42 and 50 mbsf (Cores 204-1250C-6H and 204-1250D-6H and 7H). Mousselike and soupy textures were observed in intervals 204-1250C-13H-2, 56–66 cm, and 13H-4, 87–120 cm (106–108 mbsf), just above the depth of the BSR (Fig. **F14**). No gas hydrates were sampled from this interval, although sediment observations together with negative chloride anomalies (see **"Hydrocarbon Gases,"** p. 12, in "Inorganic Geochemistry") indicate that gas hydrate was likely present in situ and dissociated upon core retrieval.

Environment of Deposition

The sedimentary succession recovered at Site 1250 is primarily composed of diatom-bearing clay and silty clay to nannofossil-rich clays near the base of the section. These fine-grained hemipelagic sediments are frequently interbedded with abundant silt and sand turbidites. The boundaries between the lithostratigraphic units at Site 1250 correspond to changes in the environment and style of deposition.

Lithostratigraphic Subunit IIIB is characterized by a high proportion of biogenic components (especially nannofossils) relative to terrigenous material in both the coarse and fine fractions. This suggests either a change in the biogenic content of the source area or a change in overall biogenic productivity prior to the deposition of Horizon A. Horizon A corresponds to the boundary between lithostratigraphic Subunits IIIB and IIIA and is a bright seismic reflector composed of several volcanic glass–rich layers interbedded with sand intervals. It was encountered at Sites 1245, 1247, 1248, and 1250, although the lithologic manifestation of this horizon varies between sites. Horizon A at Site 1250 typically contains interlayered volcanic glass–rich silts that grade upward to volcanic ash. At Sites 1250, 1245, and 1248, we interpret the ash in the sequence to be detrital, emplaced by turbidity currents, rather than a repeated air fall deposit.

A large matrix-supported clast deposit (up to 20 m thick), which we interpret as a debris flow, is found between 75 and 100 mbsf at Site 1250. This event correlates with an increase in the sedimentation rate in lithostratigraphic Unit III below Horizon Y (see **"Summary,"** p. 10, in "Biostratigraphy"). A thinner debris flow was also observed at Site 1249 between 87 and 89 mbsf. The boundary between lithostratigraphic Units III and II corresponds to a regional unconformity showing lateral variability in the 3-D seismic reflection data. The interpretation of Horizon Y as a regional unconformity is supported by subtle changes in composition of sediments across the boundary and, at this site, by the abrupt change in sedimentation rate from 15 to 2.4 cm/k.y. at ~45 mbsf (see **"Summary,"** p. 10, in "Biostratigraphy").

Though it is unresolved in the biostratigraphy, an additional decrease in sedimentation rate likely occurred between lithostratigraphic Units II and I. The presence of high-frequency turbidites in lithostratigraphic Unit II and lack of turbidites in lithostratigraphic Unit I suggests sedimentation rates were higher during the deposition of Unit II. The lack of turbidites and the relatively thin (~9.5 m) unit thickness also may indicate that lithostratigraphic Unit I is simply hemipelagic drape that has been slowly accumulating on the crest of Hydrate Ridge.

BIOSTRATIGRAPHY

Site 1250 was drilled near the carbonate chemoherm known as the Pinnacle, located near the summit of the southern Hydrate Ridge. At this site, six holes were drilled and four of these (Holes 1250C, 1250D, 1250E, and 1250F) were cored. Hole 1250C was drilled to 138.50 mbsf, with good recovery (~82%). Hole 1250F was cored from 100.00 to 181.59 mbsf, extending 43.09 m deeper than Hole 1250C. A combination of Holes 1250C and Hole 1250F yielded a complete 181-m-thick Pleistocene–Holocene sedimentary sequence at Site 1250. The biostratigraphy determined for Site 1250 was based on examination of diatoms and calcareous nannofossils in all core catcher samples from Holes 1250C and 1250F.

Diatoms

Holes 1250C and 1250E yield rare to common, poorly to moderately preserved diatoms, except for the interval from Samples 204-1250F-9H-CC to 11H-CC, where diatoms are trace or barren. Diatom assemblages in Holes 1250C and 1250F are dominated by such species as *Stephanopyxis dimorpha, Stephanopyxis* spp., *Neodenticula seminae,* and *Thalassionema nitzschioides*. Warm-water species, such as *Fragilariopsis doliolus* and *Thalassiosira oestrupii,* are frequently present throughout the sediment sequence recovered.

Proboscia curvirostris are continuously present in almost all the samples from Holes 1250C and 1250F, except for the interval from the seafloor to Sample 204-1250C-4H-CC (30.42 mbsf), where the presence of *P. curvirostris* is sporadic. Since the nannnofossil *Emiliania huxleyi* is first present at 41.30 mbsf (see **"Calcareous Nannofossils,"** p. 9) and the FO of *E. huxleyi* is younger than the last occurrence (LO) of *P. curvirostris,* the sporadic presence of *P. curvirostris* in the uppermost part of Hole 1250C was considered to represent reworked fossils. Therefore, the LO of *P. curvirostris* was placed at the top of the continuous presence of this species in Sample 204-1250C-5H-CC (41.3 mbsf). The interval above 30.42 mbsf was assigned to North Pacific Diatom Zone (NPD) 12 (*N. seminae* zone). *P. curvirostris* is continuously present from 41.30 mbsf to 181.54 mbsf. This means that the sequence at Site 1250 does not reach the level of the FO of *P. curvirostris* (1.6 Ma); therefore, the age of sediments at 181.54 mbsf is estimated to be younger than 1.6 Ma.

Calcareous Nannofossils

Core catcher samples from most intervals of the 181-m composite sequence at Site 1250 contain rare to common, moderately to well-preserved calcareous nannofossils. Calcareous nannofossils, however, are barren or poorly preserved in a few intervals (e.g., from 51.34 to 71.23 and from 109.89 to 127.14 mbsf in Hole 1250C and from 125.49 to 149.51 mbsf in Hole 1250F).

Common to rare *E. huxleyi* is continuously present from the seafloor to 41.30 mbsf, assigning this interval to the Zone NN21. *Pseudoemiliania lacunosa* is frequently present from 51.34 to 181.54 mbsf, allowing us to determine the LO of *P. lacunosa* and place the NN19b/NN20 zonal boundary at 51.34 mbsf. Samples from 51.34 to 71.23 mbsf contain a few poorly preserved small-sized *Gephyrocapsa* species. Therefore, we could not see the small *Gephyrocapsa* spp. Acme Zone in Hole 1250C

from core catcher samples analyzed. *Calcidiscus macintyrei* is present frequently, although not abundantly (from 81.89 to 181.54 mbsf), suggesting the LO of *C. macintyrei* (1.59 Ma) is at 81.89 mbsf. The sediments at 181.54 mbsf (Sample 204-1250F-13X-CC) contain common *Gephyrocapsa lumina* and were assigned to the lower part of early Pleistocene Zone NN19 with an age of younger than 1.67 Ma.

Summary

Based on analysis of diatoms and calcareous nannofossils from the composite 181-m sequence at Site 1250, four microfossil events (one diatom and three nannofossil events) were recognized (Table T2). The age at the base of Hole 1250F (181.54 mbsf) was estimated to be younger than 1.6 Ma, based on the diatom assemblage, or to be younger than 1.67 Ma, based on the nannofossil assemblage. This means that the age of the 181-m-thick composite sequence at Site 1250 is early Pleistocene–Holocene.

We estimated linear sedimentation rates using these events (Fig. F15). The sedimentation rates are 15 cm/k.y. for the interval from the top of Hole 1250C to 42 mbsf and 2.4 cm/k.y. for the interval from 42 to 76 mbsf.

T2. Bioevents, p. 80.

F15. Age-depth plot, p. 45.

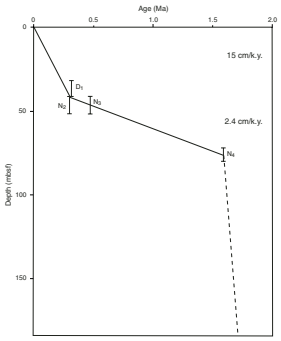

INTERSTITIAL WATER GEOCHEMISTRY

Site 1250 was drilled on the summit of Hydrate Ridge, where we expect fluid advection to be recorded by geochemical tracers as previously observed at Site 1249. At Site 1250, we collected 73 samples for interstitial water (IW) analyses from four holes. Hole 1250C was sampled at a resolution of approximately two samples per core, for a total of 31 samples. Hole 1250D was dedicated to microbiological studies, and we collected 15 samples in a coordinated program with the shipboard microbiologists. Three samples were collected from the near-surface sediments in Hole 1250E. From Hole 1250F, we collected 24 samples, 15 of which were collected at a resolution of one sample per section in the 100- to 130-mbsf interval to resolve chemical signals that could allow us to test the possibility of gas hydrate presence in the second BSR. In addition, sampling in Hole 1250F was aimed at constraining fluid flow through sediments imaged as Horizon A in the seismic data (see "Introduction," p. 1). Additional samples extended into deeper sediments that were not penetrated by prior boreholes. The IW geochemistry data are tabulated in Table T3 and are illustrated in Figure F16.

Site 1250 was cored to a TD of 180 mbsf (Hole 1250F), which is below the depth of the seismic reflector known as Horizon A. Thus, the composition of the IW at this site is influenced by gas hydrate geochemistry and by the possible migration of fluids, which might ultimately lead to the formation of authigenic carbonate deposits at and below the seafloor. The most obvious expression of authigenic carbonate formation is a massive buildup known as the Pinnacle, which is located immediately west of Site 1250.

T3. Dissolved species in pore waters, p. 81.

F16. Concentration profiles of various dissolved species, p. 46.

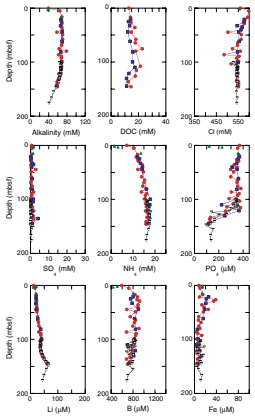

Chloride Concentration and the Presence of Gas Hydrate

The pore fluids recovered from the upper 50 mbsf at Site 1250 show an enrichment in dissolved chloride relative to background seawater

values. In Hole 1250C, Cl^- reaches a maximum value of 598 mM at 5.07 mbsf (Sample 204-1250B-2H-CC), and in Hole 1250E, it reaches 613 mM at 13.9 mbsf (Sample 204-1250C-2H-5, 140–150 cm). These enrichments are significantly lower than those measured at Site 1249, where chloride concentration in whole-round IW samples reaches 1008 mM. As discussed for Site 1249, the high chloride content in the pore fluid reveals that at Site 1250 the rate of gas hydrate formation exceeds that at which excess salts can be removed by diffusion and/or advection. (see **"Interstitial Water Geochemistry,"** p. 11, in the "Site 1249" chapter).

The chloride anomalies observed in the whole-round IW samples reflect not only the chloride enrichment in situ, but include a component of freshening resulting from gas hydrate decomposition during core retrieval and processing. We have not attempted to estimate the amount of hydrate in the upper 50 mbsf because we do not know the chloride composition of the in situ pore fluid before it is freshened by gas hydrate dissociation.

Below 50 mbsf, the chloride profile shows a gently sloping baseline toward slightly fresher values (Fig. **F17A**). The background chloride values correspond fairly well to the concentrations obtained for Site 1245, where there is no indication of chloride enrichment (see **"Interstitial Water Geochemistry,"** p. 13, in the "Site 1245" chapter). Thus, we have estimated the amount of gas hydrate in this portion of the sedimentary sequence to reach 15% of pore space, with average values ranging from 0% to 6% (Fig. **F17B**).

There is no change in the chloride concentration below the depth of the BSR at ~114 mbsf. Chloride remains at a constant value of 544 ± 3 mM from the base of the gas hydrate stability zone (GHSZ) to the bottom of the borehole (Fig. **F17**). Thus, there is no indication in the chloride data of gas hydrate presence below the BSR, as might be suggested by the second BSR observed in the seismic data (see **"Introduction,"** p. 1).

F17. Chloride concentrations and gas hydrate, p. 48.

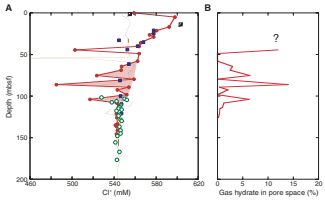

Carbon Cycling

The presence of authigenic carbonate deposition at and near the seafloor in the proximity of Site 1250 has been previously associated with methane seepage (Teichert et al., in press; Johnson et al., in press). Accordingly, sulfate concentrations are near zero in the shallowest sample (Sample 204-1250C-1H-1, 0–10 cm) and remain near zero downhole (Table **T3;** Fig. **F16**). This is because seawater sulfate and upward-moving methane are co-consumed by a consortium of microbes carrying out the net process of anaerobic methane oxidation (AMO) (e.g., Reeburgh, 1976; Boetius et al., 2000). This process has been discussed for Sites 1248 and 1249 (see **"Interstitial Water Geochemistry,"** p. 9, in the "Site 1248" chapter and **"Interstitial Water Geochemistry,"** p. 11, in the "Site 1249" chapter). Alkalinity is anomalously high in the upper tens of meters (Table **T3;** Fig. **F16**) as compared to nonseep locales like Site 1244, also reflecting advection of fluids. Alkalinity increases rapidly with depth as methane carbon, delivered to the shallow subsurface by advection, is converted to dissolved carbon dioxide by AMO.

Major and Minor Element Distributions

The advection of calcium-depleted fluids, plus the local depletion of calcium resulting from authigenic carbonate formation near the sea-

floor, results in a calcium profile showing very low calcium concentrations within the entire borehole. Similar depletion in dissolved calcium was observed at Site 1249 (see "Interstitial Water Geochemistry," p. 11, in the "Site 1249" chapter) and was reported by Torres et al. (2002) in sediments covered by bacterial mats on the summit of southern Hydrate Ridge.

Consistent with observations at Sites 1248 and 1249, we observe very high barium concentrations in the near-surface fluids, which result from upward flow of sulfate-depleted, barium-rich fluids. This barium transport results in large benthic fluxes of barium at cold-seepage sites (e.g., Torres et al., 1996).

The lithium profile (Fig. F18) shows a trend to increasing values with increasing depth, which has been observed at all sites drilled during Leg 204. This increase is believed to result from remobilization of lithium from aluminosilicates at depth, a process that has been observed at the Cascadia and other accretionary margins (e.g., Kastner et al., 1995; Chan and Kastner, 2000). Lithium shows positive deviations from this linear trend at the depths associated with the seismic reflector known as Horizon A at Sites 1245 and 1248 (see "Introduction," p. 1; and "Interstitial Water Geochemistry," p. 13, in the "Site 1245" chapter; "Interstitial Water Geochemistry," p. 9, in the "Site 1247" chapter; and "Interstitial Water Geochemistry," p. 9, in the "Site 1248" chapter). At Site 1250, a similar lithium increase is observed at the depth of the Horizon A reflector, possibly indicating transport of fluids from a depth deeper than 1 km, where the temperature has reached that exceeding the threshold needed for lithium release (>80°–100°C) (e.g., Edmond et al., 1979; Seyfried et al., 1984).

F18. Dissolved lithium data, p. 49.

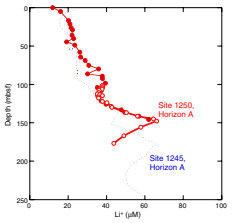

ORGANIC GEOCHEMISTRY

Site 1250 is located near the top of Hydrate Ridge and was cored to sample carbonate rocks near the Pinnacle. The shipboard organic geochemistry program at Site 1250 included analyses of hydrocarbon gases, carbonate and organic carbon, and total sulfur and total nitrogen content. A description of the methods used for these analyses is summarized in "Organic Geochemistry," p. 16, in the "Explanatory Notes" chapter.

Hydrocarbon Gases

The levels of methane (C_1), ethane (C_2), ethylene ($C_{2=}$), and propane (C_3) remaining in cores were measured using the headspace technique. The results are reported in Table T4 and plotted as parts per million by volume (ppmv) of gas component vs. depth in Figure F19. Methane content is high (>12,000 ppmv of headspace) in the shallowest cores and remains relatively constant and high throughout the cored interval down to 140 mbsf. Gas in cores was not analyzed by the headspace technique for the deeper samples in Hole 1250F. At Site 1250, there is no shallow zone with low or zero methane content, suggesting that the sulfate/methane interface is at or very near the seafloor. This is confirmed by dissolved sulfate in the pore water, which is <1 mM in the first core just beneath the seafloor consistent with prior observations (see "Carbon Cycling," p. 11, in "Interstitial Water Geochemistry") (Torres et al., 2002). The vial headspace ppmv C_1 concentration was recalculated to express the millimolar methane concentrations remaining

T4. Methane, ethane, ethylene, and propane, p. 83.

F19. C_1, C_2, $C_{2=}$, and C_3, p. 50.

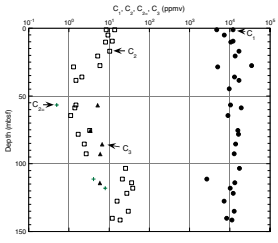

in the cores. Calculated dissolved C_1 concentration is shown in Table **T4** and, except for a few samples, is close to saturation levels for methane dissolved in seawater at surface conditions.

Headspace ethane (C_2) content is 10 ppmv near the seafloor, decreases to 1 ppmv at a depth of ~65 mbsf, and is maintained at low levels (1–3 ppmv) in the depth interval from 65 to ~105 mbsf. Ethylene ($C_{2=}$) is present at trace levels (0.5 ppmv) in only one sample above and in higher amounts (4–8 ppmv) below the BSR. Propane is present in headspace gas samples above but not below the BSR (Table **T4;** Fig. **F19**). Headspace gas analysis was not conducted in cores deeper than 140 mbsf (Hole 1250F), in order to concentrate efforts on analysis of void gas samples as discussed below.

The compositions of gas samples from voids or expansion gaps in the core liner are listed in Table **T5** and plotted on Figure **F20.** The void gas (vacutainer [VAC]) samples are relatively pure methane, with variable air contamination. The methane content in the core voids from Hole 1250B is frequently >950,000 ppmv (>95% by volume). The ethane content of void gas samples is high (700–800 ppmv) near the seafloor, then decreases to levels of 20–40 ppmv in the depth interval 58–63 mbsf. Void gas samples in the shallow zone near the seafloor also contain C_3–C_5 hydrocarbons, and gas hydrate is present near the seafloor. There is apparent hydrocarbon enrichment in the sediments near the seafloor but not at depths of 50–60 mbsf, suggesting lateral migration of wet gas hydrocarbons that have come up from depth along some focused conduit. Ethane content is maintained at low levels (127 ppmv or less) in Site 1250 sediments down to a depth of ~100 mbsf, where ethane begins to increase again and peaks at values of 1260 ppmv at depths of 115 mbsf. This is also about the estimated depth of the BSR. At other sites drilled during Leg 204, the ethane content in core void gas increases just beneath the base of methane hydrate stability, rather than above it. It appears that at Site 1250 the BSR coincides with a zone of enrichment in C_{2+} hydrocarbons. Below depths of 115 mbsf, the ethane content decreases and remains at 200–400 ppmv levels to a depth of 150 mbsf, where another zone of C_{2+} hydrocarbon enrichment is present in Horizon A.

Gas composition expressed as C_1/C_2 of headspace, and void gas is plotted vs. depth in Figure **F21.** The trends noted above for ethane and C_{2+} hydrocarbons are magnified in the C_1/C_2 ratio plot. Distinct features of Figure **F21** are three zones of C_{2+} hydrocarbon enrichment at the seafloor, at the depth of the BSR (114 mbsf), and at the depth of Horizon A (150 mbsf). These zones of anomalous heavy hydrocarbon enrichment may represent permeable pathways for lateral migration, with composition of sediment gas between these zones representing the more typical background of dominantly microbial methane.

Gas Hydrate and Pressure Cores

At Site 1250, samples from near the seafloor (1.4–6.5 mbsf) and from depths of 81.5, 86.7, and 100.2 mbsf were analyzed for the composition of gas from dissociated hydrate, with the results given in Table **T6.** The gas from the analyzed samples ranged from 55% to 98% methane, with the balance being mainly air contamination. Some of the shallowest gas hydrate samples gave off minor H_2S (400–1600 ppmv), and all samples analyzed produced CO_2 (240–5300 ppmv). Gas from several samples contained traces of propane and, in one case, some isobutane. Sample

T5. Light hydrocarbon and nonhydrocarbon gases, p. 84.

F20. Light hydrocarbons vs. depth, p. 51.

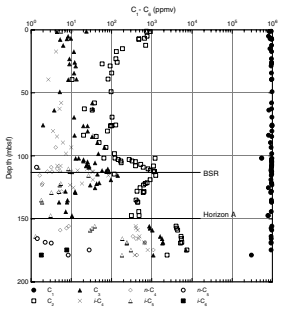

F21. C_1/C_2 ratio vs. depth, p. 52.

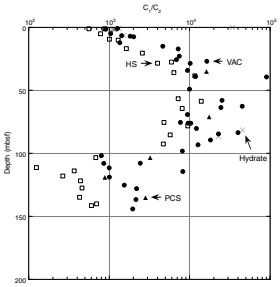

T6. Gas from decomposed gas hydrate, p. 86.

204-1250D-10H-3, 53–84 cm, produced more propane than ethane. The presence of gas components other than methane and ethane has important implications for hydrate structure. No procedures were used on the ship to evaluate hydrate structure. Many of the samples contained intermixed sediment, and it is not known if trace components could have come from dissolved gas in the sediment rather than from the hydrate itself. The C_1/C_2 ratios of gas hydrate samples are in the same range as void gas samples from the same depths at Site 1250 (Fig. **F21**), although two of the three deeper samples appear somewhat depleted in ethane.

Five deployments of the PCS successfully retrieved cores from depths of 35–120 mbsf (Cores 204-1250C-9P; 204-1250D-5P, 13P, and 18P; and 204-1250F-4P). The composition of gas samples obtained during controlled PCS degassing experiments is listed in Table **T7.** Based on the volume-averaged composition, the C_1/C_2 ratios of gas from the PCS cores fall on the VAC/void gas trend (Fig. **F21**).

T7. Composition of gas from PCS degassing experiments, p. 87.

Carbon Analyses, Elemental Analyses, and Rock-Eval Characterization

A total of 13 sediment samples were analyzed for carbonate carbon (IC), total carbon (TC), organic carbon (OC) (by difference), total nitrogen (TN), and total sulfur (TS). The results are listed in Table **T8.** IC (Fig. **F22**) varies from 0.12 to 0.65 wt% at Site 1250. When calculated as $CaCO_3$, the carbonate contents measured in the Hole 1250B sediments vary from 1.0 to 5.4 wt% (Fig. **F22**). The sediments at Site 1250 generally contain relatively low amounts of IC.

OC content varies from 1.03 to 1.64 wt% (average = 1.32 wt%) (Table **T8;** Fig. **F22**). TN contents range from 0.15 to 0.21 wt%, and the C/N ratios are all <10, consistent with a dominantly marine source of organic matter. Sediment samples have total sulfur contents ranging from 0.14 to 0.67 wt% (Table **T7**), with no distinct relation to OC content.

The results of Rock-Eval pyrolysis of selected samples are given in Table **T9.** This analysis was performed in part to evaluate the possible presence of migrated liquid hydrocarbons. Although the production index values seem moderately elevated (i.e., >0.1), they are fairly typical for continental margin sediments cored by ODP. There is no correlation between increased C_{2+} gas components and higher production index values and no definitive evidence for oil staining.

T8. IC, OC, TN, and TS, p. 88.

F22. IC, OC, TN, and TS and C/N ratios, p. 53.

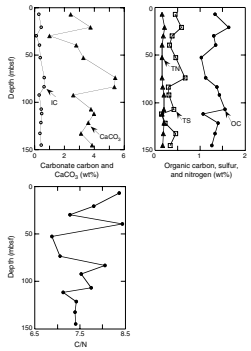

T9. Rock-Eval pyrolysis, p. 89.

MICROBIOLOGY

Site 1250 is located near the summit of Hydrate Ridge, a few hundred meters from Site 1249. As at Site 1249, methane is present all the way up to the seafloor at Site 1250 (see **"Hydrocarbon Gases,"** p. 12, in "Organic Geochemistry"). In the upper 10–20 mbsf, sulfate is essentially absent through the entire cored section (see **"Carbon Cycling,"** p. 11, in "Interstitial Water Geochemistry"). In the upper 10–20 m, hydrates are abundant (see **"Lithostratigraphy,"** p. 3), and authigenic carbonates precipitate (see **"Lithostratigraphy,"** p. 3), presumably from oxidation of advected methane (see **"Carbon Cycling,"** p. 11, in "Interstitial Water Geochemistry" and **"Hydrocarbon Gases,"** p. 12, in "Organic Geochemistry"). Site 1250 was drilled deeper than Site 1249; coring

penetrated the base of the GHSZ at ~110 mbsf and Horizon A at ~150 mbsf and reached a maximum depth of 180 mbsf.

Microbiological Sampling

Samples were taken for microbiological studies from Holes 1250D and 1250E (Table T10). Attempts were made to preserve near-surface sediments for AMO studies. The liner containing the first core from Hole 1250D was badly damaged during recovery, and the associated fluid intrusion made the core unsuitable for microbiology. Sampling began with Core 204-1250D-3H and proceeded to the TD of Hole 1250C (Core 19X). Because sulfate was not detected in any Site 1250 sediments, it seems likely that AMO takes place at the seafloor or in the very upper sediment layers. Because of interest in this zone, a total of 16 m of sediment in two cores was recovered from another hole (Hole 1250E) shot specifically for microbiology.

T10. Intervals sampled for microbiology, p. 90.

Thermal anomalies indicating hydrate were seen throughout the GHSZ in Hole 1250D (see "Infrared Scanner," p. 16, in "Physical Properties"). As at Site 1249, infrared (IR) thermal anomalies that indicated diffuse hydrate did not influence where microbiological samples were taken. Postcruise examination of IR images will help unravel the hydrate story. No samples were taken next to massive hydrates at this site. Sampling of shallow cores taken from Hole 1250E was complicated by their gassy nature. Microbiological samples from top layers were in very close proximity to readily observable, cross-cutting gas hydrate veins in multiple orientations that rapidly disappeared upon exposure.

As at other sites that intersect Horizon A, Site 1250 was influenced by heavy hydrocarbons in deeper sediment layers (see "Hydrocarbon Gases," p. 12, in "Organic Geochemistry"). Drilling in Hole 1250D was stopped at 145 mbsf and before Horizon A was penetrated, but deep sediments that contained thermogenic hydrocarbons were sampled for microbiological studies. Thermogenic sources of methane at this site may make biological production of methane unfavorable.

Contamination Tests

Perfluorocarbon Tracer

No samples for PFT analyses were taken at Site 1250.

Fluorescent Microspheres

Fluorescent microsphere tracer data are summarized in Table T11. Abundant microspheres in both outer and inner layers of samples from shallow cores taken from Hole 1250E reiterate the difficulty of sampling soft, gassy sediments. With the possible exception of Hole 1244F, microsphere quality assurance evaluations from Leg 204 suggest that all APC mudline cores should be regarded as questionable for microbiological analysis. No mudline XCB cores were taken for microbiology during this leg. In nearly all shallow cores collected during this leg, either high levels of contamination were indicated or microsphere deployment was unsuccessful and cores have an unknown amount of contamination. All cores taken from Hole 1250D were treated with microspheres, and in most cores, no interior spheres were detected.

T11. Core quality indicators, p. 91.

In view of the difficulties encountered with recovering suitable near-seafloor material under the conditions at the crest of Hydrate Ridge and

considering the microsphere tracer observations, a different method of sample collection, such as box coring or multicoring, should be used.

PHYSICAL PROPERTIES

The physical properties of sediments at Site 1250, located east of the carbonate pinnacle, are similar to those at Site 1249. At Site 1250, three holes (Holes 1250C, 1250D, and 1250F) were used for physical property analyses. Standard sampling and measurement procedures were applied as outlined in "Physical Properties," p. 22, in the "Explanatory Notes" chapter. Core recovery was generally good, and only a few data gaps are present.

In all holes cored at this site, a downhole profile of IR temperature was acquired and was used for on-catwalk hydrate detection. Twenty samples, which were thought to be hydrate, were taken on the catwalk; however, the IR images show a much higher number of cold-spot anomalies, which we interpret to indicate additional instances of the presence of hydrate.

Infrared Scanner

IR imaging of cores recovered at Site 1250 enabled the on-catwalk identification of hydrate zones in each core, as described in "Physical Properties," p. 22, in the "Explanatory Notes" chapter. This information was used to facilitate hydrate sampling and preservation for all cores. The IR thermal anomalies are cataloged in Table T12, which includes an interpretation of the overall hydrate texture for each anomaly. A large fraction (60%) of the anomalies in both Holes 1250C and 1250D are apparently created by disseminated hydrate. Vein-filled features account for 25%–28%, and nodular features account for 12%–14% of the hydrate associated with the IR anomalies. No trends with depth were identified for these three types of anomalies. The abundance of disseminated hydrate and veins or lenses parallel to bedding suggests that stratigraphy exerts a significant control on the occurrence of gas hydrate at this site.

T12. Gas hydrate, p. 92.

Successive thermal images were used to produce downcore thermal profiles for each core recovered in Holes 1250C and 1250D (Fig. F23). Extensive cold anomalies are present between 14 and 109 mbsf in Hole 1250C and between 6 and 113 mbsf in Hole 1250D, which is consistent with a BSR depth of 112 mbsf. The temperature anomalies created by hydrate have been extracted from the downcore temperature data and from direct examination of IR images (Fig. F24). Comparison of anomalies from Holes 1250C and 1250D indicates significant differences between the two holes (separated by 40 m, 20 m north and south of Hole 1250A, respectively) (Fig. F1). Overall downcore trends are similar, but Hole 1250D has more anomalies than Hole 1250C (57 vs. 40 anomalies). Most of the anomalies present in Hole 1250D are small ΔTs, but there is no obvious bias in the detection of anomalies. Larger ΔT s are present in Hole 1250C. The opposite would be expected if, for some reason, thermal anomalies were detected less effectively in Hole 1250C. Core recovery plots (Fig. F24) show that poor core recovery in the upper part of both holes limited detection of shallow hydrate if present.

F23. IR temperature profiles, p. 54.

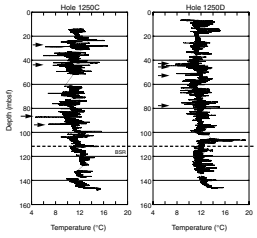

F24. Comparison of temperature anomalies, p. 55.

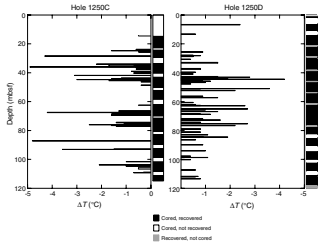

Comparison of pore water saturation (S_w) calculated from LWD (see Fig. F42) with thermal anomalies shows a generally good correlation between the two methods of hydrate detection. However, S_w estimates

suggest increasing hydrate concentration approaching the BSR (112 mbsf). IR anomalies show peak hydrate presence at ~45–80 mbsf. Comparison with wireline logging results in Hole 1250F may help to determine if this discrepancy represents heterogeneity in the presence of hydrate on a scale of 25 m horizontally or if the combined uncertainty in IR anomalies and resistivity logging data are responsible for hole-to-hole differences.

Sediment Density from Multisensor Track and Moisture and Density

Overall data trends in sediment density at Site 1250 are related to the normal compaction gradient of the sediments (Fig. F25). Densities are ~1.6 g/cm³ at the seafloor and increase to ~1.8 g/cm³ at 150 mbsf at the BOH (Table T13). There is a distinct density change at 45 mbsf that correlates to seismic Horizon Y (Fig. F26). Density increases by ~0.15 g/cm³, and porosity decreases by ~10%. There is one distinct outlier in the moisture and density (MAD) bulk density data at a depth of 40.72 mbsf with a density of 2.033 g/cm³. This data point corresponds to a sample taken in a sandy layer (Sample 204-1250C-5H-6, 30–32 cm), which is within the interval of turbidites that are present around Horizon Y (Fig. F27B). An equivalent sample from a sandy layer was taken at a depth of 133.92 mbsf (Sample 204-1250C-17H-2, 42–44 cm) with a density of 1.949 g/cm³ (Fig. F27A). The sandy layers have a lower water content than the surrounding clay-rich sediments. The MAD measurements are mass-property measurements (see **"Physical Properties,"** p. 22, in the "Explanatory Notes" chapter), and the clay-rich sediments, therefore, show a lower density than the sandy layers. The sandy layers have higher bulk density and lower porosity than the clays in the MAD data. The MAD data differ from the gamma ray attenuation (GRA) measurements by ~0.2 g/cm³ for unknown reasons.

Five PCS cores were successfully taken at this site. These were available for physical property analyses (Cores 204-1250C-16P; 204-1250D-5P, 13P, and 18P; and 204-1250F-4P). Generally, three MAD samples are taken from each PCS core. There is an apparent mismatch with the general downhole trend in bulk density and the values obtained from the PCS core samples. The density in Core 204-1250D-13P is higher than the background trend, whereas densities from Cores 18P and 204-1250C-16P are much lower. Densities derived from Core 204-1250D-5P are within the general trend. There is no change in lithology between the PCS and adjacent APC/XCB cores that could explain the observed difference in bulk density. There was also no special procedure applied to the PCS sediments to measure bulk density. A possible explanation may be the treatment of the PCS prior to MAD analyses or in the way the cores were obtained in situ compared to regular APC/XCB coring. Specifically, PCS sediments are depressurized slowly compared to APC/XCB, and PCS sediments are extruded from the PCS barrel using water pressure.

At Site 1250, seismic Horizon A was cored at ~150 mbsf. The LWD data indicate a prominent drop in sediment density by >0.4 g/cm³. There is no equivalent drop detected in the MAD and GRA data. Individual samples taken from cores follow the main background trend, except for a few samples showing higher bulk densities, which are correlated with sandy intervals. A sample taken directly at the top of interval 204-1250F-10X-4, 1–3 cm, which is an interval with a very high ash

F25. Physical properties, p. 56.

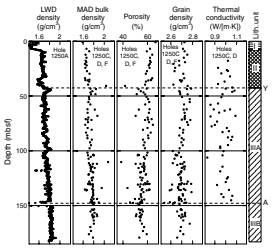

T13. MAD index properties, p. 94.

F26. Physical properties with 3-D seismic data, p. 58.

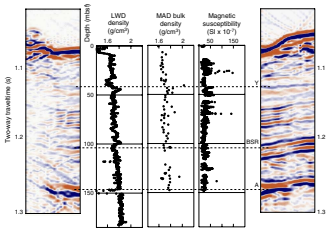

F27. High-density samples, p. 59.

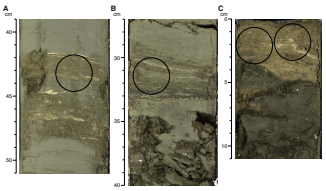

content (Fig. F27C), shows a bulk density from the MAD analyses of 1.79 g/cm³ and a grain density of 2.62 g/cm³ (indication of the ash content).

Magnetic Susceptibility

MS appears relatively uniform at Site 1250 (Fig. F26), with values generally <40 × 10^{-7} (SI). Several small-scale spikes appear in the MS data and are either associated with the presence of abundant authigenic sulfides or turbidite layers. An MS anomaly in Core 204-1250C-8H is associated with a single sulfide spot (Fig. F28). The sulfide precipitate has a diameter of <1 cm but results in an anomaly that is spread out over >5 cm, which is a function of the spatial resolution of the loop sensor with the core diameter used.

An example of stratigraphically controlled MS anomalies can be found at ~42–44 mbsf (Fig. F29). This MS anomaly is near seismic Horizon Y (see "Lithostratigraphy," p. 3). The expanded MS section and core photographs illustrate typical peaks in the record caused by magnetically susceptible minerals in the turbidites.

Compressional Wave Velocity from Multisensor Track and the Hamilton Frame

No velocity measurements were carried out at Site 1250 as a result of poor core recovery and intensive gas-expansion cracks.

Thermal Conductivity

Thermal conductivity was measured in Holes 1250C and 1250D. The three measurements at Hole 1250E are relatively low and might have been affected by gas expansion (Table T14). No distinct downhole trend was observed, and thermal conductivity is, on average, 0.967 W/(m·K).

Shear Strength

No shear strength measurements were carried out at Site 1250 because of poor core recovery and/or abundant gas-expansion cracks.

Summary and Discussion

At Site 1250, physical properties agree well with the description of the lithostratigraphic units. The boundary between lithostratigraphic Units II and III is present at a depth of 45 mbsf and is correlated with seismic Horizon Y. This horizon is interpreted as an unconformity based on observed changes in lithologic and seismic characteristics, such as a relatively sharp increase in sediment density. This is best seen in LWD and GRA density data from Hole 1250D, which had better core recovery than Hole 1250C.

The prominent seismic Horizon A was not cored in Holes 1250C and 1250D but was drilled during the LWD program (Hole 1250A) and during the revisit to Hole 1250F. There is a discrepancy between the LWD data and the laboratory density measurements. The LWD, which measured in situ properties, detects a prominent drop in sediment density, whereas no similar effect is seen in the MAD and GRA data. This discrepancy was detected in all cores from the different sites where Hori-

F28. MS anomaly, p. 60.

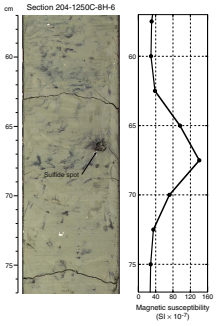

F29. MS variations of turbidite layers, p. 61.

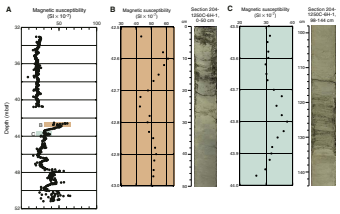

T14. Thermal conductivity, p. 95.

zon A was cored and is thought to indicate the presence of gas in situ in Horizon A.

IR imaging provided the best method for on-catwalk detection of hydrate. At Site 1250, 20 hydrate samples were collected; however, there is considerable mismatch between the S_w calculated from the LWD resistivity data and the temperature anomalies in the IR images.

DOWNHOLE TOOLS AND PRESSURE CORING

Downhole Temperature Measurements

Thirteen in situ temperature runs were made at this site: nine APCT tool and four DVTPP runs (Fig. F30). APCT data were modeled using the software program TFIT (as described in "Downhole Tools and Pressure Coring," p. 34, in the "Explanatory Notes" chapter) using measured thermal conductivities (see "Physical Properties," p. 16). Temperatures for the DVTPP runs were measured directly from the data because the longer time taken for this measurement results in temperatures that appear to have reached equilibrium. Only the deepest of the DVTPP time series shows the frictional pulse that is expected when the temperature probe is extracted. The two shallower DVTPP measurements yield temperature estimates that are slightly higher than, but generally consistent with, the APCT measurements. The DVTPP at 138.5 mbsf did not yield a reliable measurement.

The temperature estimates are given in Table T15 and shown in Figure F31. We note that at this site, no dedicated mudline temperature measurement was taken. Mudline temperatures taken for ~5 min prior to recovery are very variable and range from 4.36° to 5.51°C. The average is given in the table, but we did not include this data point in the determination of temperature gradient. The APCT data alone yield a temperature gradient of 0.053°C/m. If the DVTPP data are included, the apparent temperature gradient increases to 0.058°C/m. The apparent mismatch between the observed BSR depth of ~112 mbsf and the depth of 128–137 mbsf calculated from the temperature data, assuming a pure methane/seawater system, implies a temperature anomaly of 0.5°–1.0°C at the BSR, similar to that observed at several other sites. Although additional analysis of the data is needed to resolve questions about instrument calibration, we can conclude that the rate of vertical advection of acqueous fluid must be slow (see "Downhole Tools and Pressure Coring," p. 20, in the "Site 1249" chapter).

In Situ Pressure Measurements

Three in situ pressure measurements were made at this site using the DVTPP. They do not show the expected decay in pressure with time. Analysis will be conducted postcruise.

Pressure Core Sampler

The ODP PCS was deployed seven times at Site 1250. Five deployments were successful (i.e., a core under pressure was recovered). The ball valve did not fully close during the other deployments. The main objectives of the deployments were (1) to construct a detailed profile of concentration and composition of natural gases in the upper part of the

F30. In situ temperatures, p. 62.

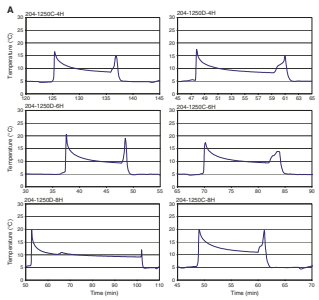

T15. Temperature measurements, p. 96.

F31. Estimated temperature, p. 64.

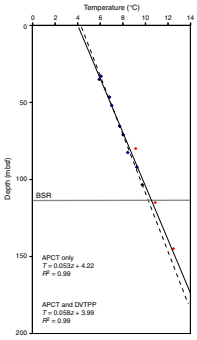

section (0–140 mbsf) and (2) to identify the presence/absence and concentrations of gas hydrate within the GHSZ.

Specific depth intervals were targeted for deployment of the PCS. Three cores (Cores 204-1250C-9P [71–72 mbsf] and 204-1250D-5P [35–36 mbsf] and 13P [103.5–104.5 mbsf]) were recovered from above the BSR at ~112 mbsf. Two other cores (Cores 204-1250D-18P [135.2–136.2 mbsf] and 204-1250F-4P [119–120 mbsf]) were recovered from below the BSR.

The PCS cores were degassed for 579–1800 min after recovery on board (Table **T15**). Pressure was recorded during degassing experiments of all cores, except for Core 204-1250F-4P (Fig. **F32**). Gas was collected in a series of sample increments (splits), and most were analyzed for molecular composition (see **"Organic Geochemistry,"** p. 12). In addition, gas splits were subsampled for onshore analyses. After degassing, the PCS was disassembled. The lengths of the cores were measured (Table **T16**), and samples were taken for analysis of physical properties (see **"Physical Properties,"** p. 16).

Gas was collected in 10- to 810-mL increments. The measured incremental and cumulative volumes are plotted vs. time on Figure **F32.** The cumulative volume of released gas varies from 1385 (Core 204-1250D-18P) to 5390 mL (Core 204-1250F-4P) (Table **T16**). The volume of the last gas splits varies from 10 (Cores 204-1250C-9P and 204-1250D-13P) to 30 mL (Core 204-1250D-5P). This observation suggests that almost all gas present in the cores was collected.

Gases released from the PCS are mixtures of air (N_2 and O_2), CH_4, CO_2, and C_{2+} hydrocarbon gases (see **"Gas Hydrate and Pressure Cores,"** p. 13, in "Organic Geochemistry"). The abundance of air components in the PCS gas samples (3.0%–8.3% of gas mixtures) suggests that air was not always properly displaced from the PCS by seawater during deployments. Methane is the dominant natural gas present in collected gas splits. The molecular composition of gases from the PCS is similar to the composition of gas voids at adjacent depths (Fig. **F21**).

Sediments in cores recovered by the PCS have lithologies similar to sediments recovered by the APC and XCB cores at adjacent depths (see **"Physical Properties,"** p. 16). Porosity values measured in APC and XCB cores taken near the PCS were averaged and used to estimate the methane concentrations in situ (Table **T16**).

The concentrations of methane in situ were estimated based on data from the degassing experiment (i.e., total volume of methane) and core examination (i.e., length of recovered core and the porosity of sediments). The calculation yields equivalent concentrations varying from 65.7 to 278.3 mM of methane in pore water. These concentrations have been compared with the theoretical methane-solubility curve extrapolated from values calculated for higher pressures (greater depths) (Handa, 1990; Duan et al., 1992) (Fig. **F33**). Preliminary analysis of gas concentrations suggests that gas hydrate may have been present in concentrations varying from 0.6% to 2.2% of pore volume in all three cores (Cores 204-1250C-9P and 204-1250D-5P and 13P) recovered from above the BSR. Interestingly, no evidence of gas hydrate presence was found in the pressure record of core degassing (Fig. **F32**). Free gas appears to be present in relatively high concentrations (perhaps around 4% of pore space) at a depth of ~7.5 m below the BSR (Core 204-1250F-4P). Only dissolved methane seems to be present in the core (Core 204-1250D-18P) retrieved from ~24 m below the BSR. Additional comparison of measured methane concentrations with theoretical methane solubility above and below the BSR will be performed on shore to better

F32. Volume-pressure-time plots for PCS, p. 65.

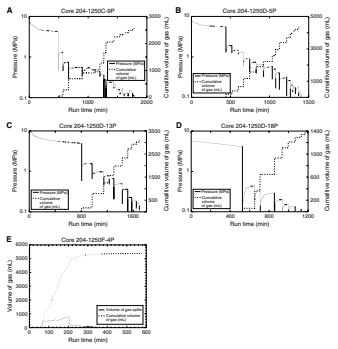

T16. Degassing experimants, p. 97.

F33. Methane concentrations, p. 66.

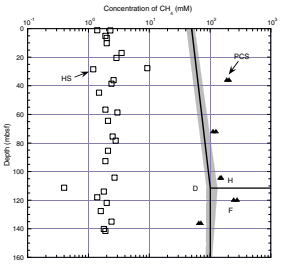

estimate if methane was present in situ in solution, in free phase, or as gas hydrate.

HYACINTH Pressure Coring and Logging

Coring Summary

The HYACINTH pressure coring tools were deployed twice at Site 1250: one with the FPC (Core 204-1250C-18Y [FPC 4]) and one with the HRC (Core 204-1250D-17E [HRC 3]). After the lessons learned from the procedures and the tool adjustments made at Site 1251, we hoped that a pressurized core might be recovered from this site. A good core was recovered with the FPC, but full retraction into the autoclave was prevented as a result of inadvertent line tension during the coring operation. The HRC, on the other hand, recovered a short core at full in situ pressure, which was considered a significant success. Core 204-1250D-17E (HRC 3) was then transferred under full pressure and logged in the V-MSCL before being depressurized. Unfortunately, the DSA tool was still dogged by technical difficulties and failed to provide any useful downhole data during the coring operations. However, the rig floor data proved valuable in analyzing some aspects of the behavior during each deployment, especially given the fact that there had been a brief tension load on the wireline during the FPC deployment.

After transferring Core 204-1250D-17E (HRC 3) to the logging chamber, the density profile was measured in the V-MSCL, where we discovered how short the core was (20 cm). This short core had sediment densities of ~1.65 g/cm^3 and produced some obvious gas layers when depressurized (Table T17).

T17. Summary of the recovery percentages, p. 98.

HYACE Rotary Corer Operations

The HRC was deployed at Site 1250 in a water depth of 796 m (see Table T18). Core 204-1250D-17E (HRC 3) was taken in the bottom of Hole 1250D at 134.2 mbsf. Lithologies at this depth were lightly indurated silty clays that were being cored with full recovery by the APC. These sediments were considered suitable for the FPC, and it was thought that they might be stiff enough to be cored using the HRC. A modified finger catcher was made and fitted for this deployment in the hope that it might help retain the core in this type of formation. The deployment went well, with the procedures being essentially the same as for previous runs (see **"Downhole Tools and Pressure Coring,"** p. 25, in the "Site 1251" chapter and **"Downhole Tools and Pressure Coring,"** p. 34, in the "Explanatory Notes" chapter). The HRC was lowered in the drill string at 72 m/min while circulating and rotating. Pumping was stopped at 890 m, the tool was lowered down slowly to the landing position, and a slack of 4 m was given on the wireline. The drill string was then lowered to TD with the wireline following. The blowout Preventer (BOP) on the wireline was closed, and pumping was started at 82 gallons per minute (gpm). A pressure spike was observed at 540 psi, indicating that coring had begun, and then pumping continued at 95 gpm for 20 min before stopping and opening the BOP. The drill string was lifted to 937 m before the BOP was closed again and pumping continued for 2 min (to ensure full stroke) at 80 gpm. The BOP was again opened, and the tool was lifted on the wireline very slowly for the first 16 m before being raised to the surface at 110 m/min. During the coring operation the weight on bit was set at ~15,000

T18. HYACINTH pressure coring summary, p. 99.

klb, and both the active and passive heave compensators were activated. The tool was recovered and placed on the trestles in the usual way. It was disassembled and the autoclave moved to the transfer system where an internal pressure of 88 kbar was measured. The core was retracted into the shear transfer chamber under full pressure where it was sheared and successfully moved into the logging chamber. After the core had been logged in the V-MSCL, it was depressurized in stages before being removed and curated as a 28-cm-long core. Note that this short core was the first of its kind to have been recovered and logged in a liner under full in situ pressure.

Fugro Pressure Corer Operations

A single FPC deployment was made at Site 1250 in a water depth of 796 m (see Table **T18**). Core 204-1250C-18Y (FPC 4) was recovered from the bottom of Hole 1250C at 137.5 mbsf. Lithologies at this depth were lightly indurated silty clays that were suited to the APC and considered suitable for the FPC hammer mechanism. Operationally, the deployment ran smoothly as per previous deployments (see **"Downhole Tools and Pressure Coring,"** p. 25, in the "Site 1251" chapter) with the downhole procedures being followed and the active heave compensator being used throughout. A good core was recovered (84 cm long) but the inner rod had not stroked out completely and the core had only partially retracted into the autoclave. The pressure was released by drilling small holes in the liner prior to removing the core. Once again during this deployment the FPC data logger worked well but the Lamont DSA tool only collected data from the very beginning part of the test. An analysis of the rig data concluded that at one time a significant tension had been applied on the wireline during the coring operation (which probably prevented a full stroke occurring) and should be avoided by paying out more slack wire on subsequent deployments.

DOWNHOLE LOGGING

Logging While Drilling

Operations

LWD operations at Site 1250 consisted of drilling two dedicated LWD boreholes in Holes 1250A and 1250B. LWD operations in Hole 1250B were conducted because of a RAB tool failure in Hole 1250A. Site 1250 LWD operations began at 0330 hr Universal Time Coordinated (UTC) on 22 July 2002 by spudding Hole 1250A at a water depth (drillers depth) of 807.00 meters below rig floor (mbrf) on the crest of southern Hydrate Ridge. The LWD tools deployed in Hole 1250A included the GeoVision Resistivity (GVR; RAB), MWD (Powerpulse), Nuclear Magnetic Resonance (NMR-MRP) tool, and Vision Neutron Density (VND) tool. Drilling proceeded at reduced ROP of 15 m/hr and low fluid circulation rates of 15 spm to minimize formation washout in the unconsolidated sediments below seafloor. No real-time MWD or NMR-MRP data were recorded over this interval, as the pump rate was insufficient to activate the turbines in the downhole tools. The ROP was increased to ~25 m/hr, fluid circulation was returned to more normal levels at a bit depth of 20 mbsf, and real-time MWD and NMR-MRP data were recorded to TD (210 mbsf). The LWD tools were pulled to the rig floor at

2215 hr on 22 July for a total bit run of ~18 hr. Data from four sequential holes (Holes 1247A, 1248A, 1249A, and 1250A) were downloaded from the LWD tools, which amounted to ~76 MB of binary data. At this point, it was determined that the battery power in the RAB tool had been unexpectedly depleted during the logging run in Hole 1250A, and resistivity and gamma data were not recorded for this hole. Drilling time for the entire four-hole suite was 65 hr.

As noted above, the reason for drilling Hole 1250B was the loss of the RAB data in Hole 1250A. LWD operations for Hole 1250B began with initialization of Azimuthal Density Neutron (ADN), RAB, and NMR-MRP tools and running the bottom-hole assembly to 60 m above the seafloor at 2400 hr on 23 July. Hole 1250B was also spudded at a water depth of 807.00 mbrf (drillers depth). Drilling proceeded to 25 mbsf with an average ROP of 20 m/hr and pump-stroke circulation rate of 15 spm. No real-time MWD or NRM-MRP data were recorded over this interval. The ROP was increased to a relatively high rate of 50 m/hr at 25 mbsf and maintained to TD at 180 mbsf in an attempt to speed up operations. The pipe was pulled up from the BOH to 160 mbsf without rotating to evaluate the effect of drilling motion on the NMR-MRP log. The tools were recovered at the rig floor at 1400 on 23 July and laid down prior to downloading data from Hole 1250B. For Hole 1250B the total bit run was ~8 hr.

Logging Quality

Figure F34 shows the quality control logs for Holes 1250A and 1250B. As noted above, the target ROP for the two LWD logging runs at Site 1250 were different (in Hole 1250A, target ROP below 20 mbsf was ~25 m/hr; in Hole 1250B, target ROP below 25 mbsf was ~50 m/hr), which provided an opportunity to compare the effects of variable drilling conditions on the LWD data obtained in both holes. The actual recorded ROP below ~20 mbsf in Hole 1250A was consistent at 25 m/hr (±5 m/hr). However, the measured ROP in Hole 1250B was more variable below 25 mbsf, with measured ROP from 30 to 70 m/hr. In Hole 1250A, an ROP of 25 m/hr was sufficient to record one sample per 4-cm interval (~25 samples per meter). With a ROP of 50 m/hr in Hole 1250B, a measurement was obtained every 10 cm (~15 samples per meter). The quality of the RAB image from Hole 1250B is quite high, and no significant resolution loss was observed with variation in ROPs. The increased pump rates below 20 mbsf (Hole 1250A) and 25 mbsf (Hole 1250B) yielded enhanced NRM-MRP porosity data, with a data sampling resolution of approximately one sample per 15-cm interval.

The differential caliper log (DCAL), which gives the distance between the tool sensor and the borehole wall as recorded by the LWD density tool, is the best indicator of borehole conditions. The DCAL values are <1 in over 96% of the total drilled section in Hole 1250A, and ~86% of Hole 1250B is characterized by DCAL measurements <1 in. Only the uppermost ~18 m of Hole 1250B contains relatively thick washout intervals of >1 in. The density correction, calculated from the difference between the short- and long-spaced density measurements, varies from 0 to ~0.12 g/cm³ in both Holes 1250A and 1250B (Fig. F34), which suggests very high quality density measurements. A standoff of <1 in between the tool and the borehole wall also indicates high-quality density measurements with an accuracy of ±0.015 g/cm³.

Below 30 mbsf in Hole 1250A, the time-after-bit (TAB) measurements were 90 ± 10 min for the density and neutron porosity logs (Fig. F34).

F34. Quality control LWD logs, p. 67.

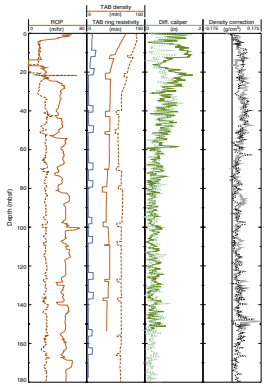

The recorded TABs for Hole 1250B (below 20 mbsf) were significantly shorter (55 ± 10 min) than those measured in Hole 1259A because of the higher ROP in Hole 1250B.

The recorded LWD data from Hole 1250B are of very high quality. The density and neutron logs from Hole 1250B closely match the logs obtained from Hole 1250A. There is minimal reduction in vertical resolution resulting from the faster ROP in Hole 1250B, and the borehole is in relatively good shape throughout the shallow interval of both LWD holes drilled at Site 1250.

The depths relative to seafloor for the LWD logs from Holes 1250A and 1250B were fixed by identifying the gamma ray signal associated with the seafloor and shifting the logging data to the appropriate depth, as determined by the drillers pipe tallies. For Holes 1250A and 1250B, it was determined that the gamma ray log pick for the seafloor was at the same depth of 806.0 m below the rig floor. The rig floor logging datum was located 11.0 m above sea level for 1250A and 11.1 m above sea level for Hole 1250B.

Wireline Logging

Operations

Hole 1250F was APC and XCB cored to a depth of 180 mbsf (drillers depth). Rig-up for conventional wireline logging (CWL) operations began at 0340 hr on 26 August and final rig-down was completed by 1405 hr on 26 August. See Table **T19** for detailed information on the Hole 1250F CWL program.

T19. CWL operations summary, p. 100.

CWL operations in Hole 1250F began with the deployment of the triple combo tool string (TAP/DIT/HLDT/APS/HNGS/QSST) (Table **T19**). The triple combo tool string initially reached a depth of 179 mbsf without difficulty and with no sticking problems. Excellent quality data were acquired during the main uphole pass, and the tool was run back to the BOH for a second pass. The second pass also reached a TD of 179 mbsf, and excellent quality data were recorded on the second ascent. The TAP temperature data and associated depth data were recorded without problems during both of the triple combo tool string lowerings. The caliper from the HLDT showed the hole to be in extremely good condition, with the hole diameter seldom >13 in. After completing the second pass, the triple string combo tool was again lowered to a depth of 179 mbsf to obtain several checkshots (10 tacked shots) with the QSST. A one-way traveltime of 632 ms was recorded at TD (179 mbsf). To calculate a checkshot interval velocity with depth, a 32-m uphole shift is necessary to take into account the position of the QSST at the top of the triple combo tool string. The triple combo logging run ended with the rig-down of the tool string being completed at 0950 hr on 26 August.

For the second CWL run in Hole 1250F, the FMS-sonic tool string (FMS/DSI/SGT) was deployed. The FMS-sonic tool string reached a maximum depth of 182 mbsf on two consecutive passes. The two FMS-sonic tool string runs confirmed the excellent condition of the hole, as observed during the triple combo logging run. The FMS images and sonic waveforms recorded from the two lowerings of the FMS-sonic tool string were of very high quality. However, the FMS-sonic tool string did not initially reenter the drill pipe (set at 58 mbsf) during the first ascent, which required the end of the first pass to be aborted prematurely. It was determined that the lockable flapper valve (LFV) had closed, pre-

venting the FMS-sonic string from reentering the drill pipe. The drilling rig mud pumps were used to pump open the LFV. During the first pass of the FMS-sonic string, the DSI tool was set at a low-frequency mode for the lower dipole, standard frequency for the upper dipole, and low frequency for the monopole. During the second pass of the DSI, a Stoneley wave mode was used instead of the upper dipole; the monopole was set at the standard frequency; and the lower dipole was set at the standard frequency. The recorded sonic waveforms from both lowerings of the DSI are of very high quality, but the very low velocity of the formation made it difficult for the automatic slowness/time coherence (STC) picking program to select accurate compressional velocities. Some adjustment of the STC parameters allowed for improved compressional (*P*)- wave velocity (V_P), but further reprocessing is required. The quality of the recorded shear wave data was very high, but it will also require additional processing.

A final run was made for seismic experiments, which will be discussed elsewhere.

Logging Quality

All logging data from the triple combo and FMS-sonic runs in Hole 1250F are of very high quality (Figs. **F35, F36, F37, F38**). The hole conditions were excellent, with an almost straight HLDT caliper measurement averaging about 12.2 in. Comparison of logs from successive passes shows good repeatability of the data. The two passes of the FMS calipers also showed that the hole was nearly cylindrical, consistent with the HLDT log caliper recorded on the triple combo runs.

The absolute depths, relative to seafloor, for all of the CWL logs were fixed by identifying the gamma ray signal associated with the seafloor and depth shifting the logging data appropriately. The gamma ray pick for the seafloor in Hole 1250F was 807 mbrf for all of the CWL runs.

Interpretation of Logging-While-Drilling and Wireline Logs

The well log data plots for Holes 1250A, 1250B, and 1250F in Figures **F35, F36, F38,** and **F39** show excellent quality LWD and CWL logs. Lower pump rates through the shallow subsurface section of Holes 1250A and 1250B greatly reduced the effect of borehole washout on the LWD logs in the near-surface unconsolidated sediments. The downhole LWD and CWL logs dramatically highlight gas hydrate–bearing sediments with high resistivities, high acoustic velocities, and RAB image anomalies. Resistivity, acoustic, and density log variations below the zone of predicted gas hydrate stability (~111 mbsf) may indicate lithologic changes and the presence of free gas. Unlike many other sites on Hydrate Ridge, no borehole breakouts were observed in the RAB images from Hole 1250B.

Logging While Drilling and Wireline Log Comparison

Figure **F37** shows a comparison of downhole LWD and CWL data from Holes 1250B and 1250F, using the gamma ray, neutron porosity, density, photoelectric cross section, and deep resistivity logs. The highly variable CWL logging data within the upper 63 mbsf of Hole 1250F was obtained through the drill pipe. A comparison of similar logging signatures in Figure **F37** reveals that the LWD logging data from

F35. CWL logging data, p. 68.

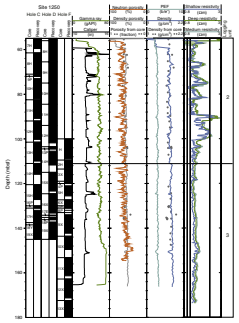

F36. CWL gamma ray logging data, p. 69.

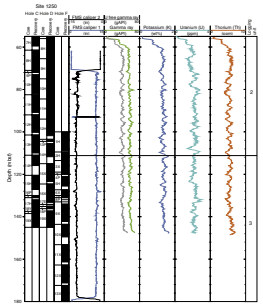

F37. LWD and CWL downhole logging data, p. 70.

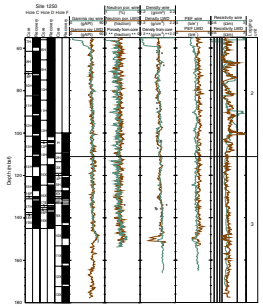

F38. CWL acoustic logging data, p. 71.

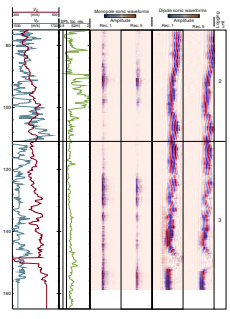

Hole 1250B are ~3 m deeper than the CWL data from Hole 1250F. This depth difference is best shown with the deep resistivity and density logs from the two holes. At a depth of ~89 mbsf in Hole 1250F the CWL density and resistivity logs show a distinct increase in value; however, this same log response is at a depth of ~92 mbsf on the LWD data from Hole 1250B. The offset could possibly be explained by local variability in the geology of this site; however, Hole 1250F was located only 15 m west of Hole 1250B. This apparent depth discrepancy will be further examined after the cruise. After taking into account the apparent depth difference between Holes 1250B and 1250F, it can be seen that the LWD and CWL data from each hole match relatively well, exhibiting similar curve shapes and absolute log values. The CWL- (Hole 1250F) and LWD-recorded (Hole 1250B) resistivity logs, however, exhibit differences in measured values with depth and a difference in the apparent vertical resolution of each device, with the LWD RAB tool yielding a log with a higher vertical resolution.

Logging Units

The logged section in Holes 1250A, 1250B, and 1250F has been divided into three "logging units" on the basis of obvious changes in the LWD gamma ray, density, electrical resistivity (Fig. **F39**), and acoustic transit-time measurements (Fig. **F38**).

Logging Unit 1 (0–29 mbsf) is characterized by a 10-m-thick high-resistivity zone (2–12 mbsf), with a measured RAB peak value exceeding 2.5 Ωm. Logging Unit 1 is also characterized by increasing densities with depth as measured by the LWD tools. However, this trend in the downhole recorded density data is probably due, in part, to degraded log measurements within the enlarged portion of the near surface of both boreholes as shown in Figure **F34.** Logging Unit 1 is located entirely within lithostratigraphic Units I and II (0–45 mbsf), which is composed of finely interbedded diatom-rich clay and silty clay sediments. In Hole 1250B, the transition from logging Unit 1 to 2 is defined by an increase in the measured resistivities (from ~0.8 to ~1.1 Ωm) and a subtle increase in LWD-derived density (from ~1.58 to ~1.68 g/cm³).

Logging Unit 2 (29–111 mbsf) is characterized by zones of distinct high resistivities and high acoustic velocities, with the resistivity in one relatively thin zone >3.0 Ωm (at a depth of ~100 mbsf) and V_P recorded at >1.63 km/s. The gamma ray log in logging Unit 2 shows a characteristic cyclicity that may reflect the interbedded nature of the sand, silt, and clay turbidite sequences described by the shipboard sedimentologists for Lithostratigraphic Unit III (45–100 mbsf) (see **"Lithostratigraphic Unit III,"** p. 5, in "Lithostratigraphic Units" in "Lithostratigraphy"). The downhole log-measured densities generally increase with depth in logging Unit 2 (1.65 g/cm³ at the top to near 1.8 g/cm³ at the bottom). In Hole 1250F (Fig. **F38**), the V_P log has been used to precisely select the depth of the boundary between logging Units 2 and 3, which is considered to be the base of the deepest gas hydrate presence as inferred form the available LWD and CWL data. The boundary between logging Units 2 and 3 is marked by a subtle drop in resistivity (to ~0.5 Ωm) and V_P (to ~1.45 km/s). The boundary between logging Units 2 and 3 corresponds, roughly, to the depth of the BSR at this site.

Logging Unit 3 (111–210 mbsf, TD of Hole 1250A) coincides with lithostratigraphic Unit II (45–148 mbsf), which is again described as an interbedded sand, silt, and clay turbidite sequence (see **"Lithostrati-**

F39. LWD logging data, p. 72.

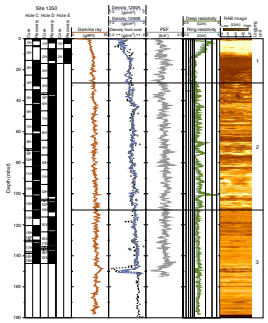

graphic Unit II," p. 5, in "Lithostratigraphic Unit" in "Lithostratigraphy"). In Hole 1250B, logging Unit 3 is generally characterized by more uniform resistivities compared to Unit 2. A 2-m-thick anomalous interval, characterized by variable V_P (ranging from ~1.50 to ~1.55 km/s), variable resistivities (ranging from ~1.1 to ~1.7 Ωm), and low densities (>1.5 g/cm^3) occurs in logging Unit 3 within the depth interval from 146 to 151 mbsf, which suggests the presence of a free gas–saturated sand. This apparent free gas–bearing interval corresponds to the seismic Horizon A (see "Introduction," p. 1).

Resistivity-at-the-Bit and Formation MicroScanner Images

Both the RAB and FMS tools produce high-resolution images of the electrical resistivity characteristics of the borehole wall that can be used for detailed sedimentological and structural interpretations. The RAB and the FMS tools can also be used to make high-resolution electrical images of gas hydrates in the borehole, thus yielding information about the nature and texture of gas hydrate occurrences. The resolution of the RAB images is considerably lower than the resolution of the FMS images. The RAB images have about a 5- to 10-cm vertical resolution, whereas the FMS tool can resolve features such as microfractures with widths <1 cm. However, the RAB tool provides 360° coverage of the borehole, whereas FMS images cover only ~30% of the hole.

In Figure F40, we have cross correlated a RAB image (Hole 1250B) and an FMS image (Hole 1250F) from the stratigraphic interval that contains Horizon A, which has been identified as a prominent regional seismic reflector (see "Introduction," p. 1). In this figure, Horizon A appears as a complex interbedded zone of high and low resistivities. More detailed examination of the FMS image shows distinct lateral variability within this interval and apparent fine-scale sedimentologic structures.

F40. RAB and FMS images showing Horizon A, p. 73.

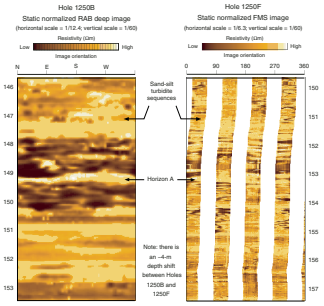

Logging Porosities

Sediment porosities can be determined from analyses of recovered cores and from numerous borehole measurements (see "Physical Properties," p. 22, and "Downhole Logging," p. 43, both in the "Explanatory Notes" chapter). Data from the LWD density, neutron, and NRM-MRP logs have been used to calculate sediment porosities for Holes 1250A and 1250B. Core-derived physical property data, including porosities (see "Physical Properties," p. 16), were used to both calibrate and evaluate the log-derived sediment porosities.

The VND LWD log-derived measurements of density in Holes 1250A and 1250B (Fig. F39) increase with depth and are relatively consistent within both holes, with values ranging from ~1.6 near the top of each hole to >1.85 g/cm^3 near the BOHs. The density log measurements are slightly degraded in the very top of each hole. The LWD log-derived density measurements from Holes 1250A and 1250B were used to calculate sediment porosities (ϕ) using the standard density-porosity relation,

$$\phi = (\rho_m - \rho_b)/(\rho_m - \rho_w).$$

Water density (ρ_w) was assumed to be constant and equal to 1.05 g/cm^3; however, variable core-derived grain/matrix densities (ρ_m) were as-

sumed for each log density porosity calculation. The core-derived grain densities (ρ_m) in Hole 1250A ranged from an average value at the seafloor of 2.73 to ~2.68 g/cm³ at the BOH, whereas the core-derived grain densities (ρ_m) in Hole 1250B ranged from an average value of 2.71 g/cm³ at the top of the hole to about 2.68 g/cm³ at TD (see "Physical Properties," p. 16). The density log-derived porosities in Holes 1250A and 1250B were similar and ranged from ~50% to 75% (Figs. F41).

The LWD neutron porosity logs from Holes 1250A and 1250B (Fig. F41) yielded sediment porosities ranging from an average value at the top of the logged section of ~60% to ~50% at the BOH. The "total" sediment porosities derived by the NMR-MRP tool in Holes 1250A and 1250B (Fig. F41) ranged from about 70% near the seafloor to about 40% near the BOH. The NMR-MRP porosity logs from Holes 1250A and 1250B exhibit several relatively thin (2–3 m thick) intervals of significantly low porosities (at depths of about 60, 66, 80, and 82 mbsf). These apparent decreases in NMR-MRP porosities can be attributed to the presence of gas hydrate. Porosity logs in gas hydrate–bearing reservoirs are subject to error because most downhole porosity devices are calibrated to the physical properties of water-bearing sediments (as reviewed by Collett and Ladd, 2000). Therefore, downhole log-derived porosities need to be corrected for the presence of gas hydrate. The required correction for density and neutron-derived porosities is relatively small. But NMR-MRP porosities are more significantly affected by gas hydrate. The effect of gas hydrate on the downhole log-derived porosities from Site 1250 will be further examined after the cruise.

The comparison of core- and log-derived porosities in Figure F41 reveals that the neutron-, density-, and NMR-MRP–derived porosities are generally similar to the core porosities in logging Units 2–3 (29–210 mbsf). However, the density-derived porosities are slightly higher than the core-derived porosities in logging Unit 1.

F41. LWD log- and core-derived porosities, p. 74.

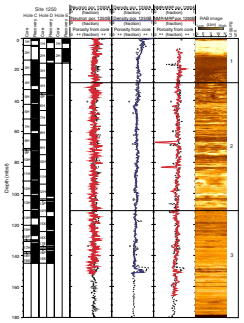

Gas Hydrate

The presence of gas hydrate at Site 1250 was documented by direct sampling, with numerous specimens of gas hydrate being recovered in Holes 1250C–1250E from near the seafloor to a depth of 86.35 mbsf. It was inferred, based on geochemical core analyses (see "Interstitial Water Geochemistry," p. 10), IR image analysis of cores (see "Physical Properties," p. 16), and downhole logging data that disseminated gas hydrate is present in logging Units 1 and 2. As previously discussed (see "Downhole Logging," p. 43, in the "Explanatory Notes" chapter), the presence of gas hydrate is generally characterized by increases in log-measured electrical resistivities and acoustic velocities. Logging Unit 2 at Site 1250 contains distinct zones that exhibit stepwise increases in both electrical resistivities and V_P. As discussed above, a portion of logging Unit 1 is also characterized by high resistivity measurements. Because the drill pipe was set at a depth of 73 mbsf for CWL logging, no acoustic logging data were collected from logging Unit 1.

Resistivity log data from Hole 1250B have been used to quantify the amount of gas hydrate at Site 1250. For the purpose of discussion, it is assumed that the high resistivities measured in logging Units 1 and 2 are due to the presence of gas hydrate. Archie's Relation,

$$S_w = (aR_w/\phi^m R_t)^{1/n}$$

(see "Downhole Logging," p. 43, in the "Explanatory Notes" chapter), was used with resistivity data (R_t) from the LWD RAB tool and porosity data (ϕ) from the LWD density tool to calculate water saturations in Hole 1250B. It should be noted that gas hydrate saturation (S_h) is the measurement of the percentage of pore space occupied by gas hydrate, which is the mathematical complement of Archie-derived S_w, with

$$S_h = 1 - S_w.$$

For Archie's Relation, the formation water resistivity (R_w) was calculated from recovered core water samples, and the Archie a and m variables were calculated using a crossplot technique, which compares the downhole log-derived resistivities and density porosities. See Collett and Ladd (2000) for the details on how to calculate the required formation water resistivities and Archie variables. The values used for Site 1250 were a = 1, m = 2.8, and n = 1.9386.

Archie's Relation yielded water saturations (Fig. F42) ranging from a minimum value of only ~50% in logging Unit 1 and near the bottom of logging Unit 2, to a maximum of 100% in portions of logging Units 1 and 2 (0–111 mbsf), which implies the gas hydrate saturation in Hole 1250A ranges from 0% to 50%. The low water saturations shown in logging Unit 3 (Fig. F42) below the GHSZ probably indicate the presence of free gas–bearing sediments (as discussed previously in this chapter).

F42. Log-derived gas hydrate saturations, p. 75.

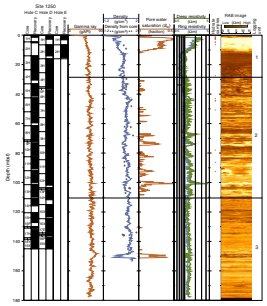

Temperature Data

The TAP tool was deployed on the triple combo tool string in Hole 1250F (Fig. F43). During the process of coring and drilling, cold seawater is circulated in the hole, cooling the formation surrounding the borehole. Once drilling ceases, the temperature of the fluids in the borehole gradually rebounds to the in situ equilibrium formation temperature. Thus, the temperature data from the TAP tool cannot be easily used to assess the nature of the in situ equilibrium temperatures. However, the plot of the first pass downgoing temperature profile in Figure F43 reveals several gradient changes, which were caused by borehole temperature anomalies. The temperature anomaly at ~73 mbsf is the base of the drill pipe during the initial descent of the triple combo tool string. The break in the slope of the first pass downgoing temperature log at a depth ~130 mbsf is ~20 m below the depth of the BSR (111 mbsf) at this site.

F43. TAP tool temperatures, p. 76.

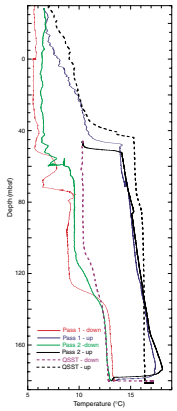

REFERENCES

Boetius, A., Ravenschlag, K., Schubert, C.J., Rickert, D., Widdel, F., Gieseke, A., Amann, R., Jørgensen, B.B., Witte, U., and Pfannkuche, O., 2000. Microscopic identification of a microbial consortium apparently mediating anaerobic methane oxidation above marine gas hydrate. *Nature,* 407:623–626.

Bohrmann, G., Suess, E., Greinert, J., Teichert, B., and Naehr, T., 2002. Gas hydrate carbonates from Hydrate Ridge, Cascadia convergent margin: indicators of near-seafloor clathrate deposits. *Fourth Int. Conf. Gas Hydrates:* Yokohama, Japan, 19023:102–107.

Chan, L.-H., and Kastner, M., 2000. Lithium isotopic compositions of pore fluids and sediments in the Costa Rica subduction zone: implications for fluid processes and sediment contribution to the arc volcanoes. *Earth Planet. Sci. Lett.,* 183:275–290.

Clague, D., Maher, N., and Paull, C.K., 2001. High-resolution multibeam survey of Hydrate Ridge, offshore Oregon. *In* Paull, C.K., and Dillon, W.P. (Eds), *Natural Gas Hydrates: Occurrence, Distribution, and Detection.* Am. Geophys. Union, Geophys. Monogr. Ser., 124:297–306.

Collett, T.S., and Ladd, J., 2000. Detection of gas hydrate with downhole logs and assessment of gas hydrate concentrations (saturations) and gas volumes on the Blake Ridge with electrical resistivity log data. *In* Paull, C.K., Matsumoto, R., Wallace, P.J., and Dillon, W.P. (Eds.), *Proc. ODP, Sci. Results,* 164: College Station, TX (Ocean Drilling Program), 179–191.

Duan, Z., Møller, N., Greenberg, J., and Weare, J.H., 1992. The prediction of methane solubility in natural waters to high ionic strengths from 0° to 250°C and from 0 to 1600 bar. *Geochim. Cosmochim. Acta,* 56:1451–1460.

Edmond, J.M., Measures, C., McDuff, R.E., Chan, L.H., Collier, R., and Grant, B., 1979. Ridge crest hydrothermal activity and the balances of the major and minor elements in the ocean: the Galapagos data. *Earth Planet. Sci. Lett.,* 46:1–18.

Handa, Y.P., 1990. Effect of hydrostatic pressure and salinity on the stability of gas hydrates. *J. Phys. Chem.,* 94:2652–2657.

Johnson, J.E., Goldfinger, C., and Suess, E., in press. Geophysical constraints on the surface distribution of authigenic carbonates across the Hydrate Ridge region, Cascadia margin. *Mar. Geo.*

Kastner, M., Sample, J.C., Whiticar, M.J., Hovland, M., Cragg, B.A., and Parkes, J.R., 1995. Geochemical evidence for fluid flow and diagenesis at the Cascadia convergent margin. *In* Carson, B., Westbrook, G.K., Musgrave, R.J., and Suess, E. (Eds.), *Proc. ODP, Sci. Results,* 146 (Pt 1): College Station, TX (Ocean Drilling Program), 375–384.

Reeburgh, W.S., 1976. Methane consumption in Cariaco Trench waters and sediments. *Earth Planet. Sci. Lett.,* 28:337–344.

Seyfried, W.E., Jr., Janecky, D.R., and Mottl, M.J., 1984. Alteration of the oceanic crust: implications for geochemical cycles of lithium and boron. *Geochim. Cosmochim. Acta,* 48:557–569.

Teichert, B.M.A., Eisenhauer, A., Bohrmann, G., Haase-Schramm, A., Bock, B., and Linke, P., in press. U/Th systematics and ages of authigenic carbonates from Hydrate Ridge, Cascadia margin: recorders of fluid flow variations. *Geochim. Cosmochim. Acta.*

Torres, M.E., Bohrmann, G., and Suess, E., 1996. Authigenic barites and fluxes of barium associated with fluid seeps in the Peru subduction zones. *Earth Planet. Sci. Lett.,* 170:1–15.

Torres, M.E., McManus, J., Hammond, D.E., de Angelis, M.A., Heeschen, K.U., Colbert, S.L., Tryon, M.D., Brown, K.M., and Suess, E., 2002. Fluid and chemical fluxes in and out of sediments hosting methane hydrate deposits on Hydrate Ridge. *Earth Planet. Sci. Lett.,* 201:525–540.

Figure F1. Bathymetric map showing locations of holes drilled at Site 1244. Bathymetry from EM300 data acquired by Monterey Bay Aquarium Research Institute (MBARI) (Clague et al., 2001).

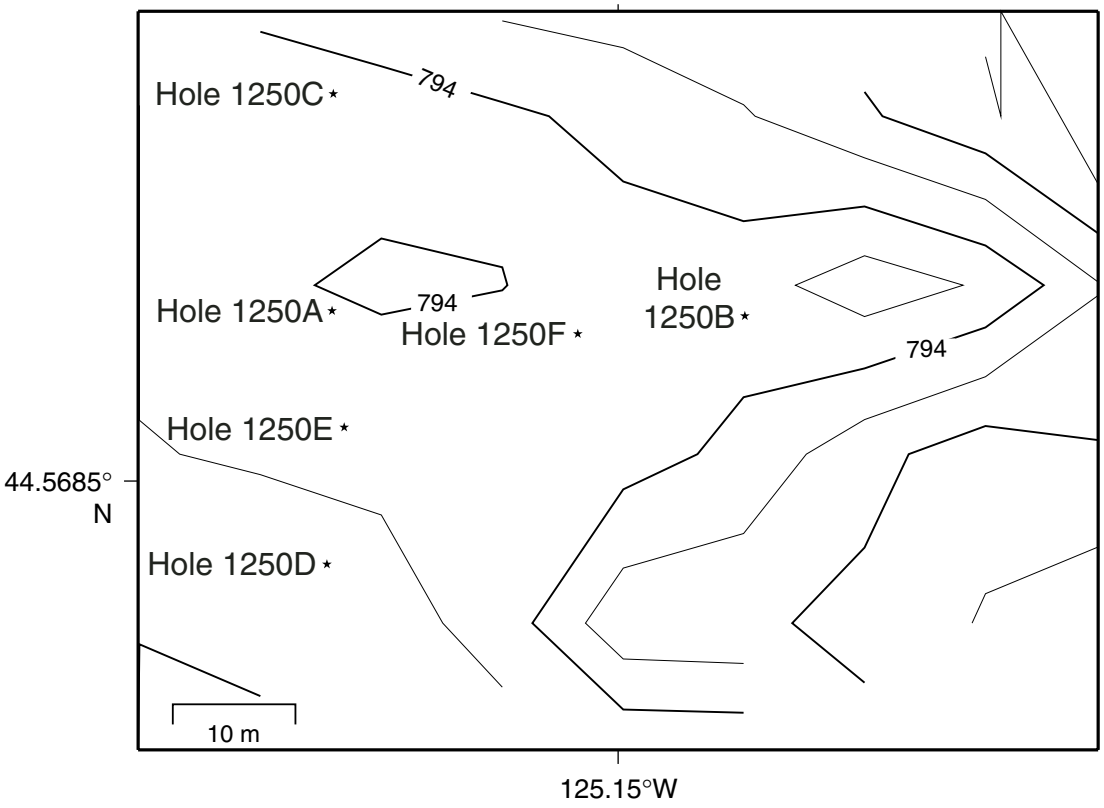

Figure F2. Lithostratigraphic summary for Hole 1250D.

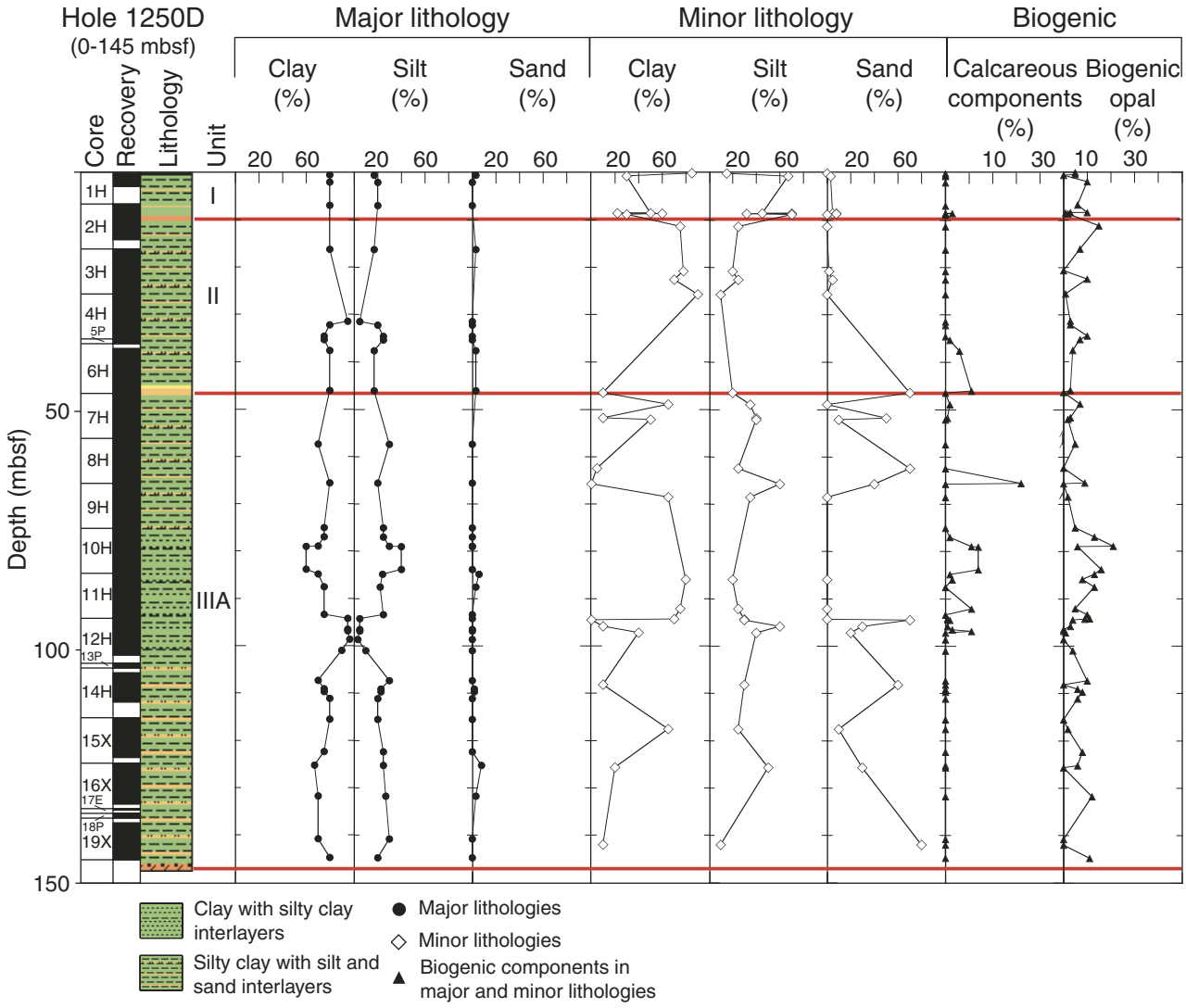

Figure F3. Lithostratigraphic summary for Hole 1250F.

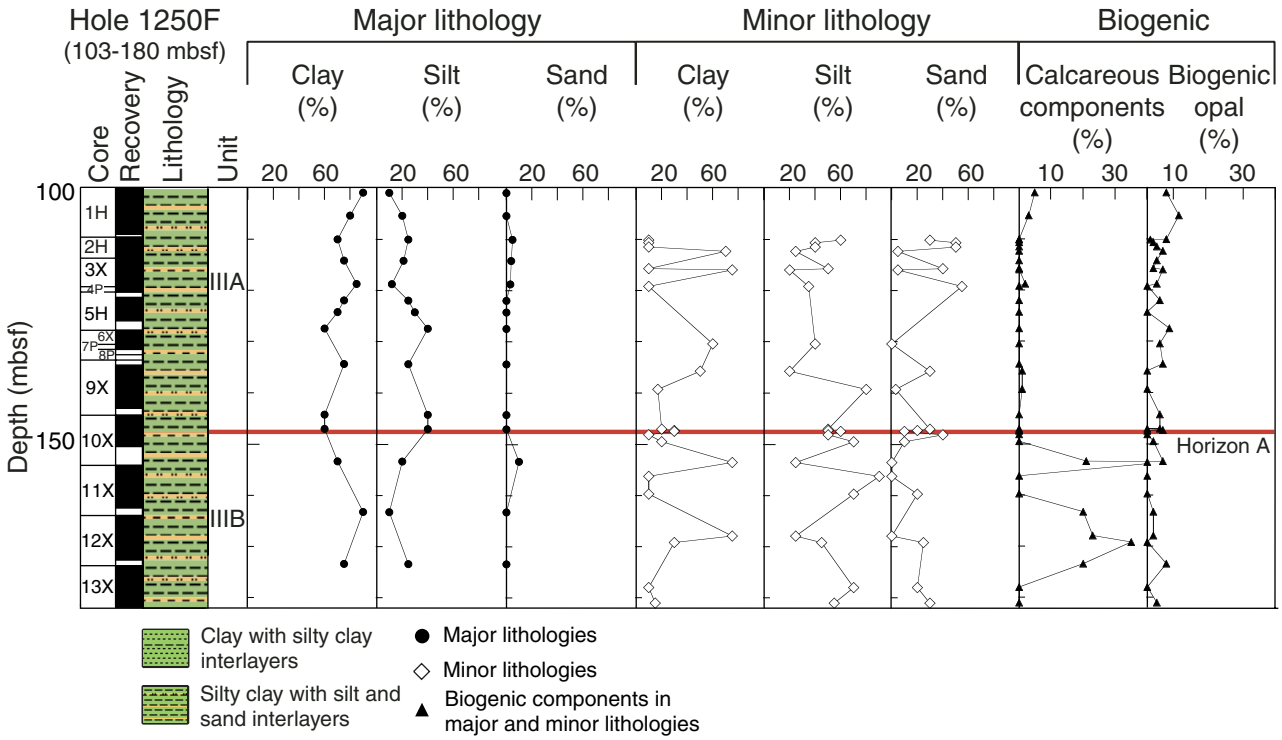

Figure F4. Seismic reflection profile from west (left) to east (right) and LWD data (electrical resistivity, left, and density, right) across Site 1250. Lithostratigraphic units and subunits distinguished at Site 1250 are shown. SF = seafloor, BSR = bottom-simulating reflector.

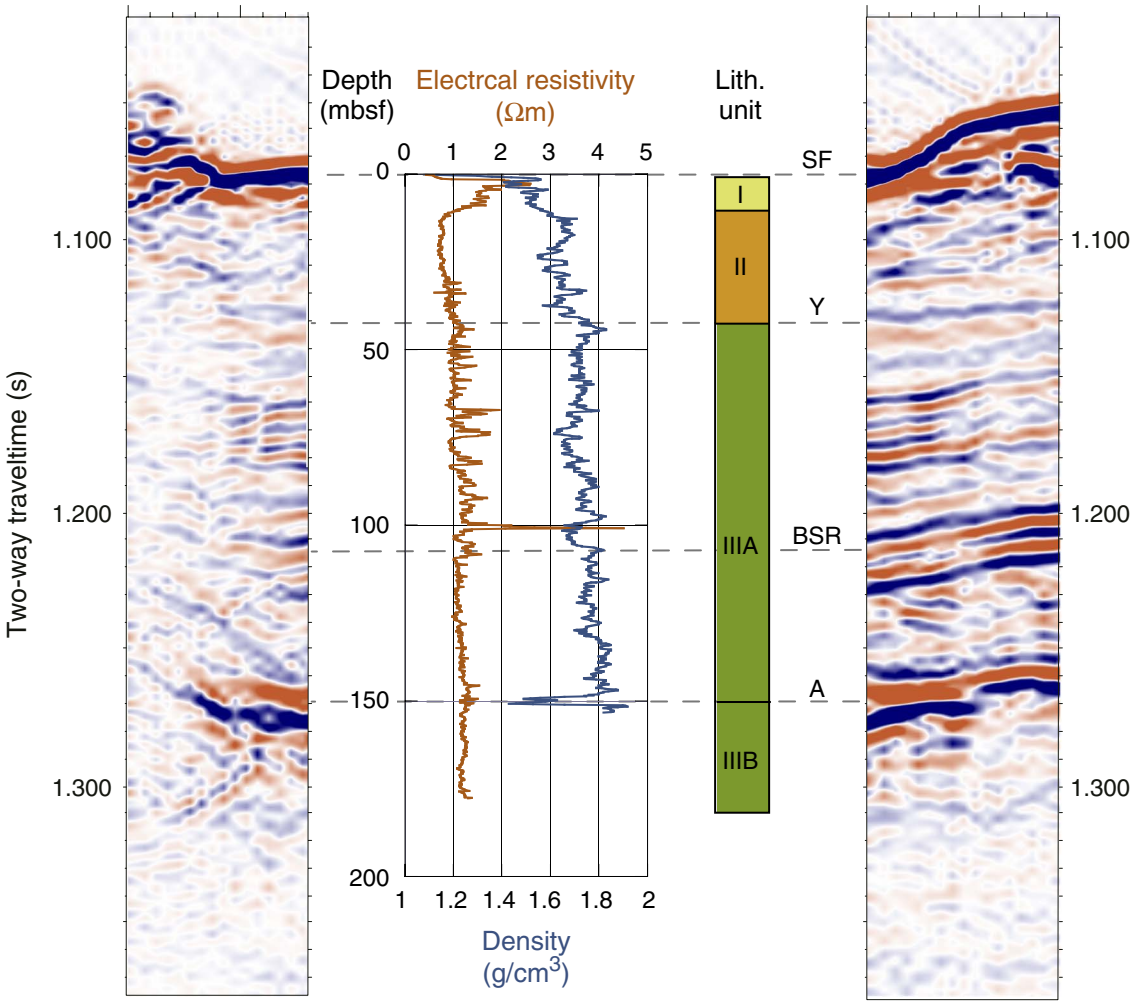

Figure F5. Distribution of grain-size classes (major and minor lithologies) vs. depth in Holes 1250C and 1250D based on smear slide descriptions. Main lithostratigraphic units and boundaries are depicted. Grey colored interval corresponds to the debris flow deposit located in lithostratigraphic Unit IIIA between 75 and 100 mbsf.

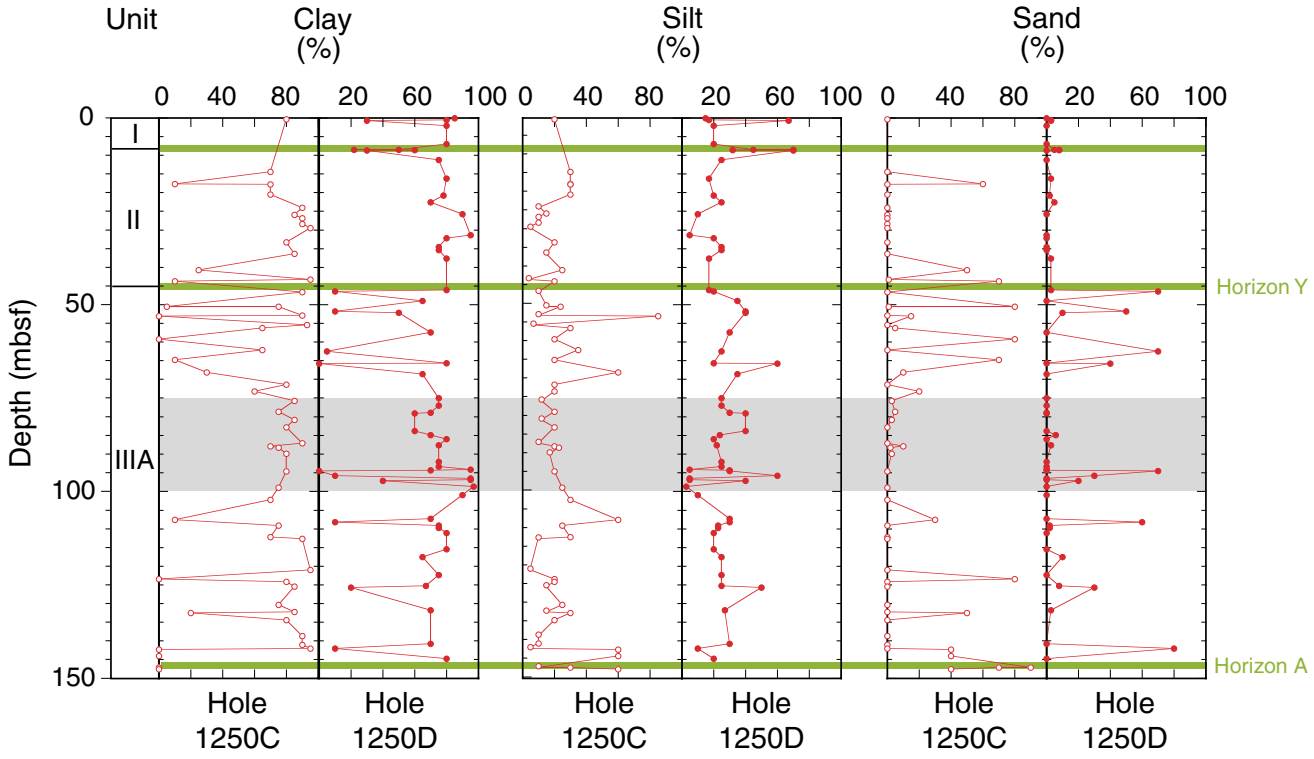

Figure F6. Close-up photograph of the base of lithostratigraphic Unit I showing the volcanic glass couplet observed at 9.5 mbsf. **A.** Interval 204-1250E-2H-2, 114–139 cm. **B.** Interval 204-1250D-2H-2, 98–111 cm. **C.** Interval 204-1250D-2H-3, 15–27 cm.

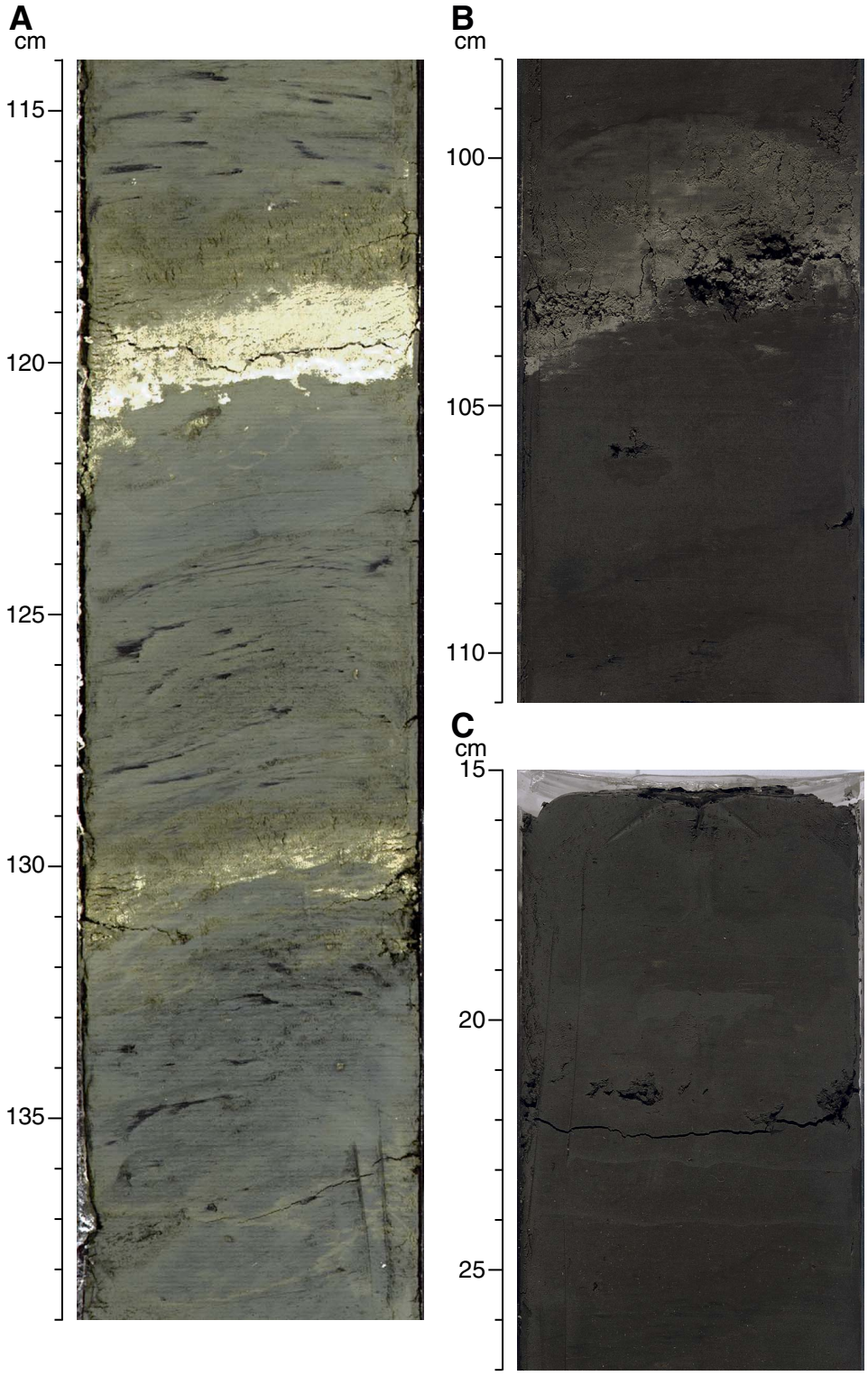

Figure F7. XRD record from a carbonate-rich interval in lithostratigraphic Unit I (Sample 204-1250D-1H-1, 72–76 cm).

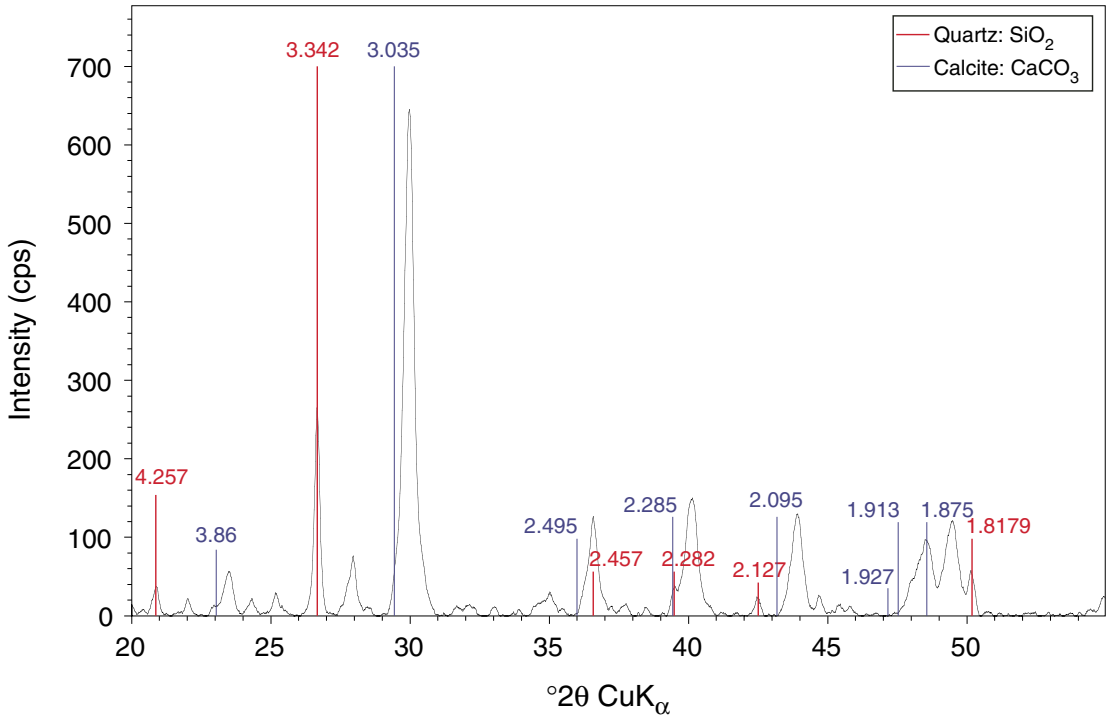

Figure F8. Distribution of biogenic components (calcareous and siliceous) vs. depth in Holes 1250C and 1250D based on smear slide descriptions. Main lithostratigraphic units and seismic horizons are depicted. A gray-colored interval corresponds to the debris flow deposit located between 75 and 100 mbsf.

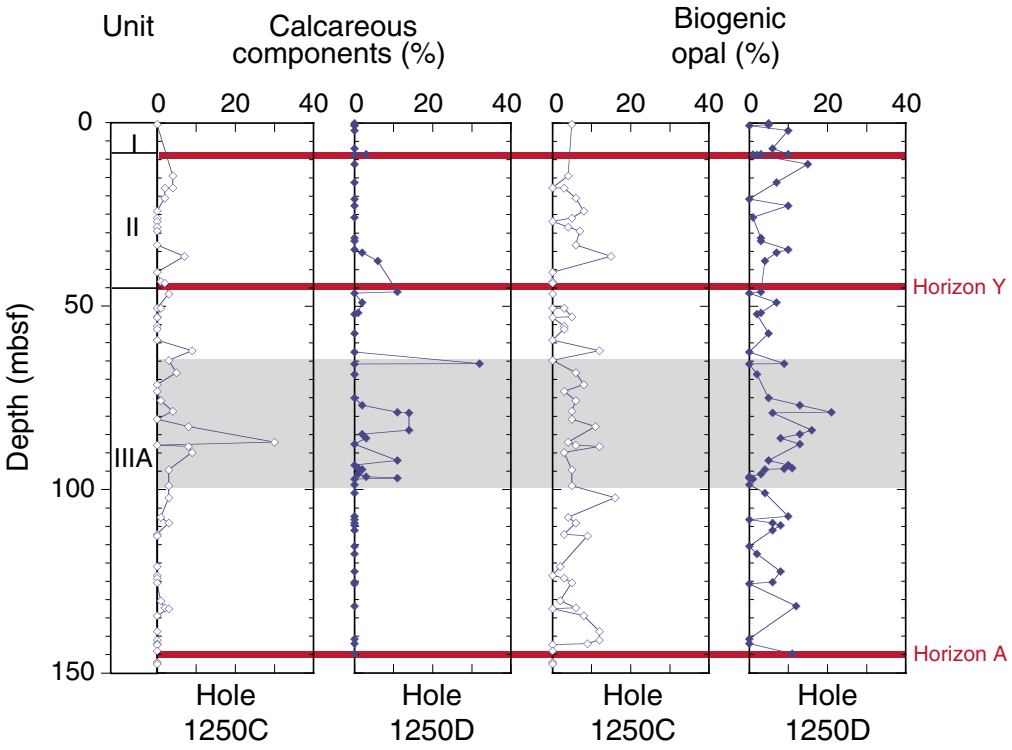

Figure F9. Close-up photographs of turbidite sequences located around Horizon Y at the boundary between lithostratigraphic Unit II and Subunit IIIA. **A.** Base of lithostratigraphic Unit II (interval 204-1250C-6H-1, 113–138 cm). **B.** Top of lithostratigraphic Subunit IIIA (interval 204-1250C-6H-3, 44–55 cm). **C.** Top of lithostratigraphic Subunit IIIA (interval 204-1250C-6H-7, 8–22 cm).

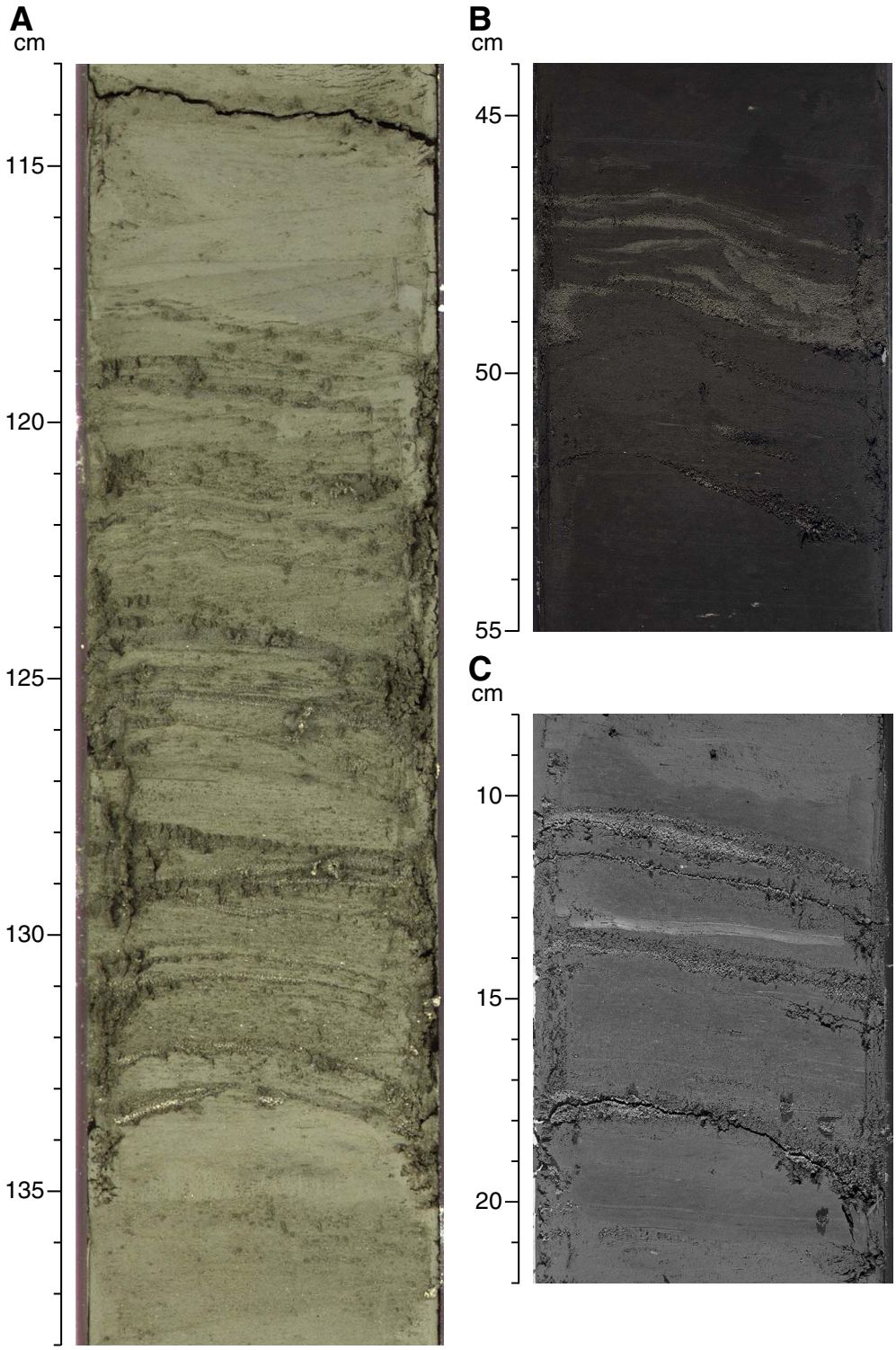

Figure F10. Close-up photograph of the debris flow deposit located in lithostratigraphic Unit IIIA (interval 204-1250C-10H-1, 81–107 cm).

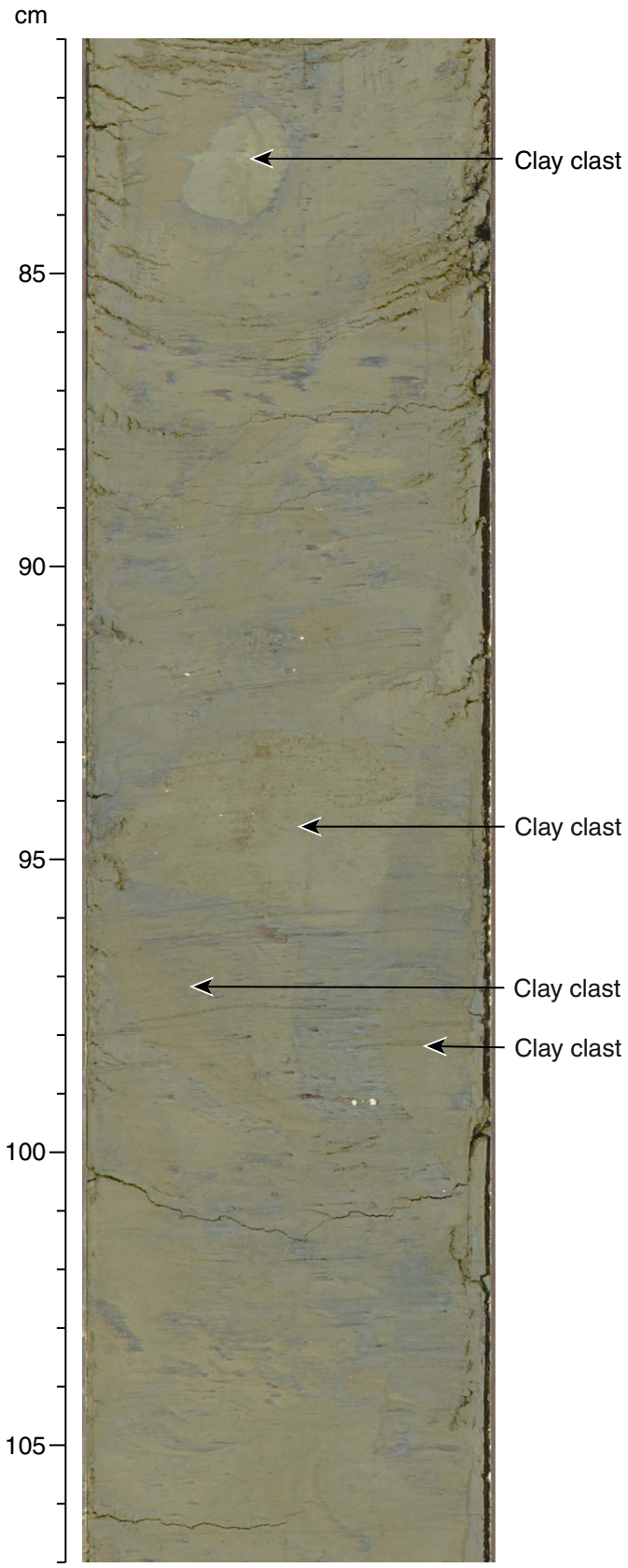

Figure F11. Close-up photograph of some of the volcanic glass–rich layers constituting Horizon A at the boundary between lithostratigraphic Subunits IIIA and IIIB. **A.** Last occurrence of volcanic glass (interval 204-1250C-19X-7, 5–23 cm). **B.** Thick volcanic glass–rich layer (interval 204-1250F-10X-4, 0–10 cm).

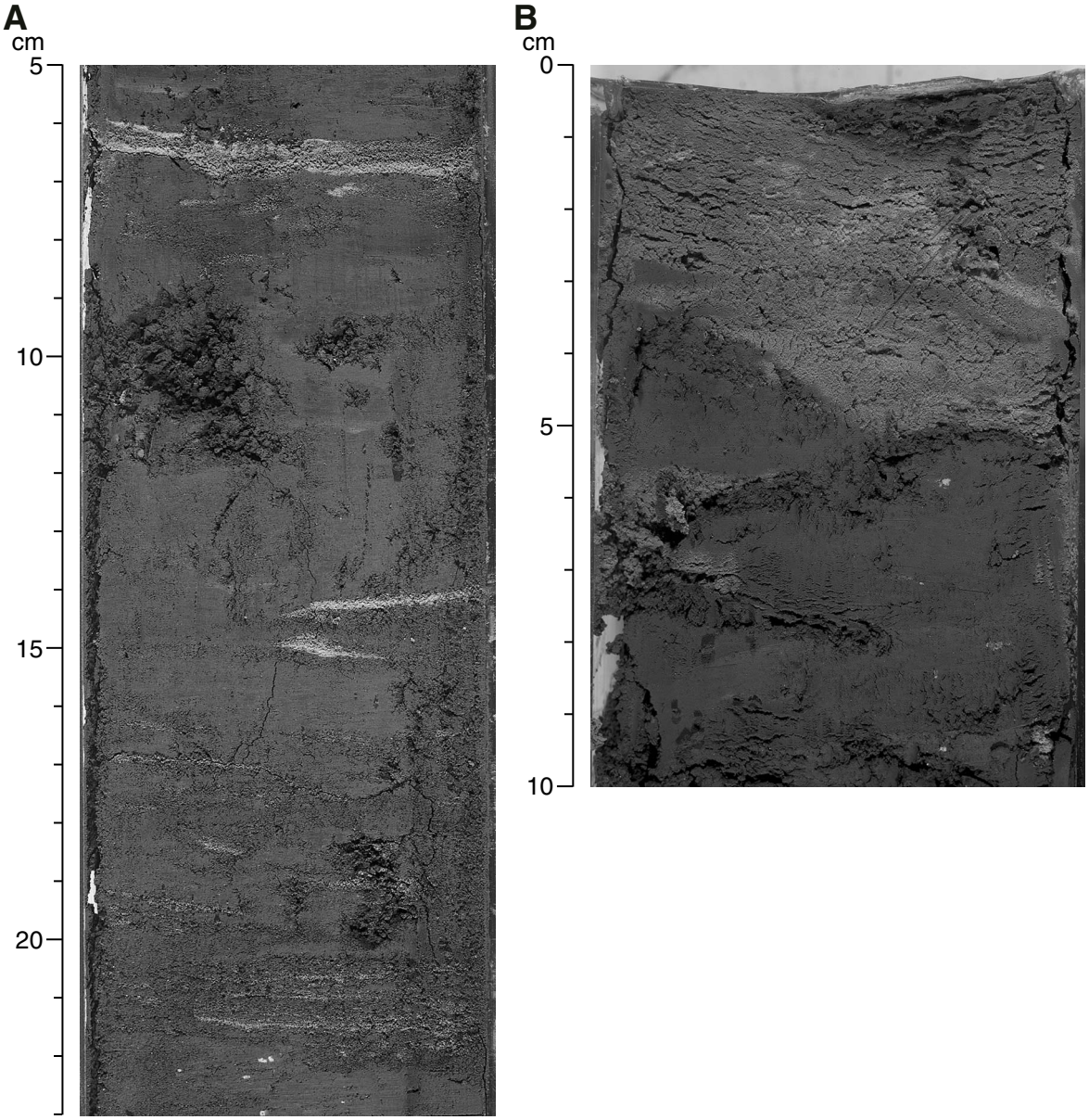

Figure F12. Distribution of the volcanic glass with depth in Holes 1250C, 1250D, 1250E, and 1250F determined from smear slides analysis. Glass layers identified at each of the sites are correlated by a thick blue line.

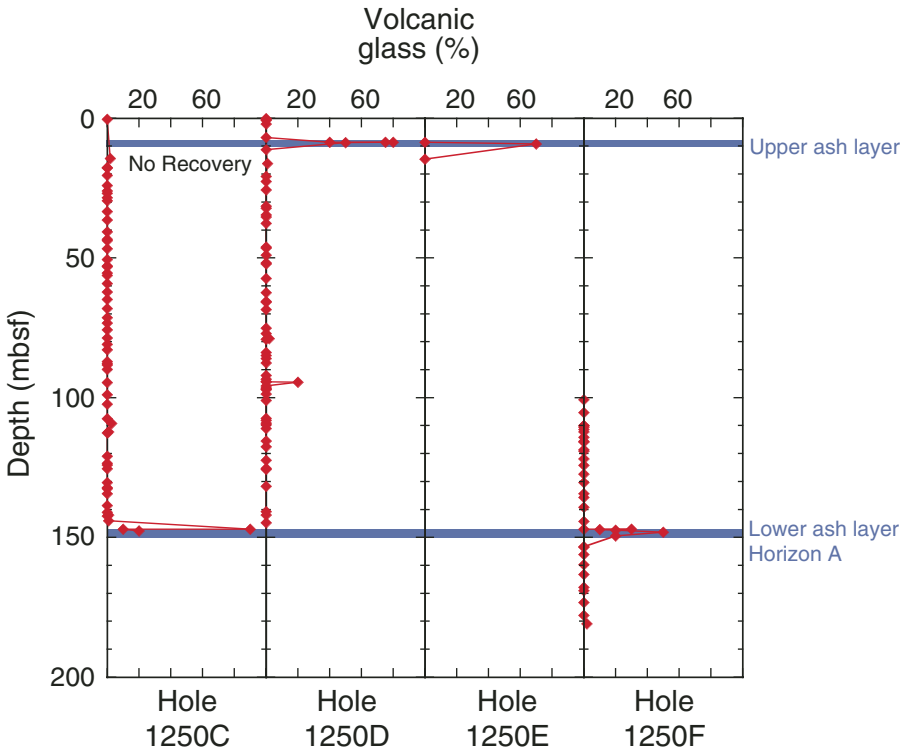

Figure F13. Color reflectance and high-resolution MS vs. depth across Horizon A in Hole 1250F. Gray lines = different glass layers identified (see **"Lithostratigraphic Unit III,"** p. 5, in "Lithostratigraphic Units" in "Lithostratigraphy.").

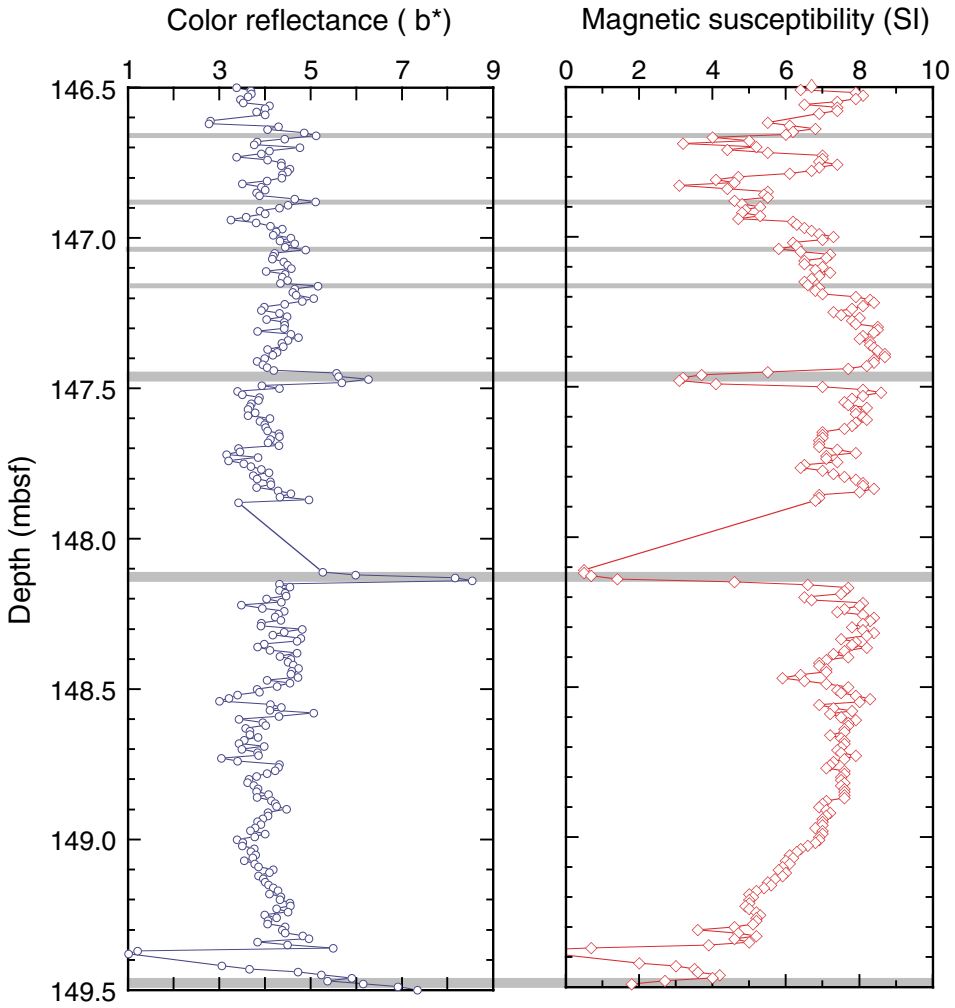

Figure F14. Close-up photograph of mousselike (middle and bottom) and soupy (top) textures found in interval 204-1250C-13H-4, 109–122 cm.

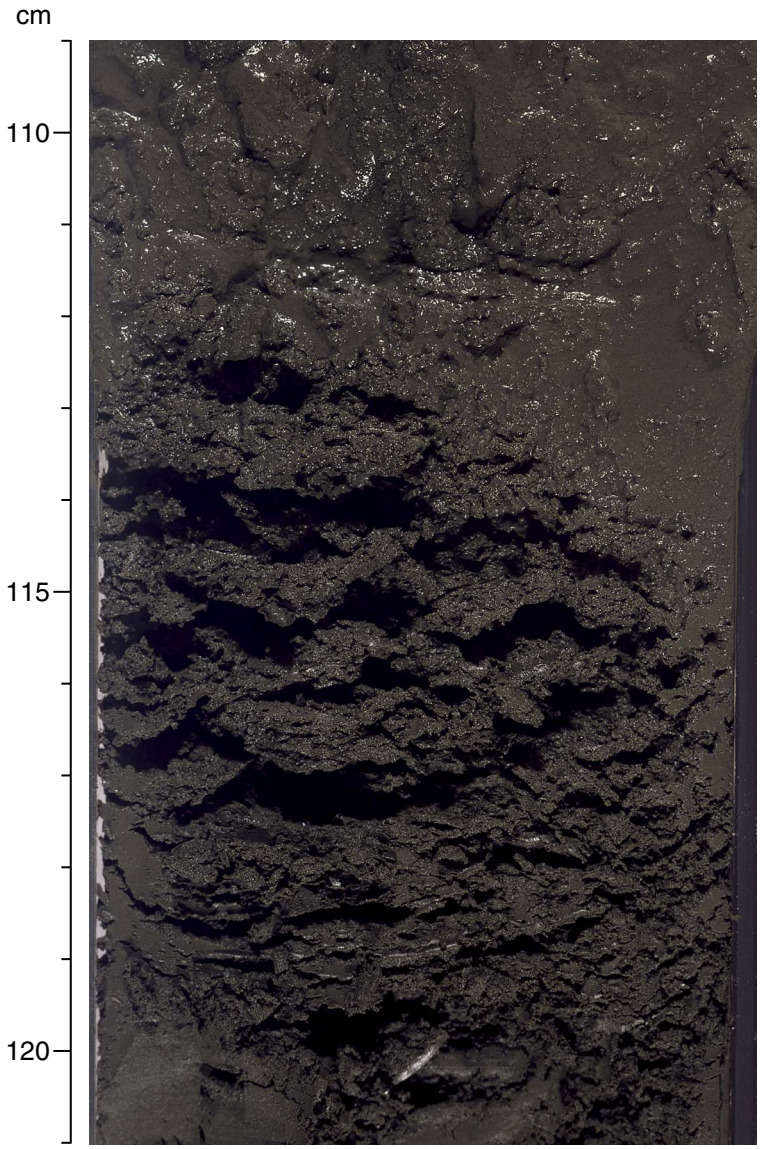

Figure F15. Age-depth plot for Hole 1250C based on diatom and calcareous nannofossil bioevents. The detailed age and depth of control points are shown in Table T2, p. 80. D = diatom event, N = nannofossil event.

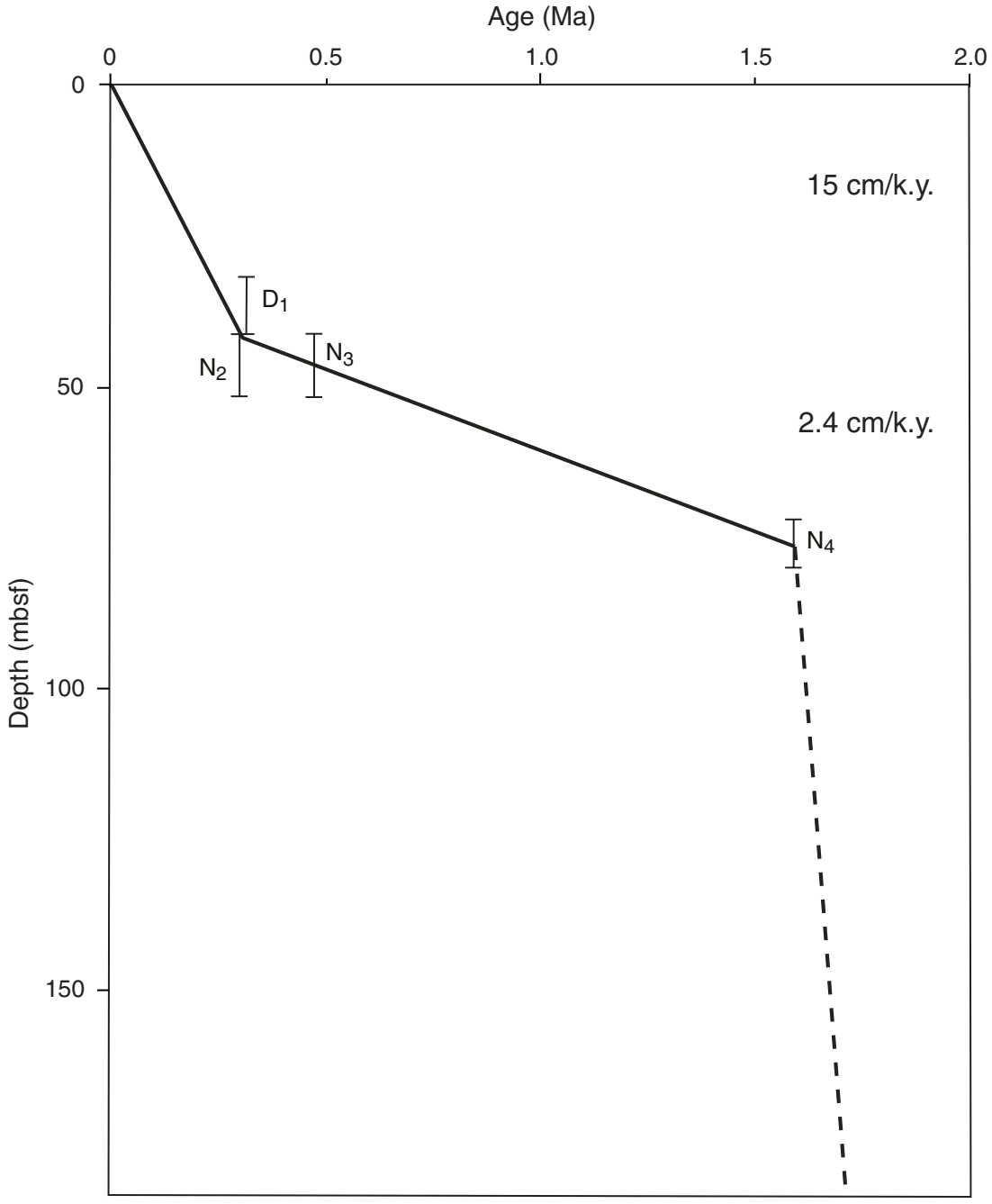

Figure F16. Concentration profiles of various dissolved species in pore waters from Holes 1250C (red circles), 1250D (blue squares), 1250E (green triangles), and 1250F (open triangles). DOC = dissolved organic carbon. (Continued on next page.)

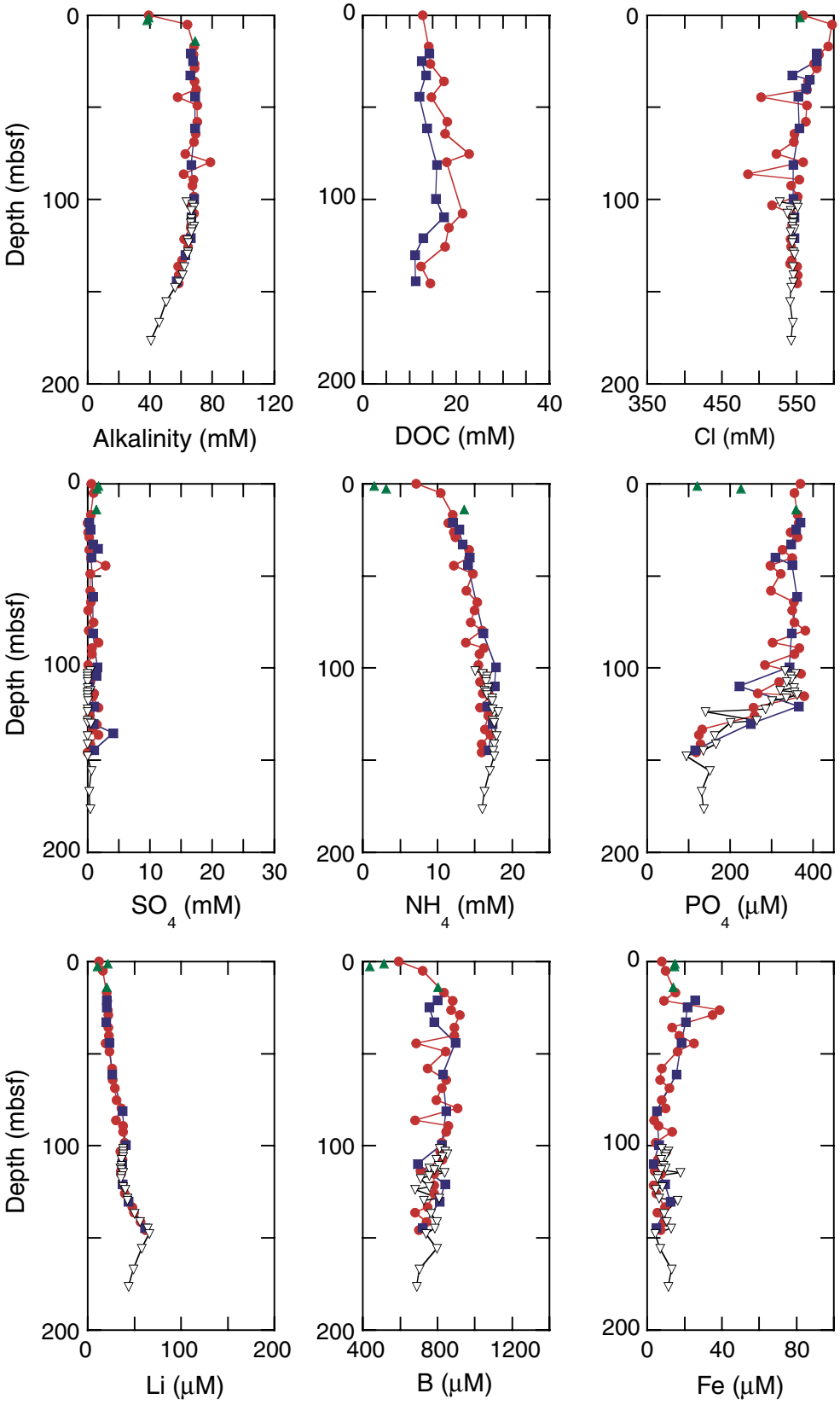

Figure F16 (continued).

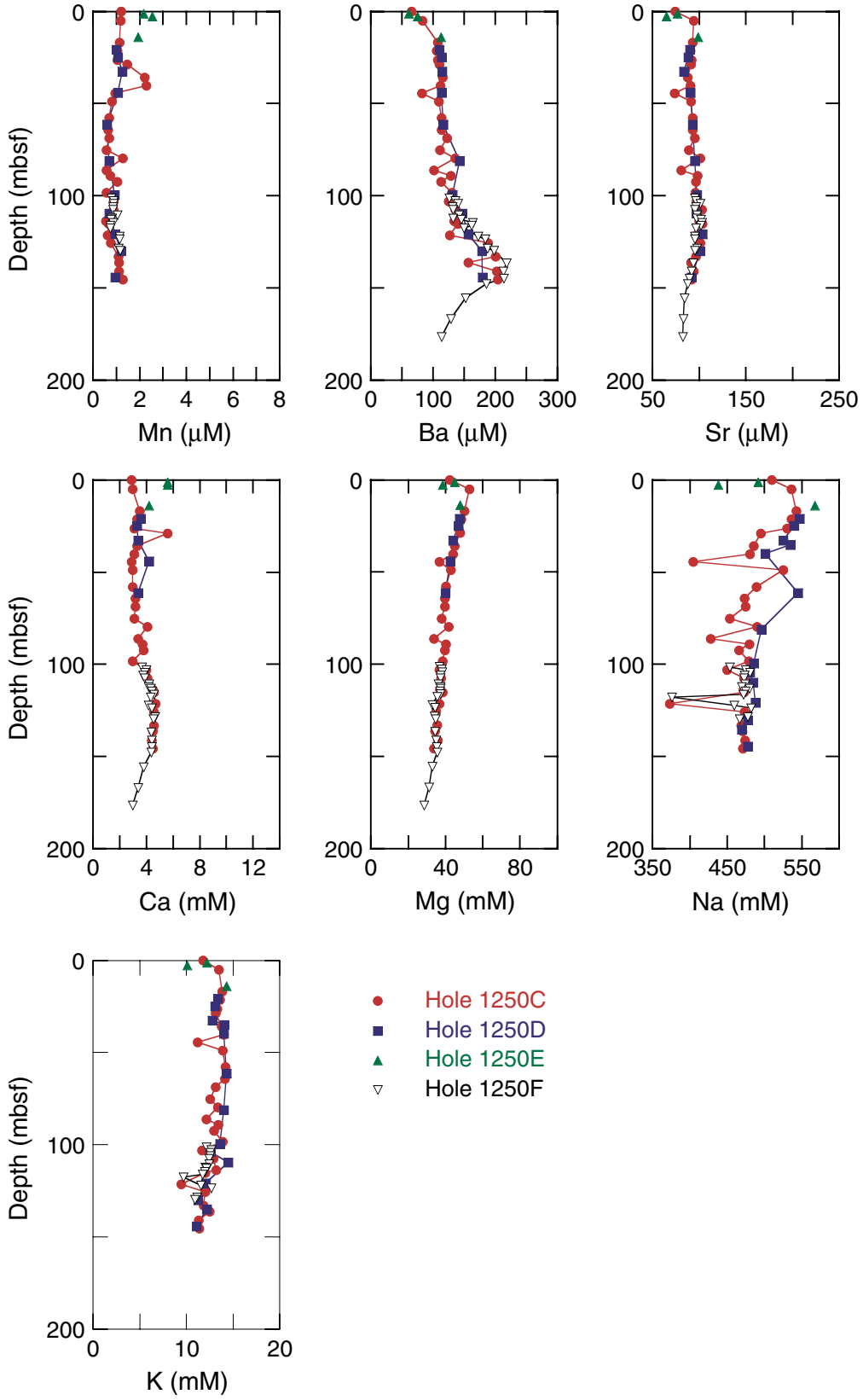

Figure F17. Chloride (Cl^-) concentration profiles and gas hydrate estimates based on these chloride data at Site 1250. **A.** Chloride data (red circles) are shown with data from Site 1245 (fine orange line) for comparison. Chloride concentration data from Holes 1250B (closed red circles), 1250C (closed blue squares), 1250E (semiopen black squares), and 1250F (open green circles). For comparison, the chloride profile from Site 1245 (fine, brown line) is also shown. Note that in the upper 40 mbsf, the chloride concentrations are commonly above seawater values (~560 mM). Below 50 mbsf, the chloride data form a sloping baseline toward slightly fresher values similar to that of Site 1245. There are no anomalies in the chloride concentration below 110 mbsf. **B.** Estimates of the amount of gas hydrate in the sediments of Site 1250. No gas hydrate estimates given above 50 mbsf because the chloride concentration of in situ pore water is unknown. Below 50 mbsf, the establishment of a firm chloride baseline allows a first-order estimate of gas hydrate amounts that peak at 15% of pore space but commonly range between 0% and 6%.

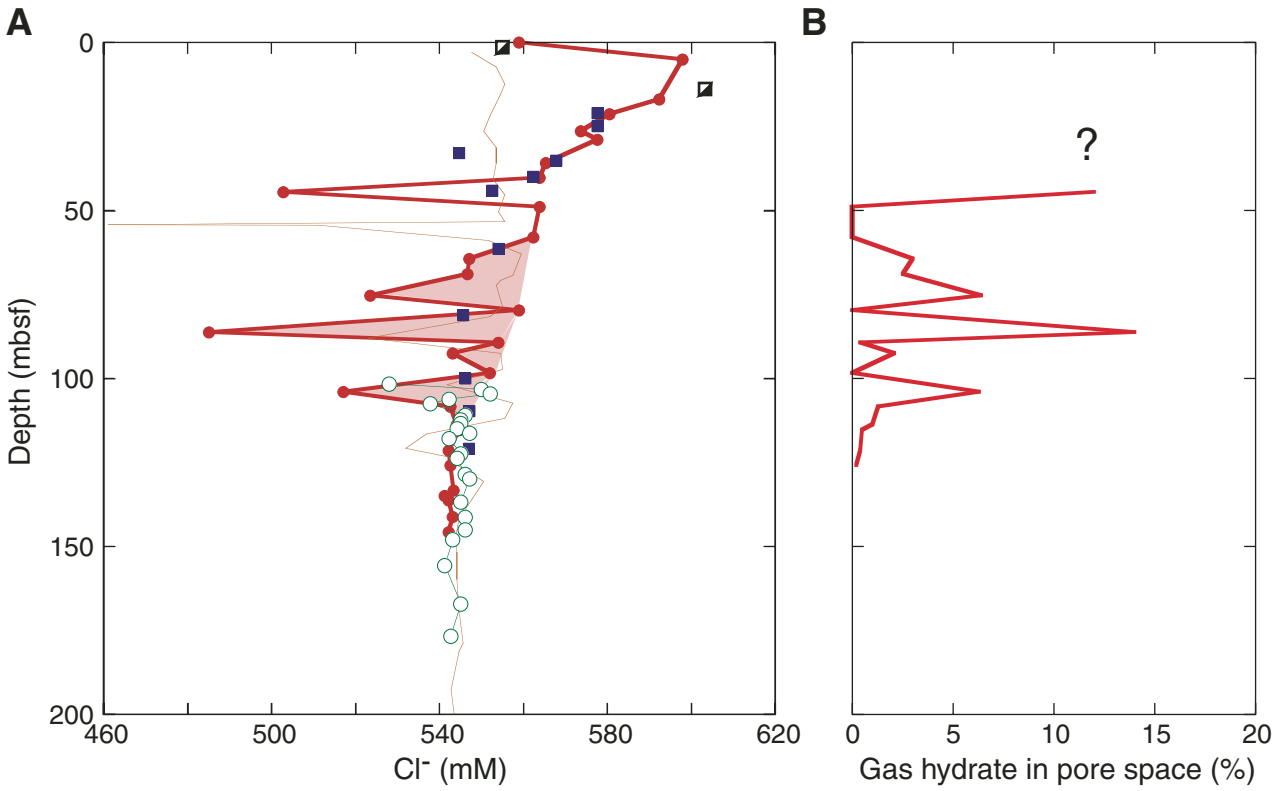

Figure F18. Dissolved lithium data from Site 1250 (red circles) shown with lithium concentration data from Site 1245 (dotted line) and their relationship to Horizon A at each site. Note that each site exhibits a sloping baseline showing increasing lithium concentration with depth. Both sites also show locally higher concentrations of dissolved lithium at Horizon A, with a similar magnitude of lithium enrichment.

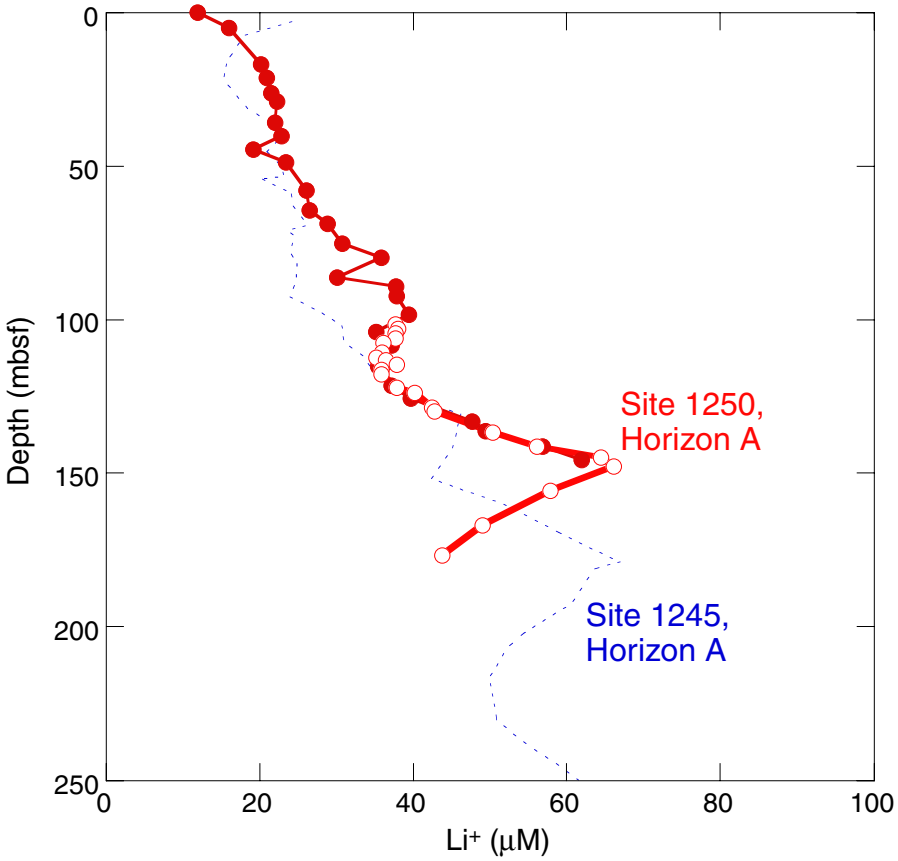

Figure F19. Headspace gas concentrations of C_1, C_2, $C_{2=}$, and C_3 vs. depth for Site 1250.

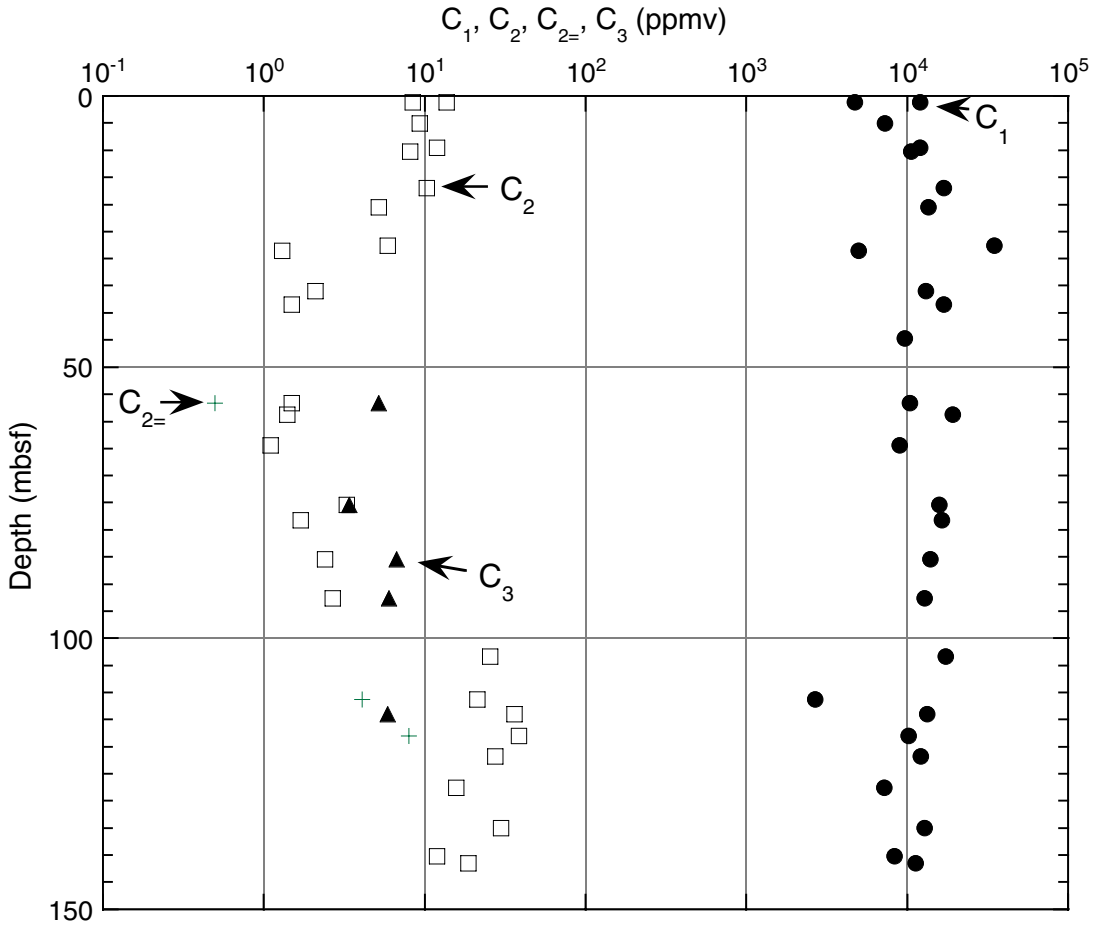

Figure F20. Concentrations of C_1, C_2, C_3, i-C_4, n-C_4, i-C_5, n-C_5, and C_6 in core void gas vs. depth for Site 1250.

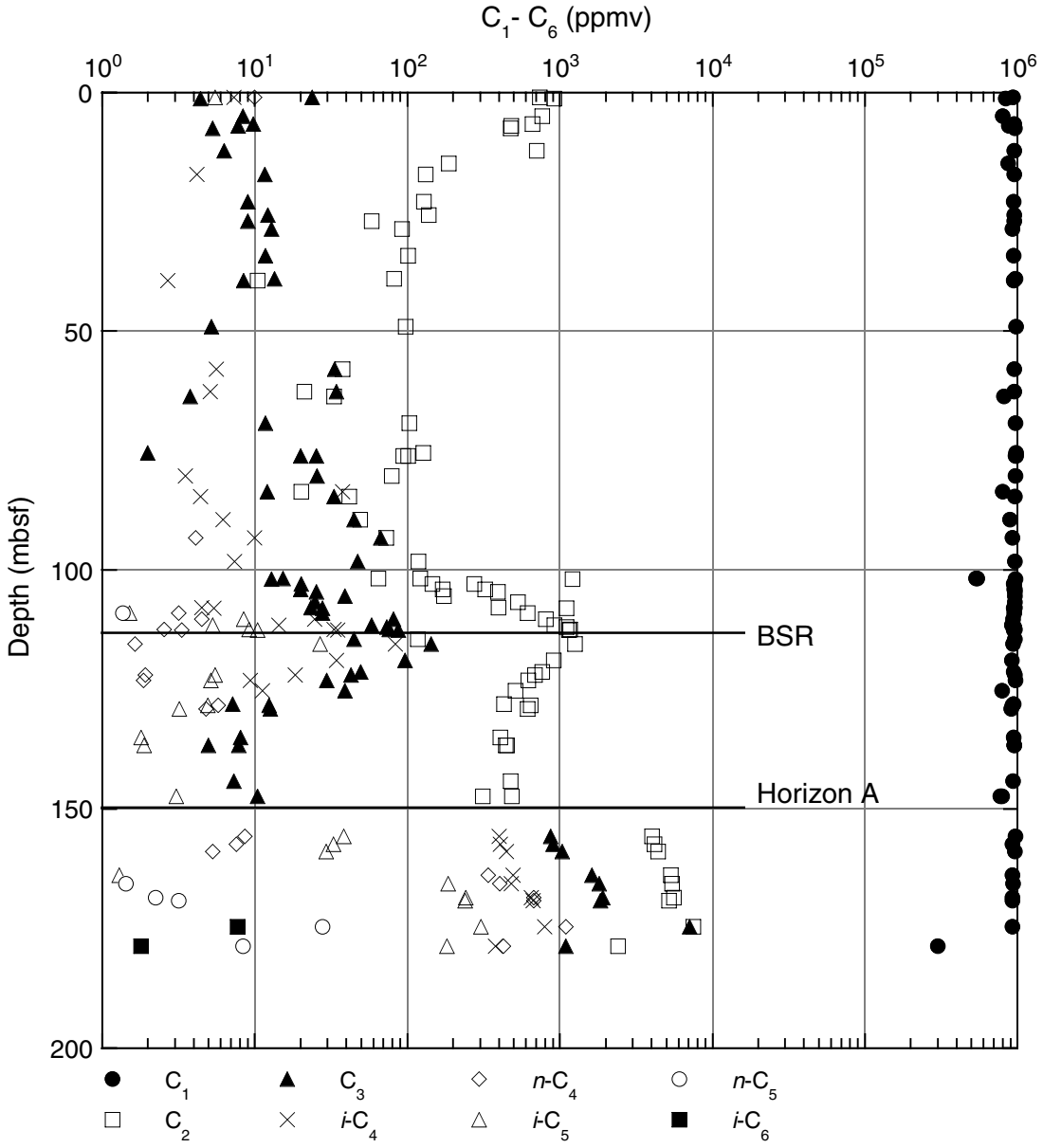

Figure F21. C_1/C_2 ratio vs. depth for Site 1250. VAC = void gas. HS = headspace gas, PCS = pressure core sampler. BSR = bottom-simulating reflector.

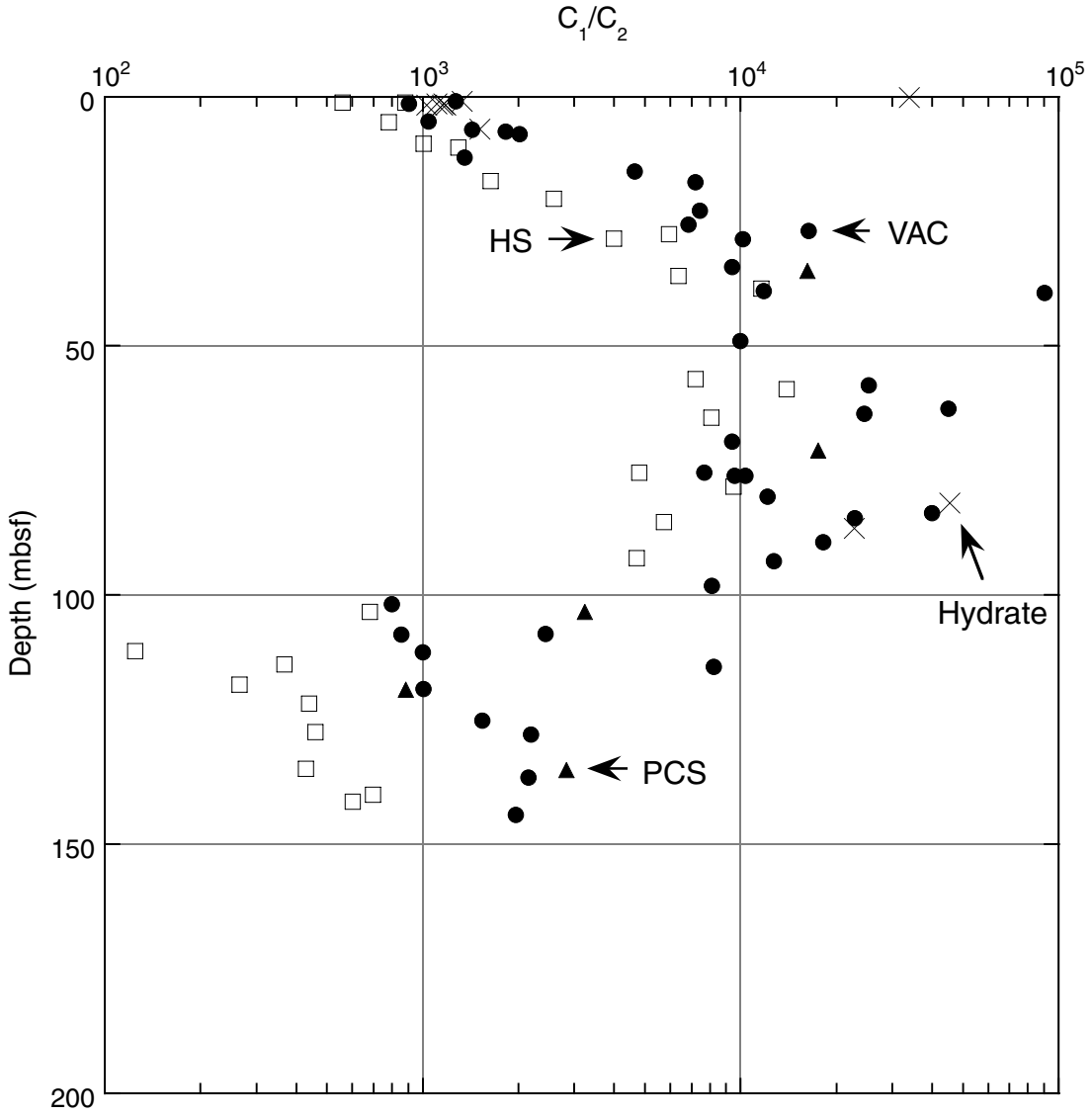

Figure F22. Downcore variation in carbonate carbon (IC), organic carbon (OC), total nitrogen (TN), and total sulfur (TS) and C/N ratios in sediment from Site 1250.

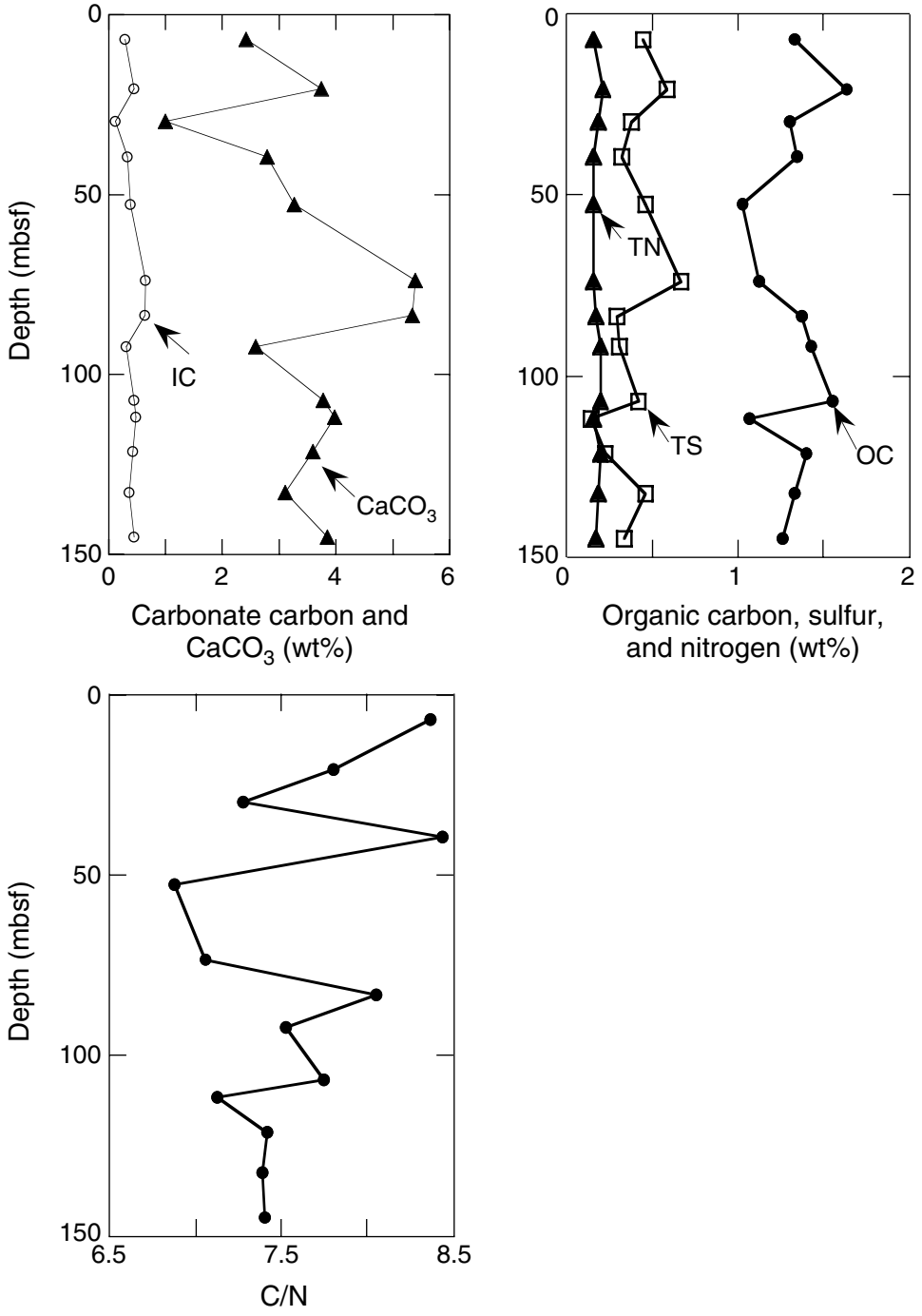

Figure F23. Downhole IR temperature profiles from Holes 1250C and 1250D. Arrows indicate depths where samples thought to contain hydrate were collected. BSR = bottom-simulating reflector.

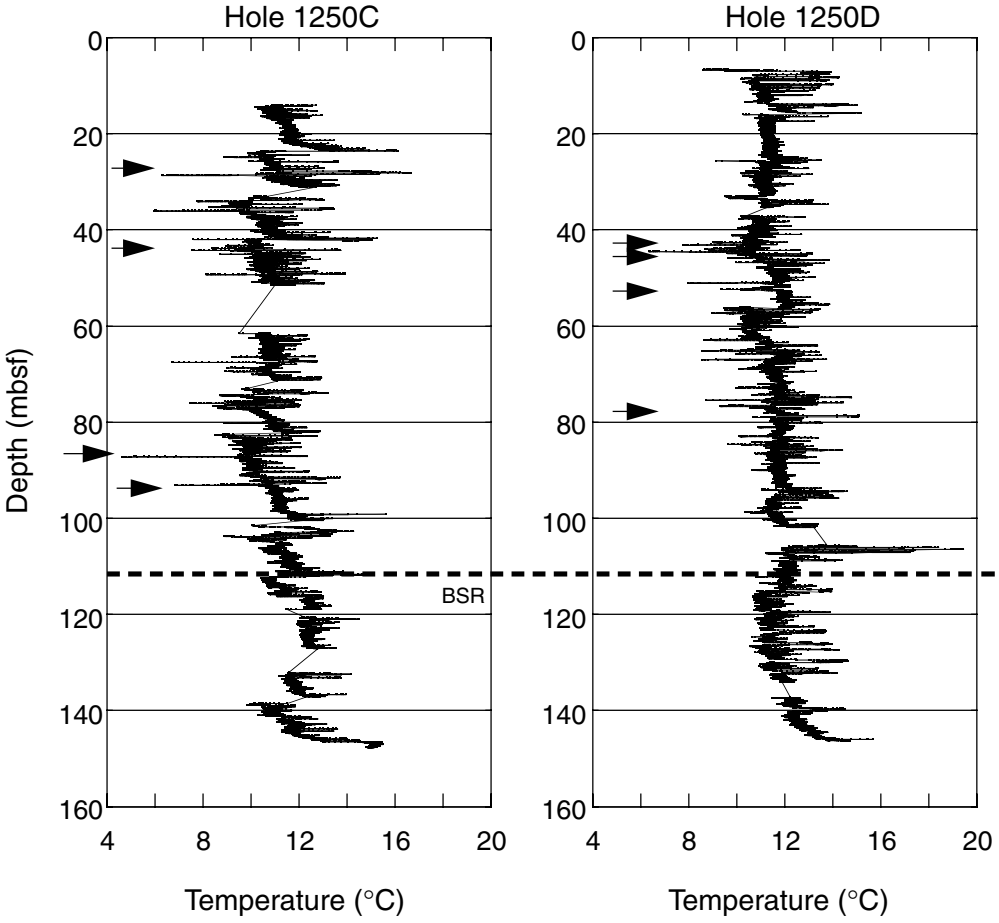

Figure F24. Comparison of temperature anomalies (ΔT) in Holes 1250C and 1250D.

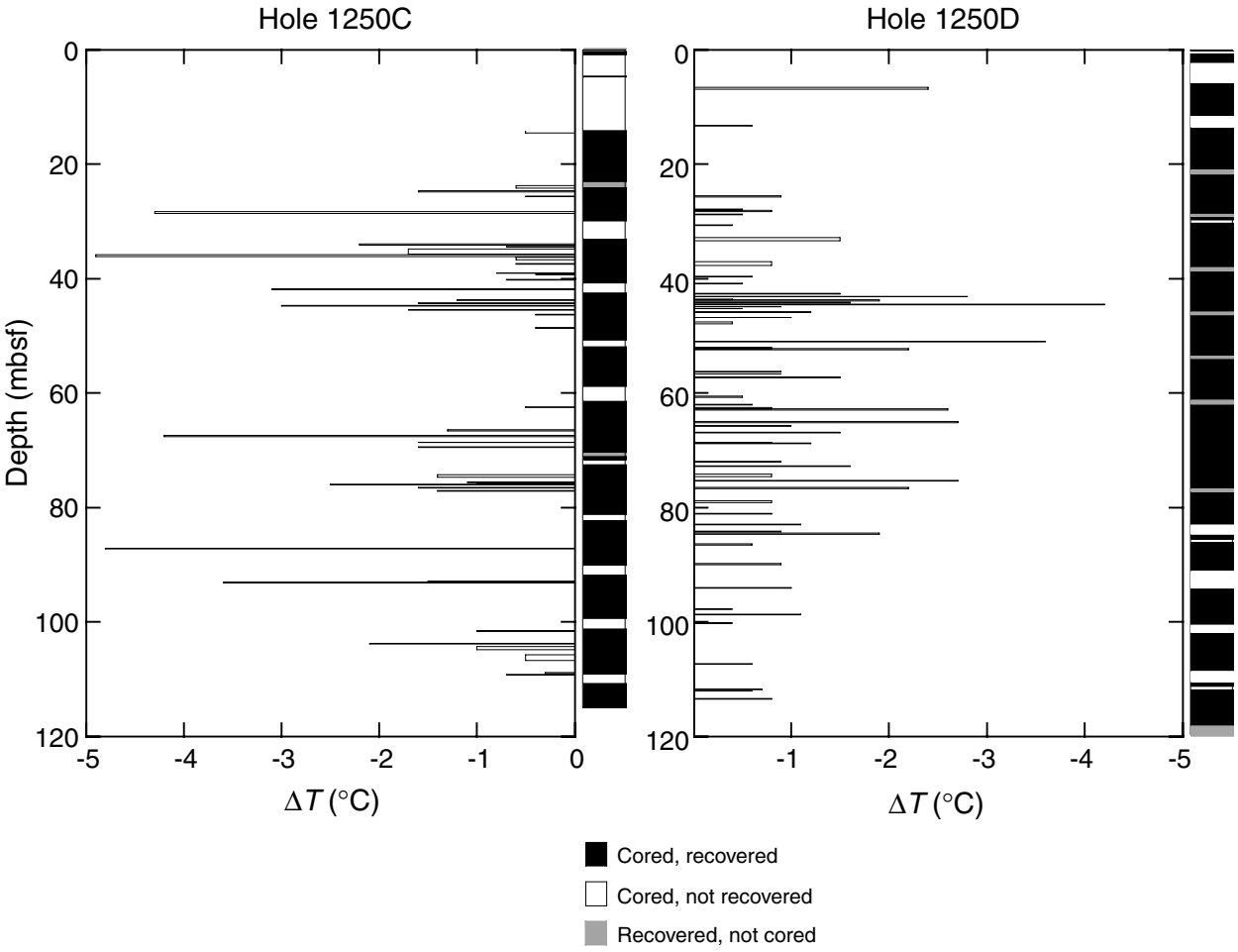

Figure F25. Overview of physical properties measured at Site 1250. LWD = logging-while-drilling, MAD = moisture and density, GRA = gamma ray attenuation. (Continued on next page.)

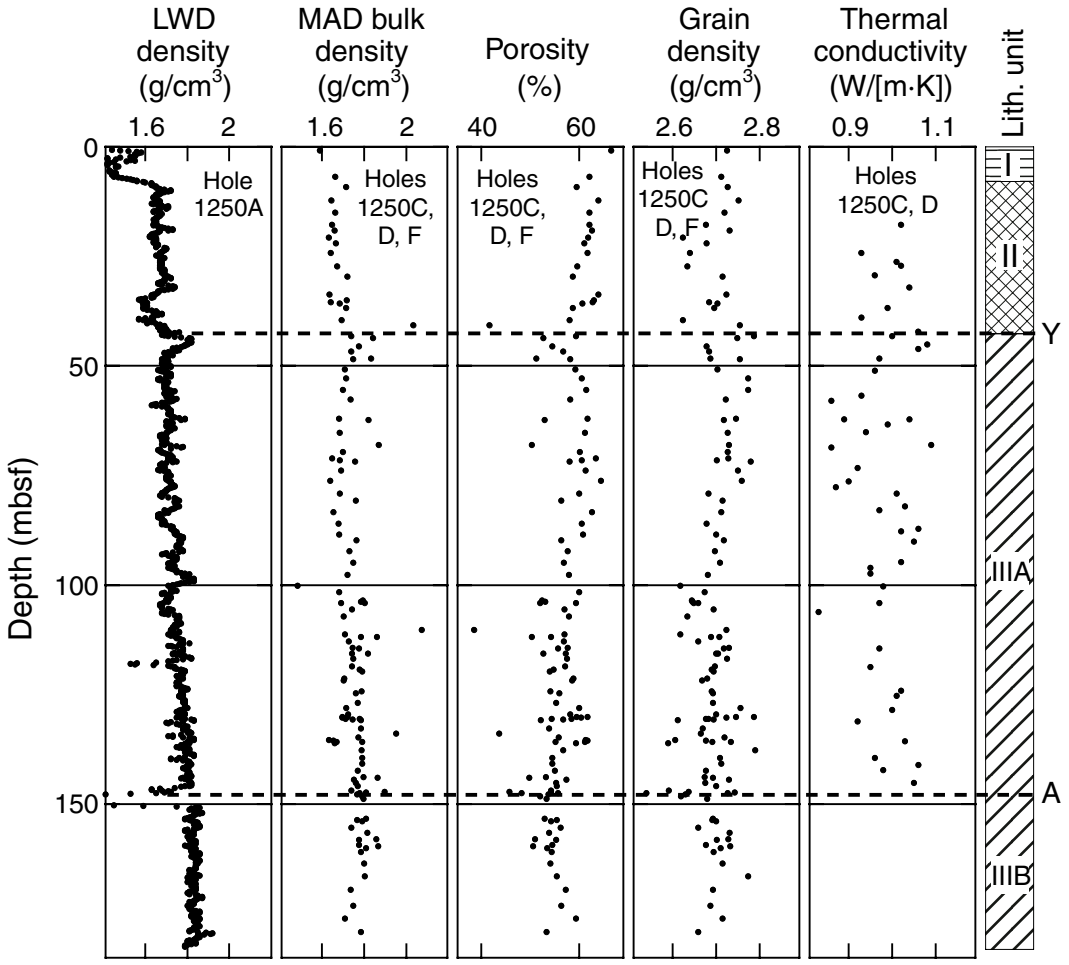

Figure F25 (continued).

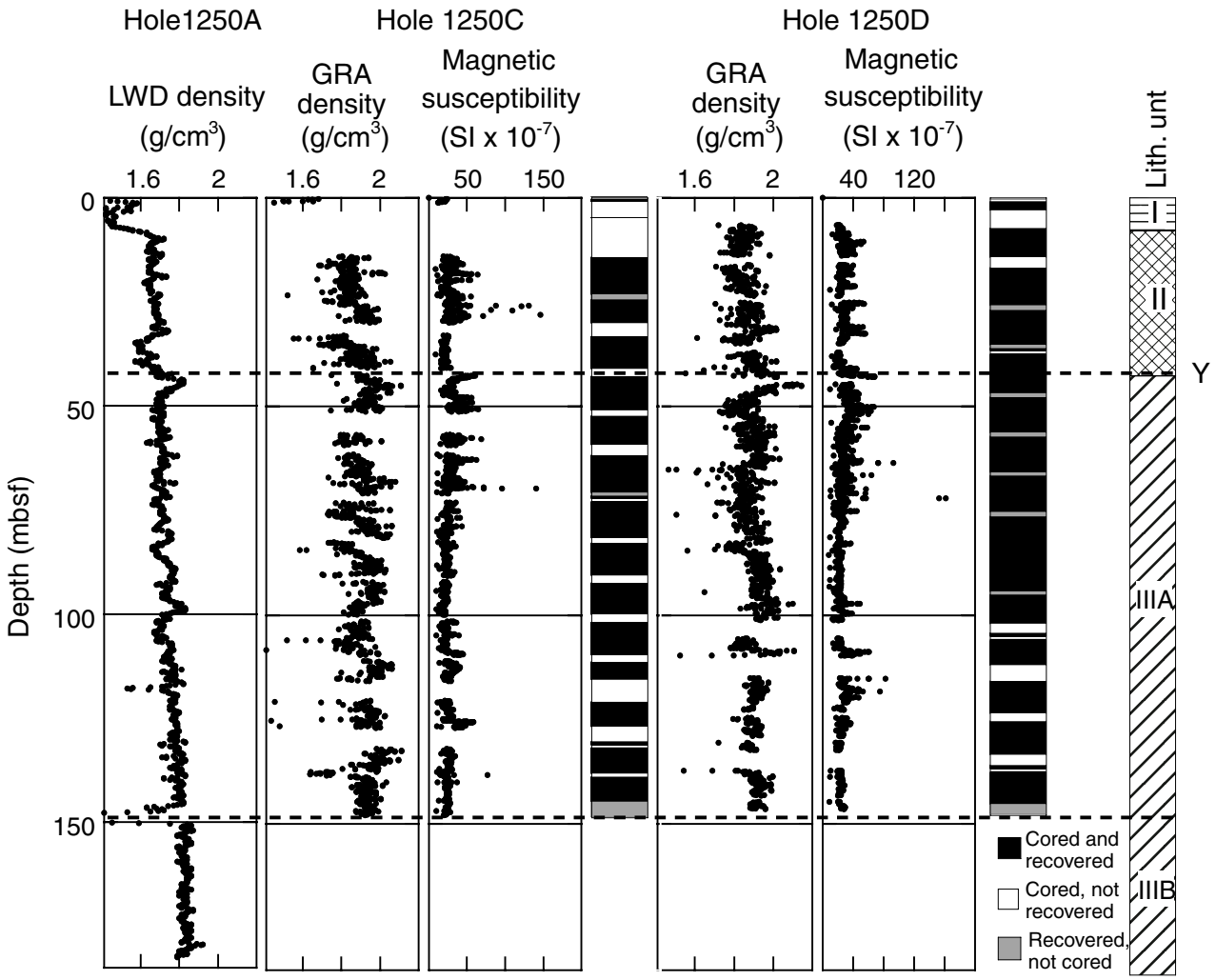

Figure F26. Comparison of physical properties with 3-D seismic data at Site 1250. LWD = logging-while-drilling, MAD = moisture and density.

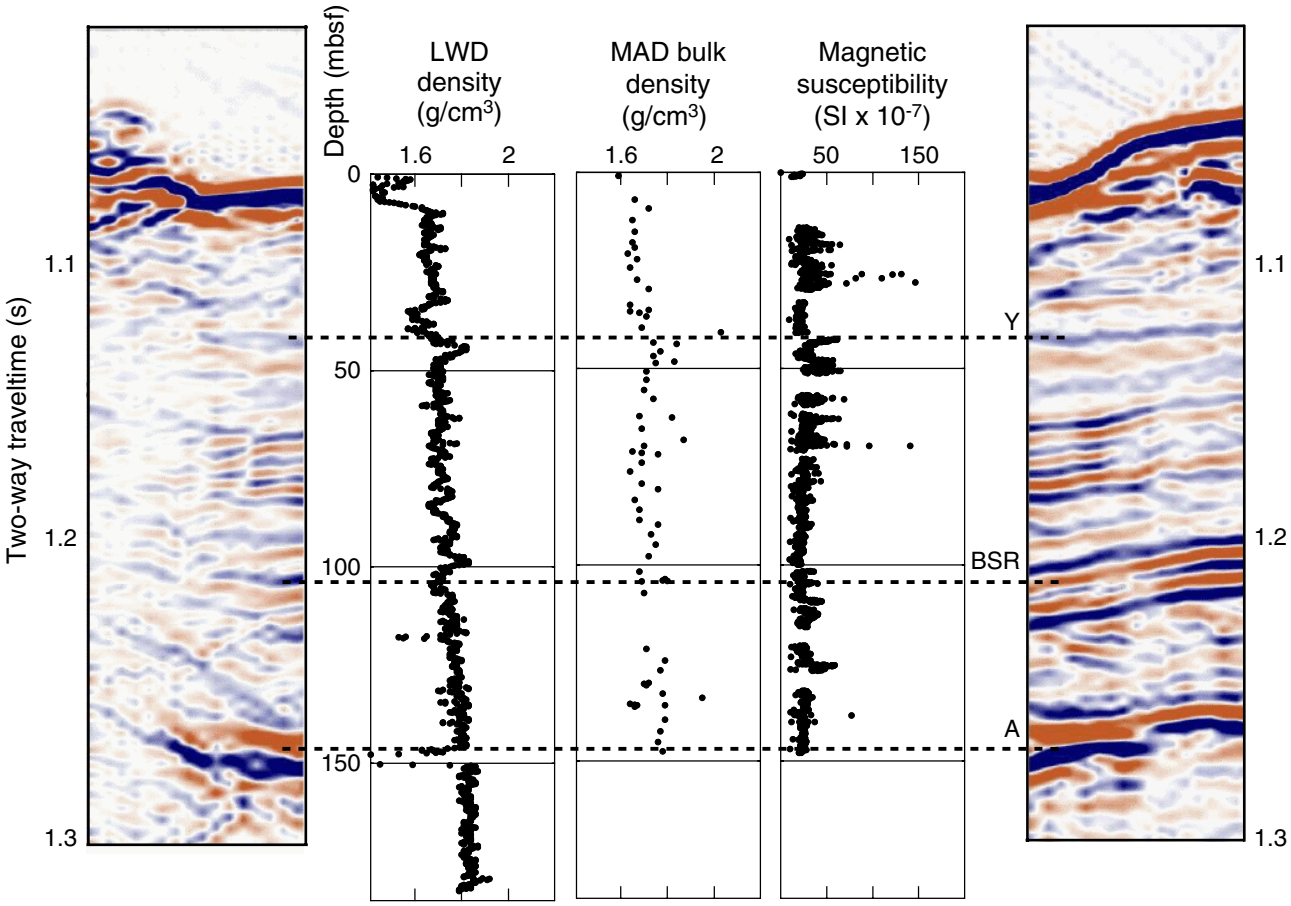

Figure F27. Examples of high-density samples associated with sandy layers. **A.** Interval 204-1250C-5H-6, 39–51 cm. **B.** Interval 204-1250C-17H-2, 27–40 cm. **C.** Ash layer from interval 204-1250F-10X-4, 0–3 cm.

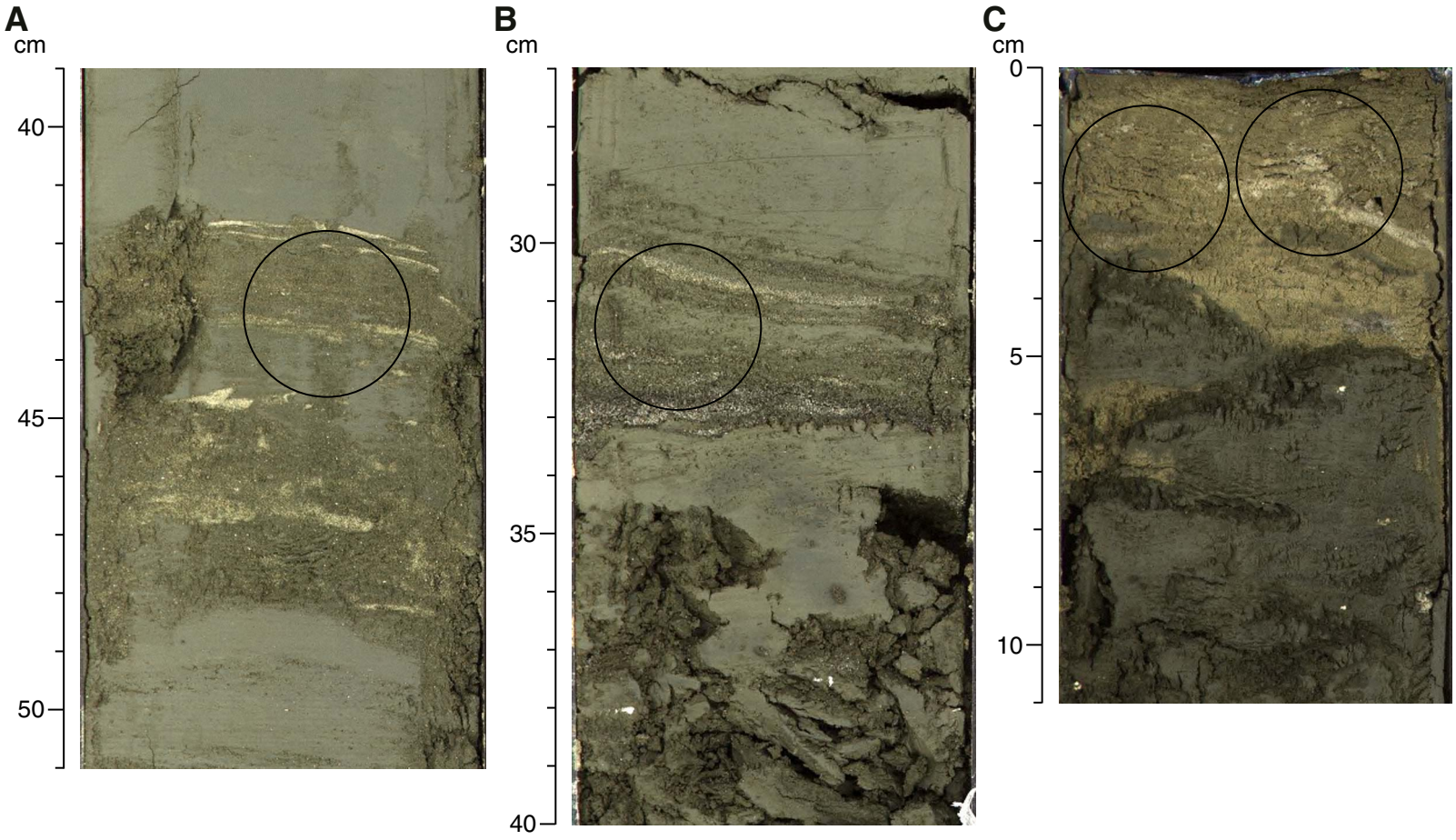

Figure F28. Example of an MS anomaly associated with the presence of a single sulfide precipitation.

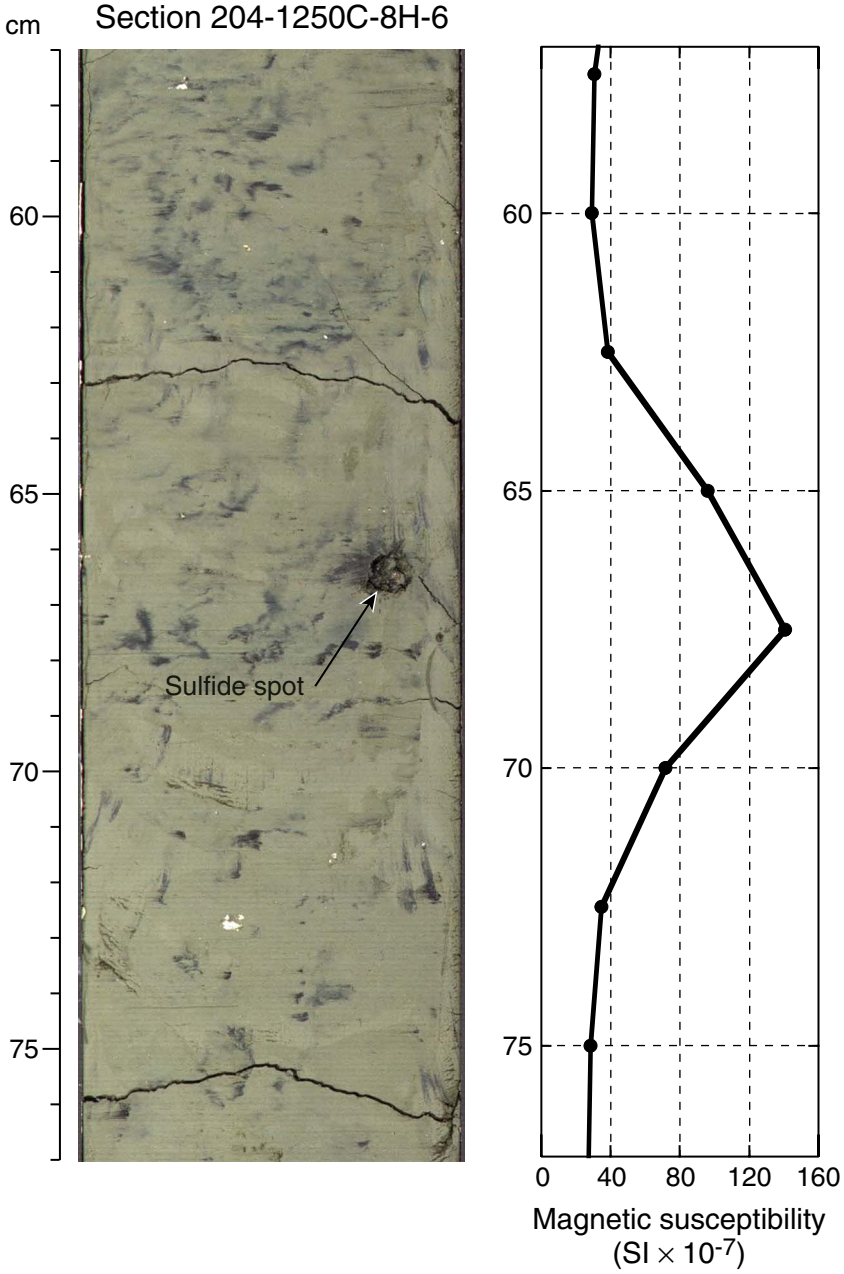

Figure F29. Example of MS variations of turbidite layers associated with Horizon Y in Hole 1250C. **A.** Overall plot of MS as a function of depth. **B.** Detailed plot of MS and the corresponding core photograph of sediments from 42.5 to 43.0 mbsf. **C.** Detailed plot of MS the corresponding core photograph of sediments from 43.5 to 44.0 mbsf.

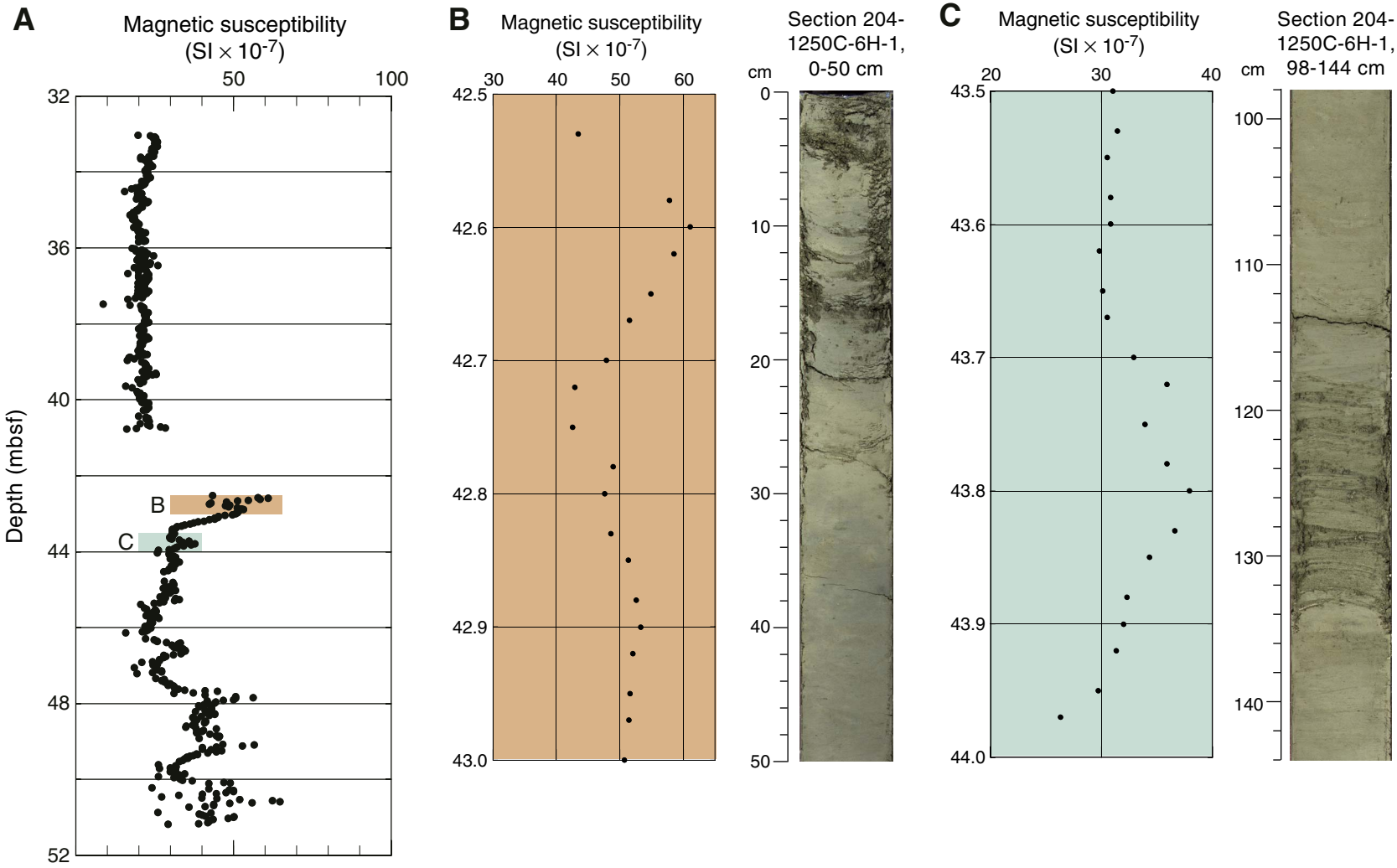

Figure F30. Raw data for estimating in situ temperatures. **A.** APCT tool data. Only the portion of data immediately before, during, and immediately after penetration of the probe into the subsurface is shown. For an example of the entire temperature history of a deployment see **"Downhole Tools and Pressure Coring,"** p. 34, in the "Explanatory Notes" chapter. The ODP core identification number associated with each run of the APCT tool is indicated in the upper left corner of the graph. (Continued on next page.)

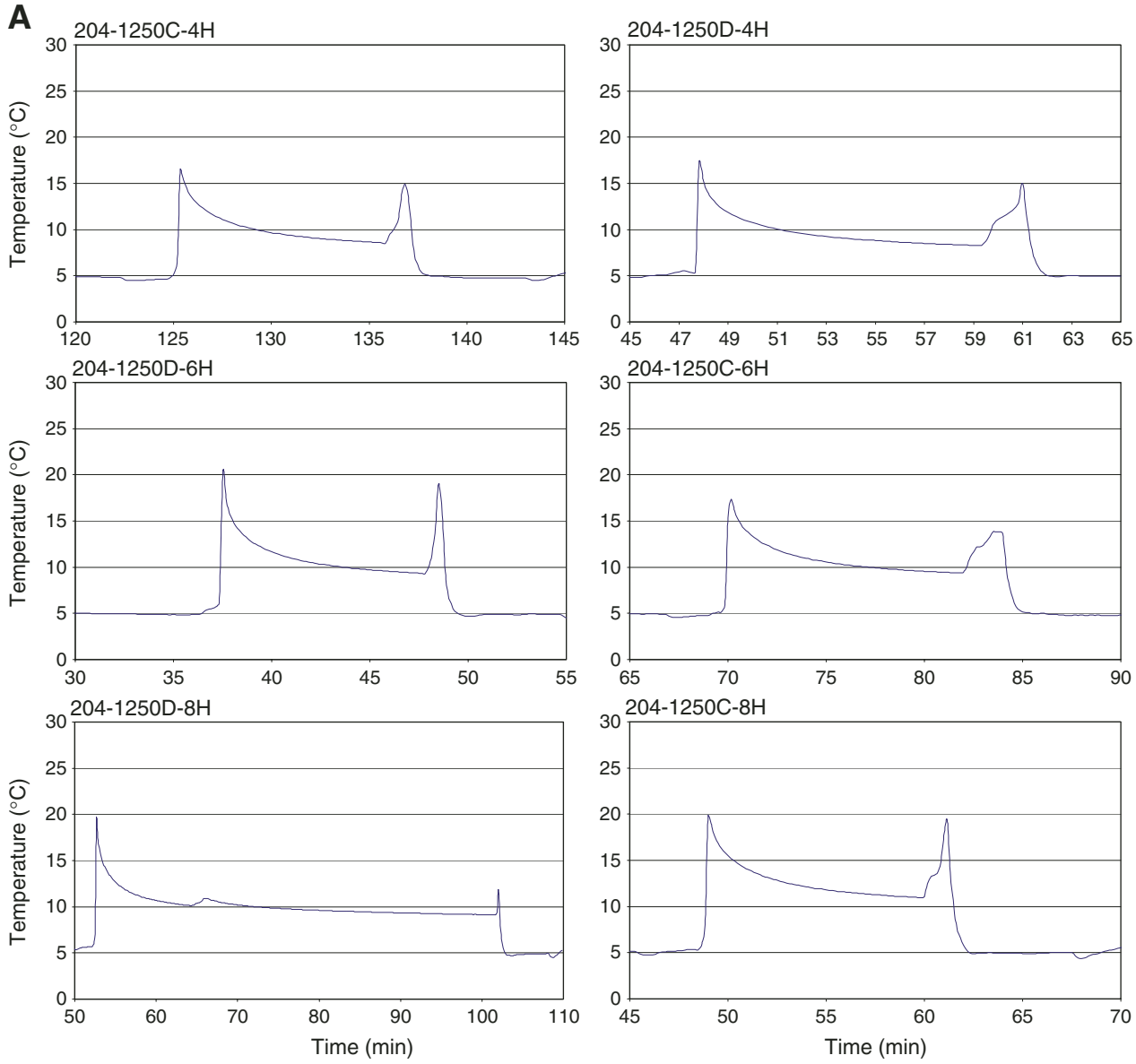

Figure F30 (continued). B. DVTPP temperature and pressure data. The ODP identification for the cores preceding and following tool deployment is indicated.

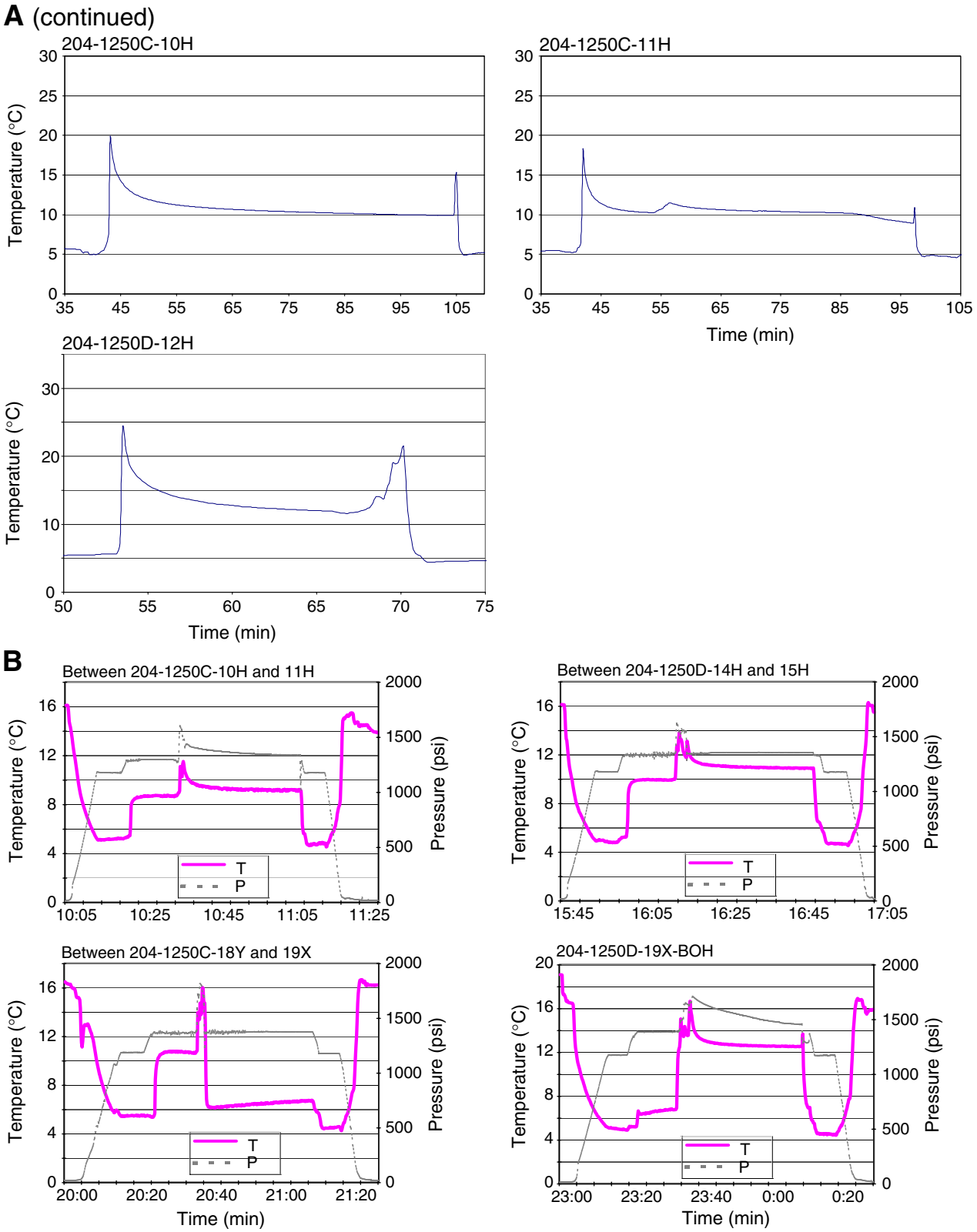

Figure F31. Estimated temperature as a function of depth at Site 1250. Red symbols = DVTPP, blue symbols = APCT tool, dashed line = APCT tool data, solid line = all data. APCT = advanced piston corer temperature tool, DVTP = Davis-Villinger Temperature Probe.

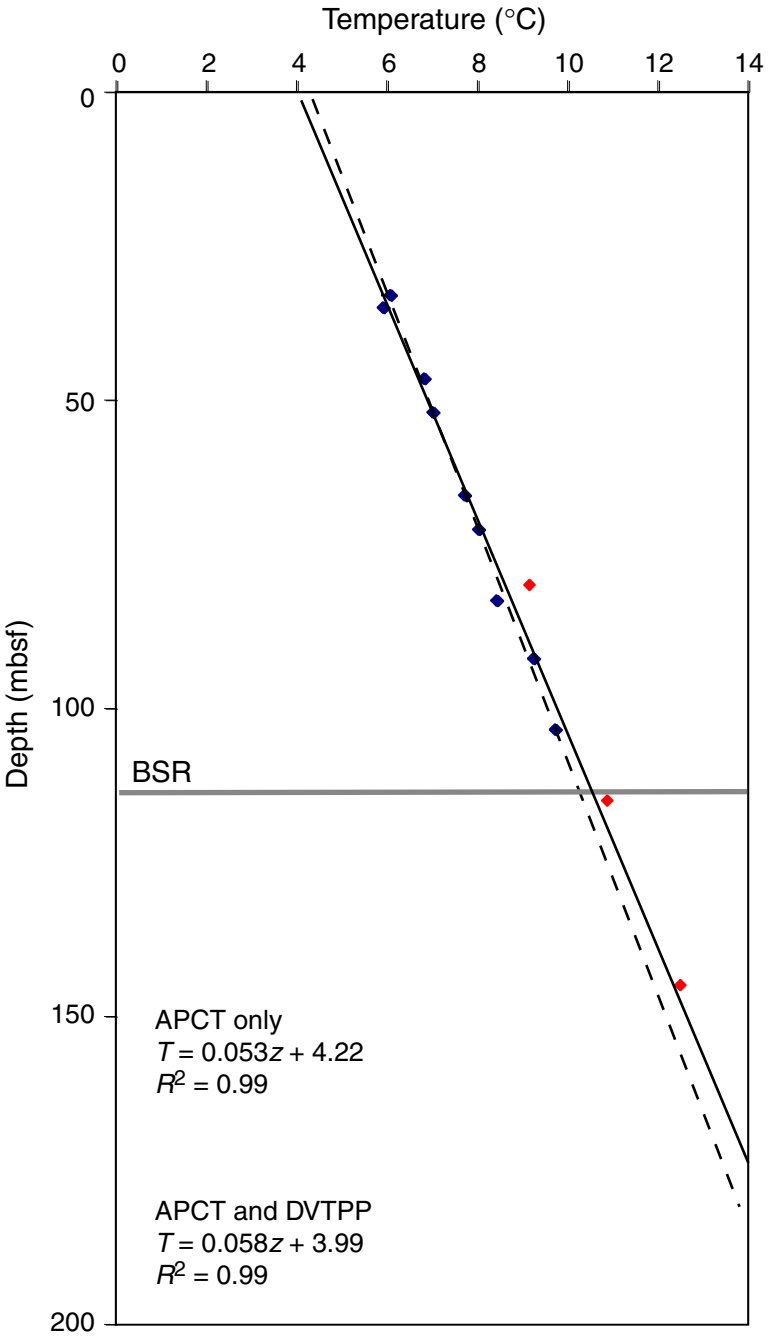

Figure F32. Volume-pressure-time plots for PCS deployed at Site 1250. **A.** Core 204-1250C-9P. **B.** Core 204-1250D-5P. **C.** Core 204-1250D-13P. **D.** Core 204-1250D-18P. **E.** Core 204-1250F-4P.

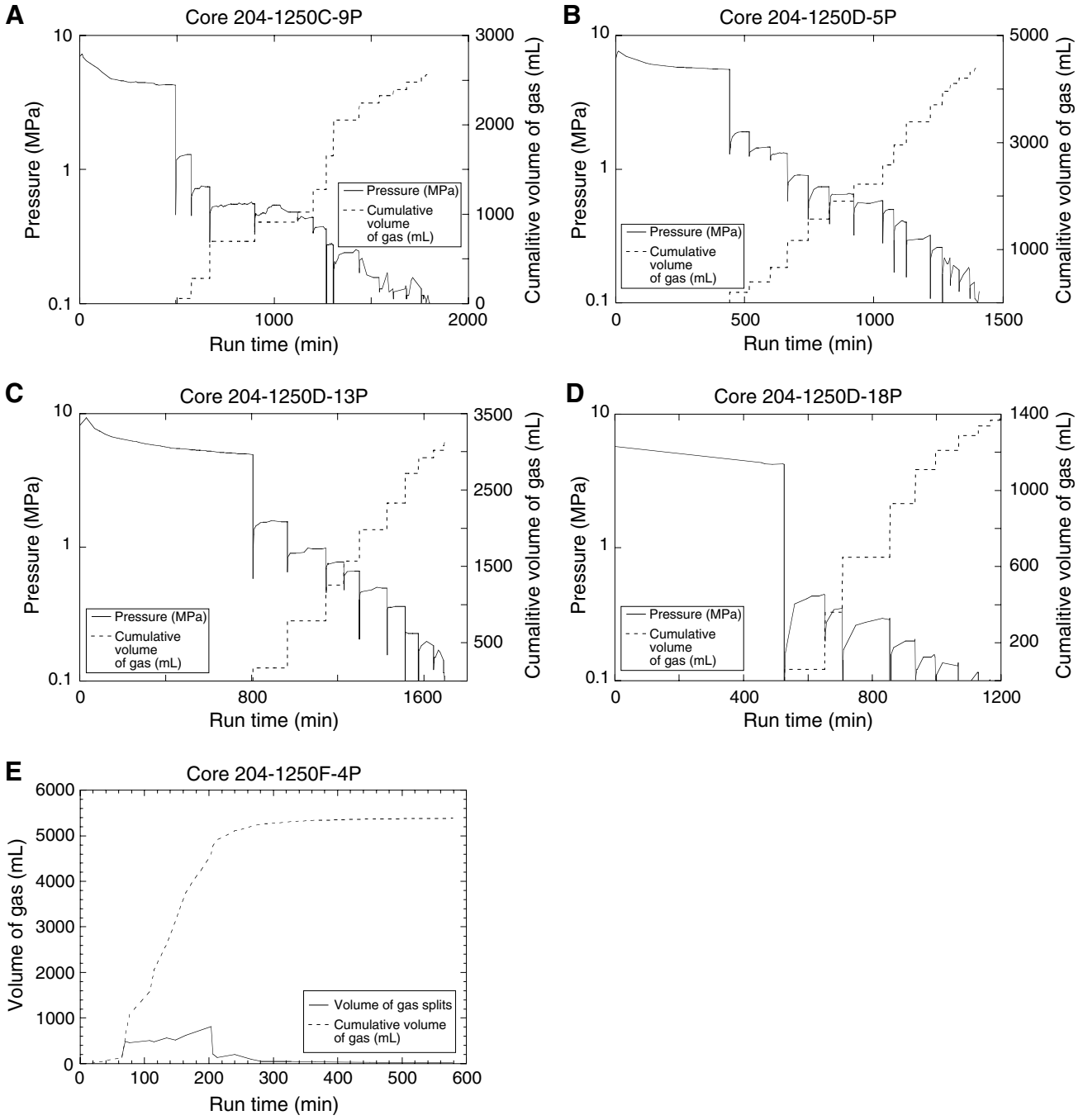

Figure F33. Methane (CH_4) concentration in sediments based on headspace (HS) and pressure core sampler (PCS) data at Site 1250. Estimated theoretical solubility of methane in pore water (extrapolated from values calculated for higher pressures; depths) (Handa, 1990; Duan et al., 1992) is shown and fields of dissolved methane (D), methane hydrate (H), and free methane (F) are depicted. The gray areas indicate the uncertainties in the position of the boundaries.

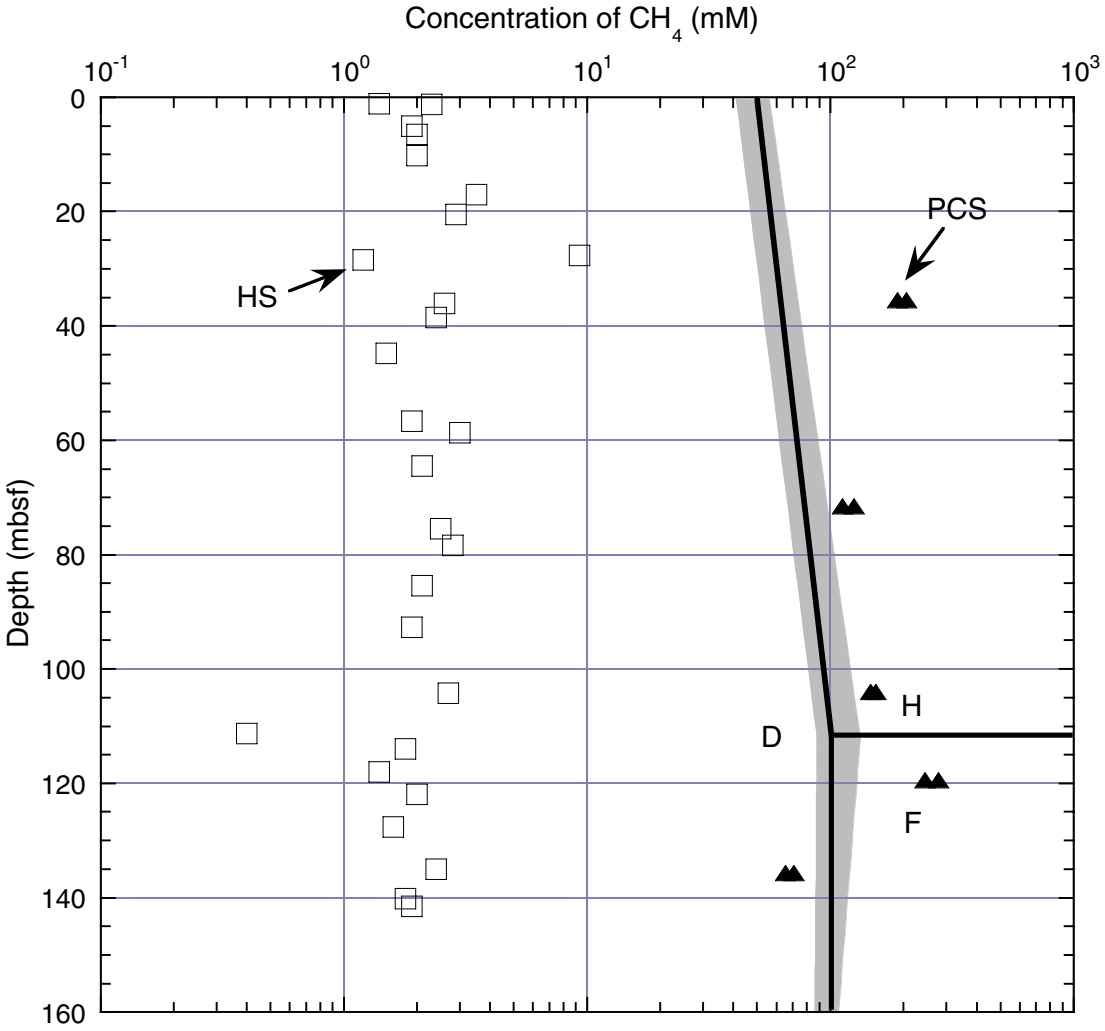

Figure F34. Quality control LWD logs from Holes 1250A and 1250B. The solid line curves represent the logging data from Hole 1250B, whereas the dashed lines represent the logging data from Hole 1250A. ROP = rate of penetration, TAB = time after bit, Diff. = differential.

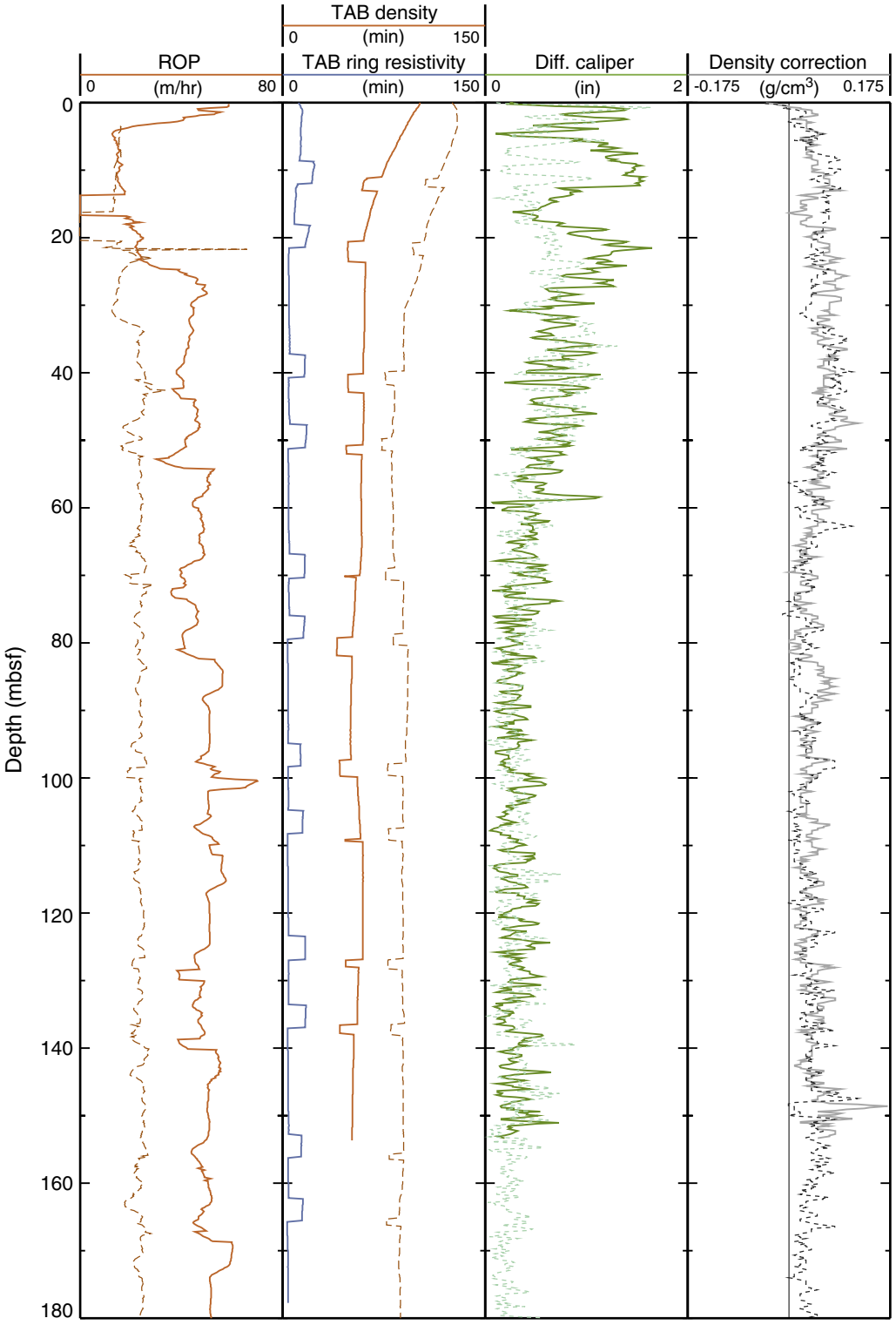

Figure F35. Summary of LWD logging data from Hole 1250A and Hole 1250B. The solid line curves represent the logging data from Hole 1250B, whereas the dashed lines represent the logging data from Hole 1250A. gAPI = American Petroleum Institute gamma ray units, PEF = photoelectric effect factor, RAB = resistivity at the bit.

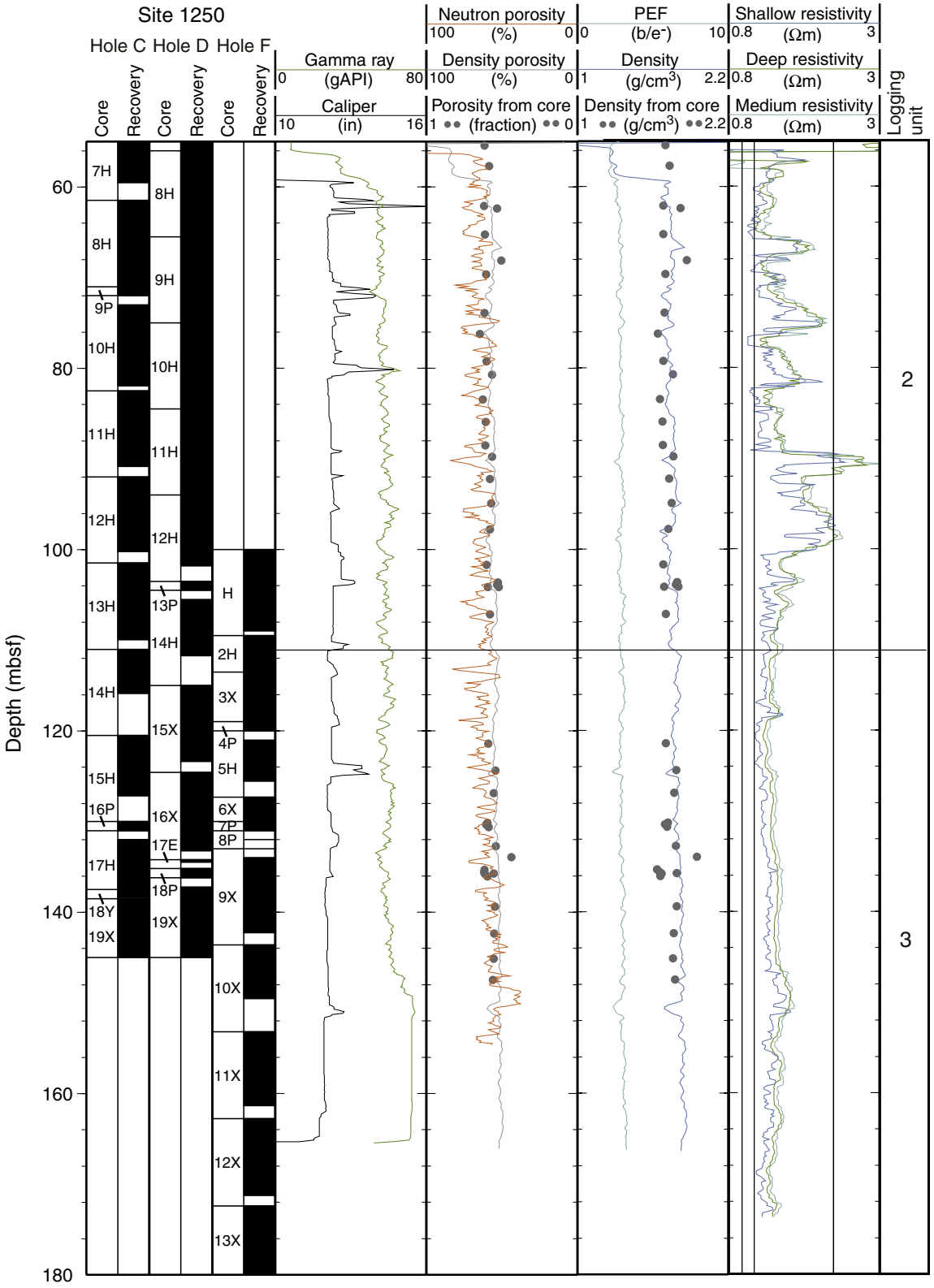

Figure F36. CWL gamma ray logging data from Hole 1250F. FMS = Formation MicroScanner, gAPI = American Petroleum Institute gamma ray units.

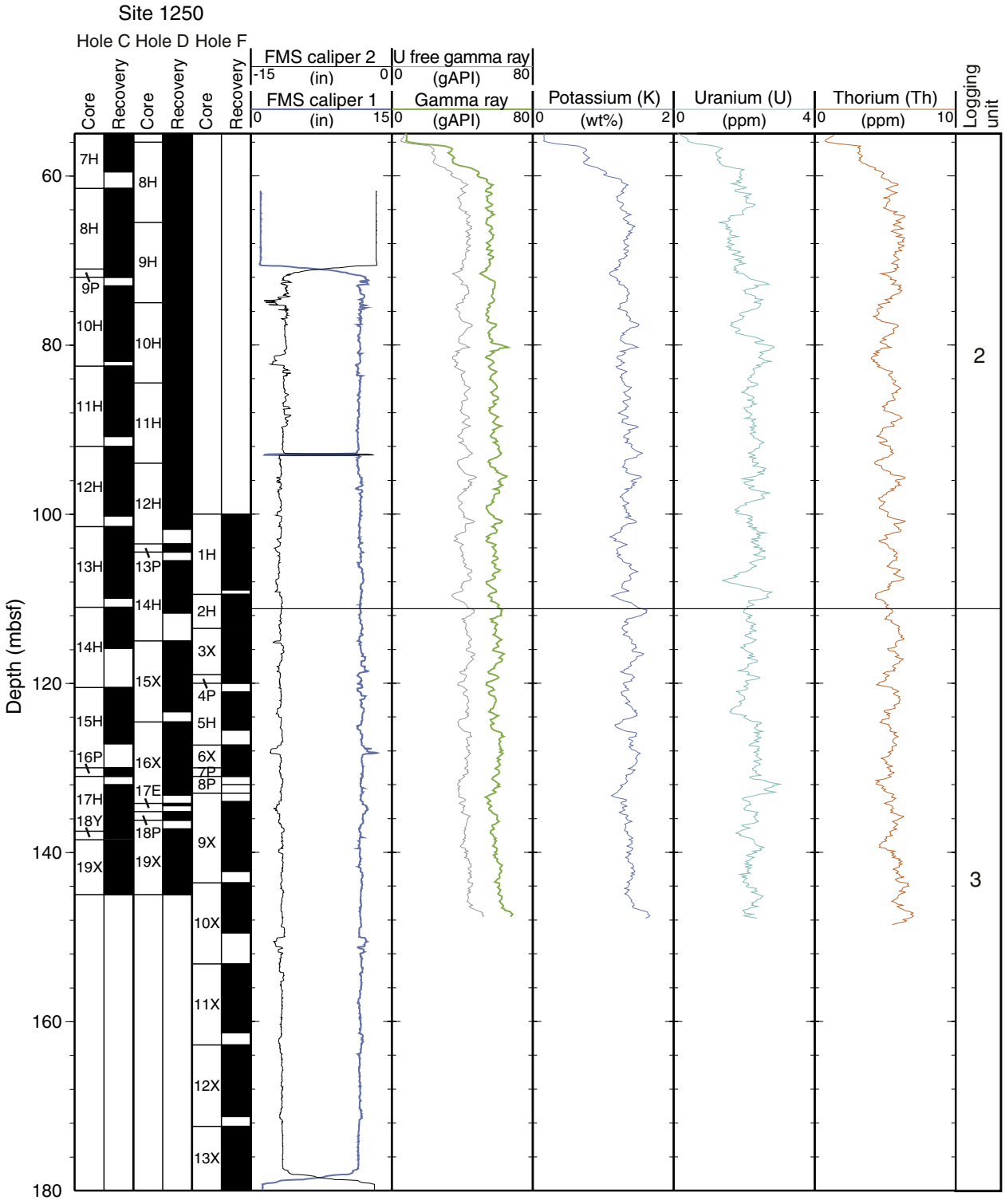

Figure F37. Comparison of logging-while-drilling (LWD) and CWL downhole logging data from Holes 1250B and 1250F. gAPI = American Petroleum Institute gamma ray units, PEF = photoelectric effect factor, RAB = resistivity at the bit, por. = porosity.

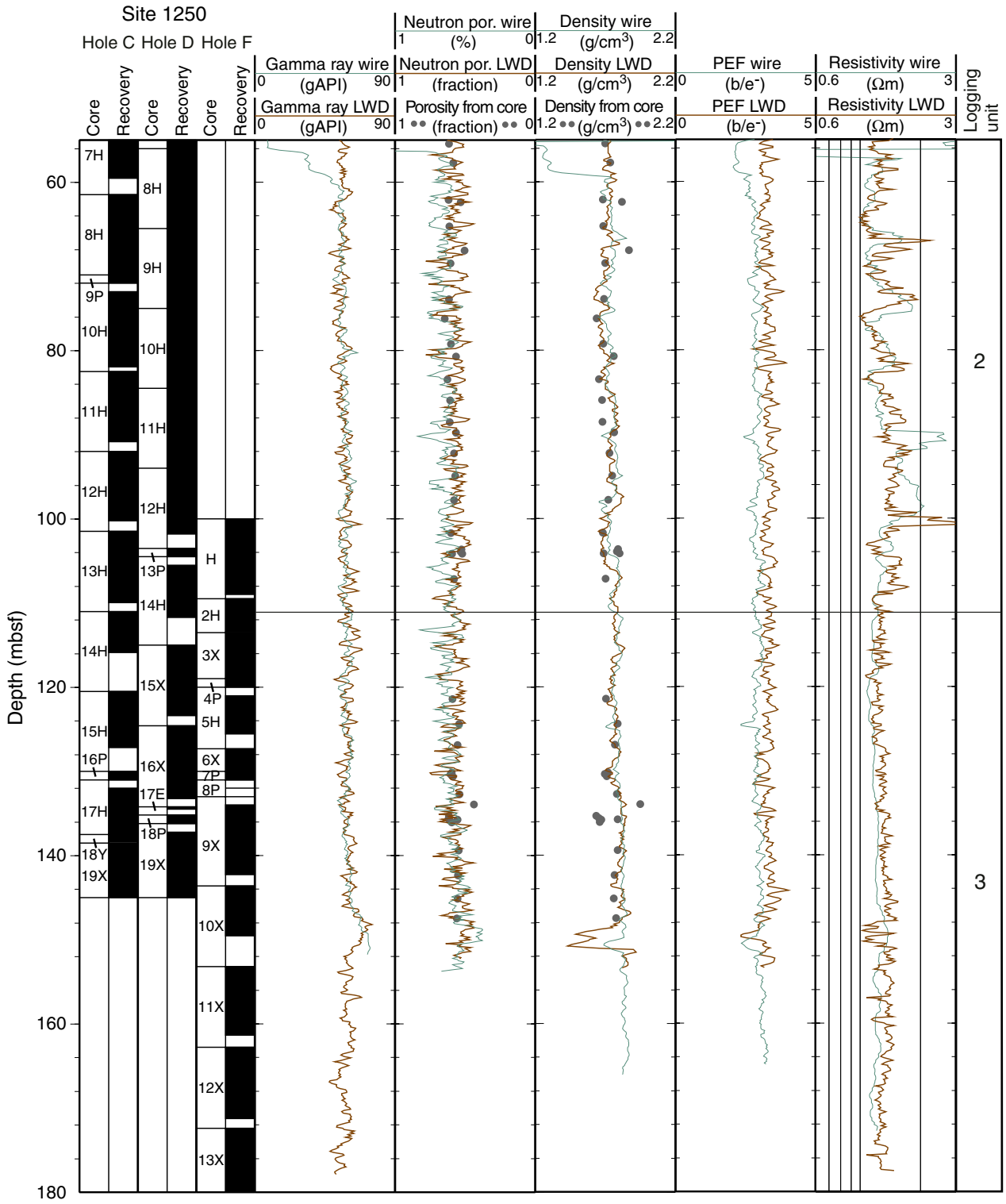

Figure F38. CWL acoustic logging data from Hole 1250F. The resistivity log is used as a reference indicator of the presence of gas hydrate. Low sonic waveform amplitudes are also possible indicators of gas hydrate. SPh. foc. res. = spherically focused resistivity.

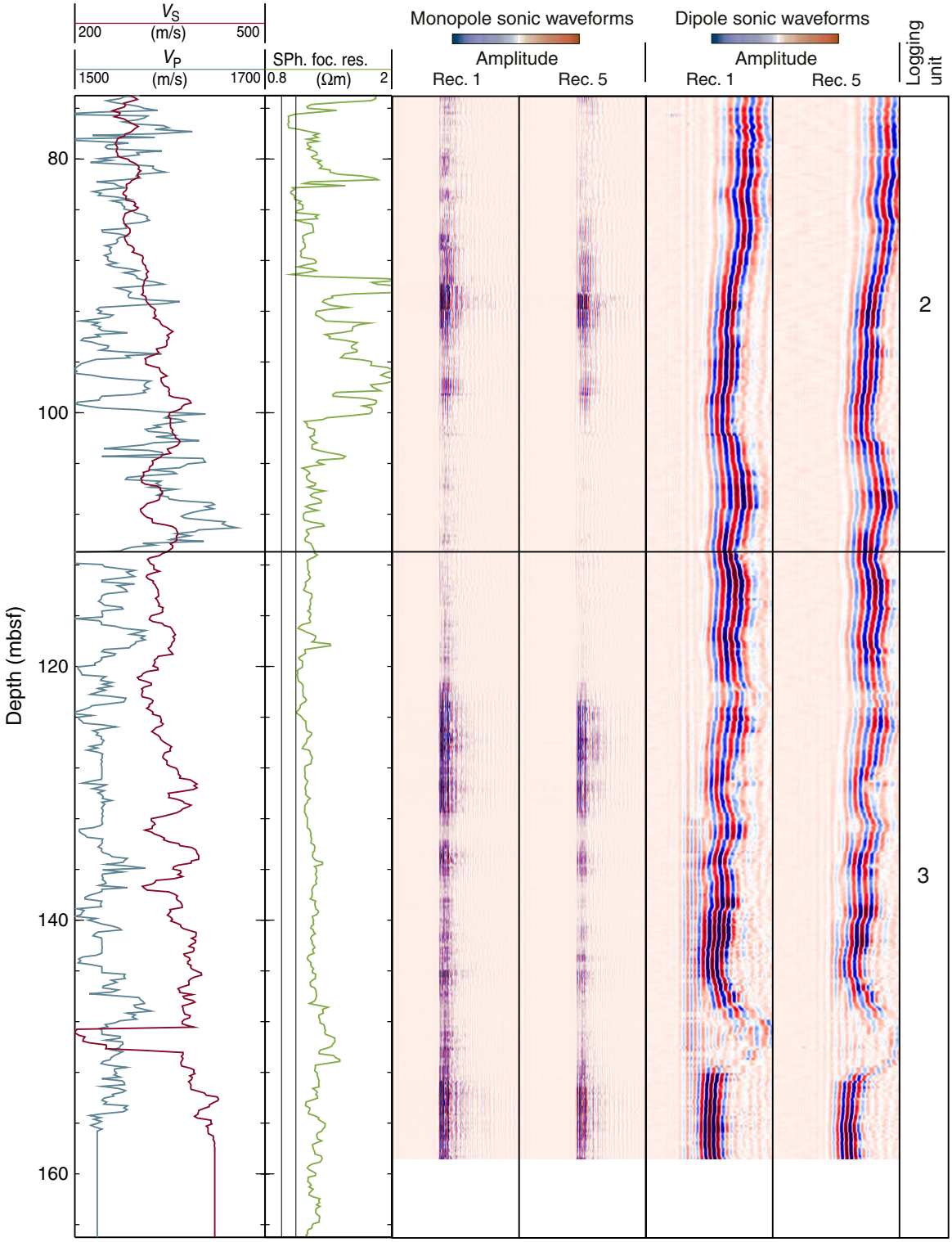

Figure F39. Summary of CWL logging data from Hole 1250F. gAPI = American Petroleum Institute gamma ray units, PEF = photoelectric effect factor, RAB = resistivity-at-the-bit.

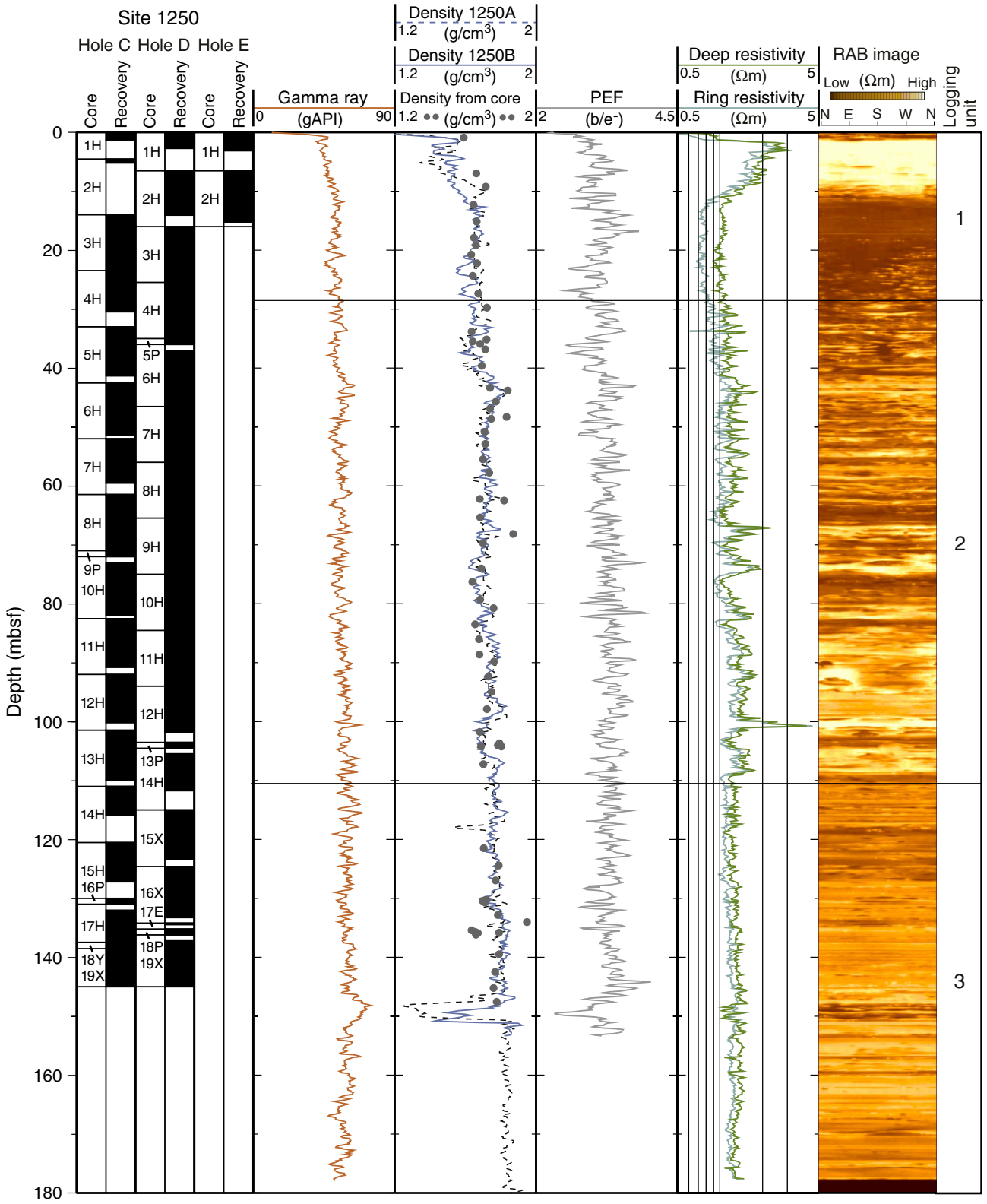

Figure F40. Resistivity-at-the-bit (RAB) and Formation MicroScanner (FMS) images showing Horizon A characterized by interbedded bright, resistive, and dark conductive layers from Hole 1250B and 1250F.

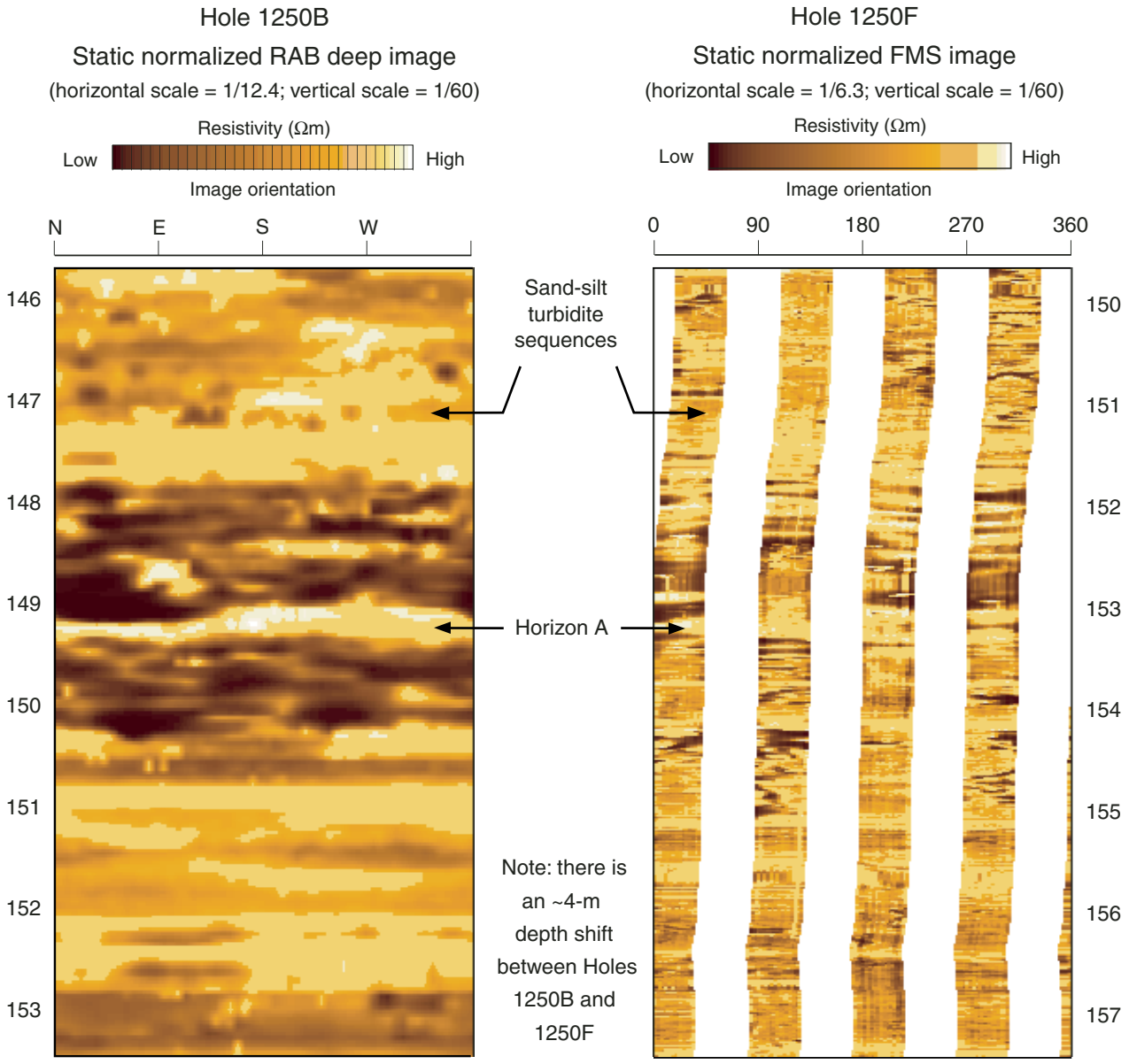

Figure F41. LWD- and core-derived porosities from Hole 1250A and 1250B. The solid line curves represent the logging data from Hole 1250B, whereas the dashed lines represent the logging data from Hole 1250A. NMR-MRP = Nuclear Magnetic Resonance tool, por. = porosity, RAB = resistivity-at-the-bit.

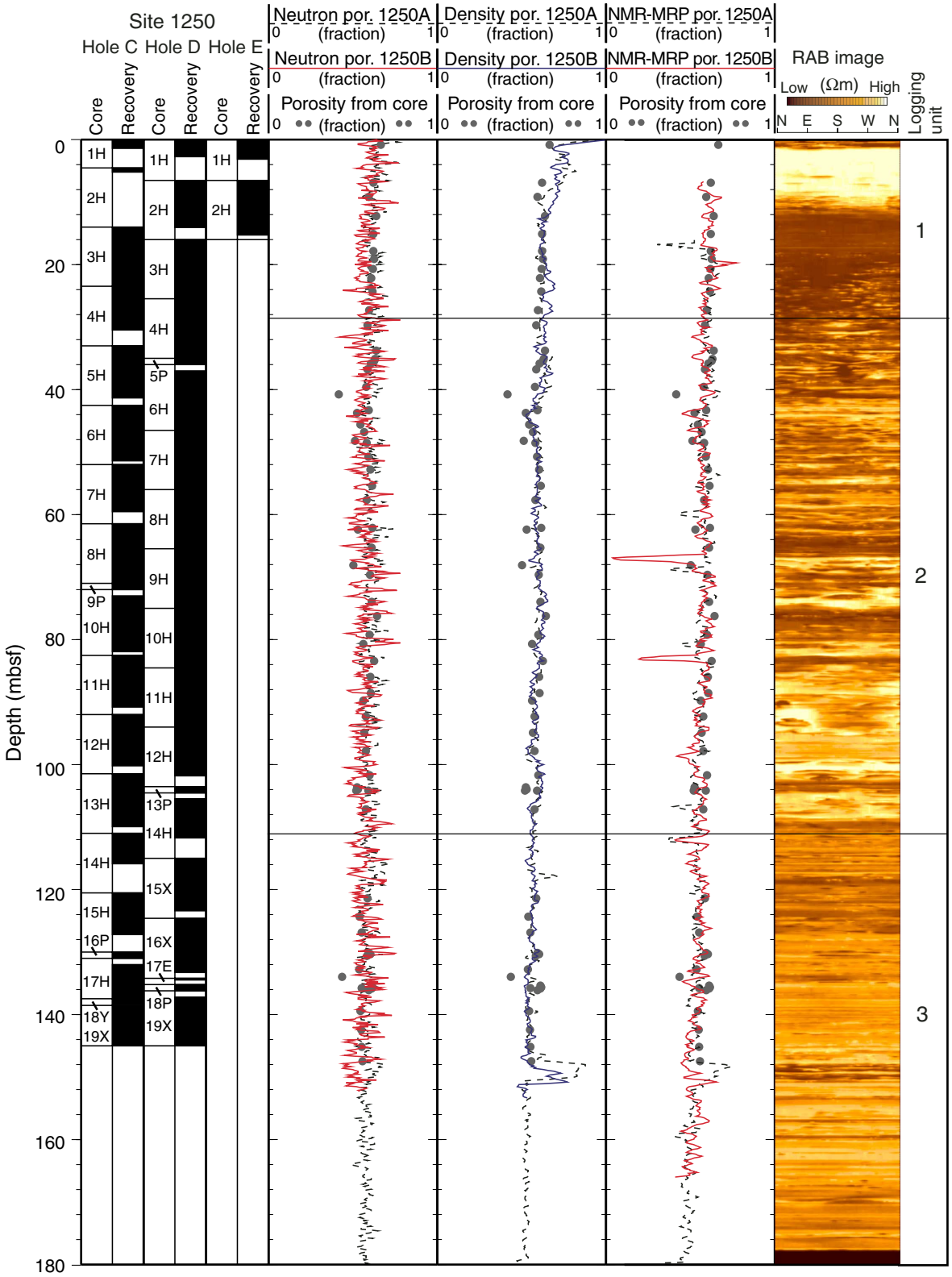

Figure F42. Logging-derived gas hydrate saturations from Hole 1250B. gAPI = American Petroleum Institute gamma ray units, RAB = resistivity-at-the-bit.

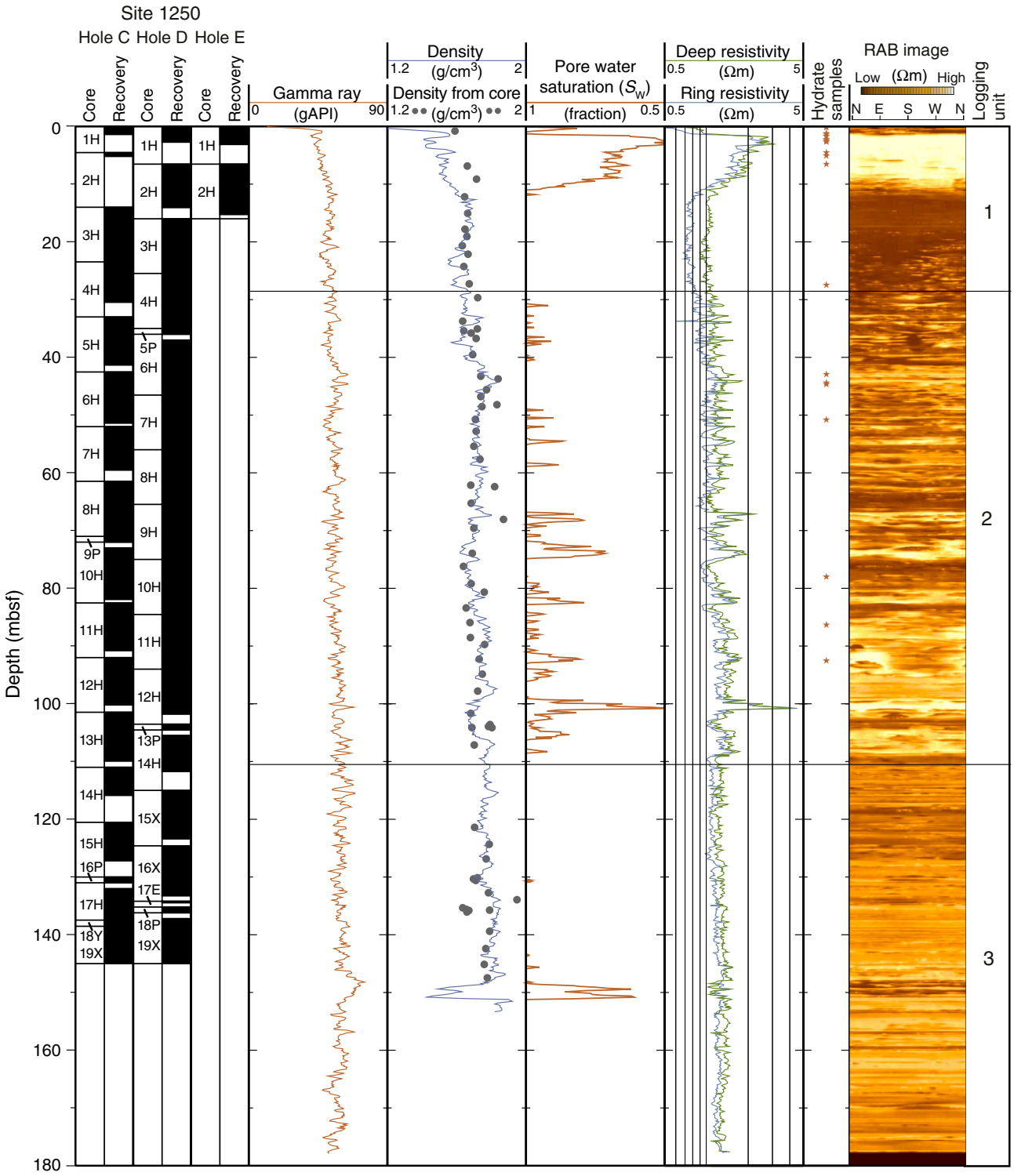

Figure F43. Borehole temperatures recorded with the TAP tool during the down and up pass of the three runs of the triple combo tool string in Hole 1250F.

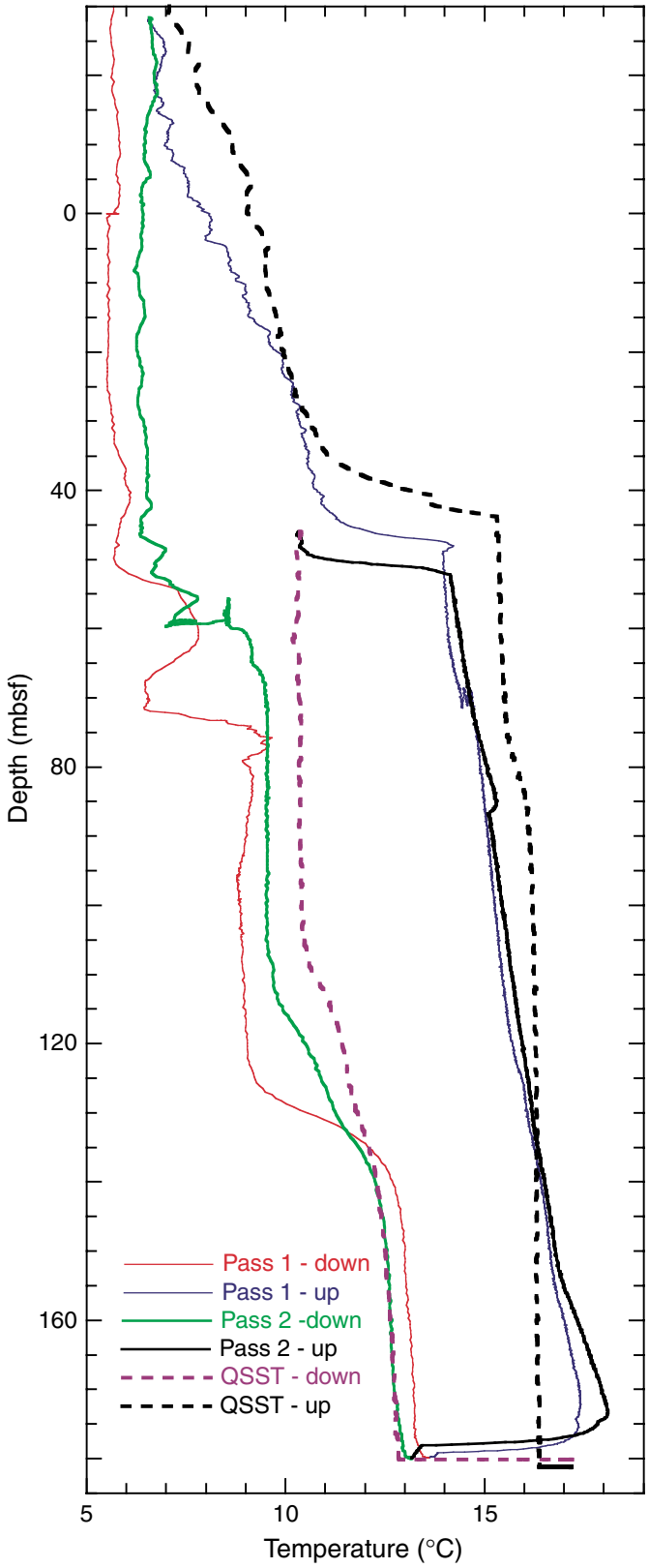

Table T1. Coring summary, Site 1250. (Continued on next two pages.)

Hole 1250A
Latitude: 44°34.1176′N
Longitude: 125°9.0179′W
Time on site (hr): 172 (1630 hr, 21 Jul–1245 hr, 22 Jul 2002)
Time on hole (hr): 20.25 (1630 hr, 21 Jul–1245 hr, 22 Jul 2002)
Seafloor (drill pipe measurement from rig floor, mbrf): 807
Distance between rig floor and sea level (m): 11
Water depth (drill pipe measurement from sea level, m): 796
Total depth (drill pipe measurement from rig floor, mbrf): 1017
Total penetration (meters below seafloor, mbsf): 210
Total number of cores: 0
Total number of drilled intervals: 1
Total length of cored section (m): 0
Total core recovered (m): 0
Core recovery (%): 0

Hole 1250B
Latitude: 44°34.1174′N
Longitude: 125°8.9921′W
Time on hole (hr): 19.5 (1400 hr, 23 Jul–0930 hr, 24 Jul 2002)
Seafloor (drill pipe measurement from rig floor, mbrf): 807
Distance between rig floor and sea level (m): 11.1
Water depth (drill pipe measurement from sea level, m): 795.9
Total depth (drill pipe measurement from rig floor, mbrf): 987
Total penetration (meters below seafloor, mbsf): 180
Total number of cores: 0
Total number of drilled intervals: 1
Total length of cored section (m): 0
Total core recovered (m): 0
Core recovery (%): 0

Hole 1250C
Latitude: 44°34.1273′N
Longitude: 125°9.0178′W
Time on hole (hr): 28.5 (1230 hr, 2 Aug–1700 hr, 3 Aug 2002)
Seafloor (drill pipe measurement from rig floor, mbrf): 807
Distance between rig floor and sea level (m): 11.4
Water depth (drill pipe measurement from sea level, m): 795.6
Total depth (drill pipe measurement from rig floor, mbrf): 952
Total penetration (meters below seafloor, mbsf): 145
Total number of cores: 19
Total number of drilled intervals: 2
Total length of cored section (m): 143
Total core recovered (m): 117.29
Core recovery (%): 82

Hole 1250D
Latitude: 44°34.1063′N
Longitude: 125°9.0182′W
Time on hole (hr): 26 (1700 hr, 3 Aug–1900 hr, 4 Aug 2002)
Seafloor (drill pipe measurement from rig floor, mbrf): 807
Distance between rig floor and sea level (m): 11.2
Water depth (drill pipe measurement from sea level, m): 795.8
Total depth (drill pipe measurement from rig floor, mbrf): 952
Total penetration (meters below seafloor, mbsf): 145
Total number of cores: 19
Total number of drilled intervals: 3
Total length of cored section (m): 142
Total core recovered (m): 133.67
Core recovery (%): 94.1

Table T1 (continued).

Hole 1250E
Latitude: 44°34.1124′N
Longitude: 125°9.0171′W
Time on hole (hr): 3.5 (1900 hr, 4 Aug–2230 hr, 4 Aug 2002)
Seafloor (drill pipe measurement from rig floor, mbrf): 807
Distance between rig floor and sea level (m): 11.3
Water depth (drill pipe measurement from sea level, m): 795.7
Total depth (drill pipe measurement from rig floor, mbrf): 823
Total penetration (meters below seafloor, mbsf): 16
Total number of cores: 2
Total number of drilled intervals: 0
Total length of cored section (m): 16
Total core recovered (m): 11.93
Core recovery (%): 74.6

Hole 1250F
Latitude: 44°34.1166′N
Longitude: 125°9.0025′W
Time on hole (hr): 74.25 (1915 hr, 24 Aug–2130 hr, 27 Aug 2002)
Seafloor (drill pipe measurement from rig floor, mbrf): 807
Distance between rig floor and sea level (m): 11.6
Water depth (drill pipe measurement from sea level, m): 795.4
Total depth (drill pipe measurement from rig floor, mbrf): 987
Total penetration (meters below seafloor, mbsf): 180
Total number of cores: 13
Total number of drilled intervals: 4
Total length of cored section (m): 77
Total core recovered (m): 69.1
Core recovery (%): 89.7

Core	Date (Aug 2002)	Local time (hr)	Depth (mbsf) Top	Depth (mbsf) Bottom	Length (m) Cored	Length (m) Recovered	Recovery (%)
204-1250A-							
			*****Drilled from 0 to 210 mbsf*****				
204-1250B-							
			*****Drilled from 0 to 180 mbsf*****				
204-1250C-							
1H	2	1510	0.0	4.5	4.5	1.39	30.9
2H	2	1615	4.5	14.0	9.5	0.71	7.5
3H	2	1745	14.0	23.5	9.5	10.14	106.7
4H	2	1910	23.5	33.0	9.5	6.97	73.4
5H	2	2005	33.0	42.5	9.5	8.35	87.9
6H	2	2120	42.5	52.0	9.5	8.89	93.6
7H	2	2210	52.0	61.5	9.5	7.54	79.4
8H	2	2325	61.5	71.0	9.5	9.78	102.9
9P	3	0100	71.0	72.0	1.0	1.00	100.0
			*****Drilled from 72 to 73 mbsf*****				
10H	3	0235	73.0	82.5	9.5	8.94	94.1
11H	3	0600	82.5	92.0	9.5	8.32	87.6
12H	3	0630	92.0	101.5	9.5	8.21	86.4
13H	3	0710	101.5	111.0	9.5	8.44	88.8
14H	3	0750	111.0	120.5	9.5	4.87	51.3
15H	3	0845	120.5	130.0	9.5	6.69	70.4
16P	3	1055	130.0	131.0	1.0	1.00	100.0
			*****Drilled from 131 to 132 mbsf*****				
17H	3	1140	132.0	137.5	5.5	5.56	101.1
18Y	3	1255	137.5	138.5	1.0	0.89	89.0
19X	3	1530	138.5	145.0	6.5	9.60	147.7
				Cored totals:	143.0	117.29	82.0
				Drilled total:	2.0		
				Total:	145.0		
204-1250D-							
1H	3	1755	0.0	6.5	6.5	2.76	42.5
2H	3	1910	6.5	16.0	9.5	7.57	79.7
3H	3	2020	16.0	25.5	9.5	10.15	106.8
4H	3	2140	25.5	35.0	9.5	9.89	104.1
5P	3	2255	35.0	36.0	1.0	1.00	100.0
			*****Drilled from 36 to 37 mbsf*****				

Table T1 (continued).

Core	Date (Aug 2002)	Local time (hr)	Depth (mbsf) Top	Depth (mbsf) Bottom	Length (m) Cored	Length (m) Recovered	Recovery (%)
6H	3	2345	37.0	46.5	9.5	10.01	105.4
7H	4	0045	46.5	56.0	9.5	9.92	104.4
8H	4	0220	56.0	65.5	9.5	9.80	103.2
9H	4	0310	65.5	75.0	9.5	10.17	107.1
10H	4	0400	75.0	84.5	9.5	9.55	100.5
11H	4	0450	84.5	94.0	9.5	9.85	103.7
12H	4	0610	94.0	103.5	9.5	7.82	82.3
13P	4	0745	103.5	104.5	1.0	1.00	100.0
			*****Drilled from 104.5 to 105.5 mbsf*****				
14H	4	0825	105.5	115.0	9.5	6.21	65.4
15X	4	1100	115.0	124.6	9.6	8.39	87.4
16X	4	1200	124.6	134.2	9.6	8.65	90.1
17E	4	1345	134.2	135.2	1.0	0.28	28.0
18P	4	1515	135.2	136.2	1.0	1.00	100.0
			*****Drilled from 136.2 to 137.2 mbsf*****				
19X	4	1600	137.2	145.0	7.8	9.65	123.7
				Cored totals:	142.0	133.67	94.1
				Drilled total:	3.0		
				Total:	145.0		
204-1250E-							
1H	4	1950	0.0	6.5	6.5	3.16	48.6
2H	4	2115	6.5	16.0	9.5	8.77	92.3
				Cored totals:	16.0	11.93	74.6
				Drilled total:	0.0		
				Total:	16.0		
204-1250F-							
			*****Drilled from 0 to 100 mbsf*****				
1H	25	0210	100.0	109.5	9.5	8.99	94.6
2H	25	0300	109.5	113.5	4.0	3.94	98.5
3X	25	0410	113.5	119.0	5.5	5.81	105.6
4P	25	0445	119.0	120.0	1.0	1.00	100.0
			*****Drilled from 120 to 121 mbsf*****				
5H	25	0525	121.0	127.3	6.3	4.54	72.1
6X	25	0635	127.3	130.0	2.7	3.79	140.4
7P	25	0730	130.0	131.0	1.0	1.00	100.0
			*****Drilled from 131 to 132 mbsf*****				
8P	25	0910	132.0	133.0	1	0.00	0.0
			*****Drilled from 133 to 134 mbsf*****				
9X	25	1020	134.0	143.6	9.6	8.29	86.4
10X	25	1110	143.6	153.2	9.6	5.96	62.1
11X	25	1205	153.2	162.8	9.6	8.12	84.6
12X	25	1400	162.8	172.4	9.6	8.47	88.2
13X	25	1445	172.4	180.0	7.6	9.19	120.9
				Cored totals:	77.0	69.10	89.7
				Drilled total:	103.0		
				Total:	180.0		

Table T2. Bioevents, Hole 1250C.

Age (Ma)	Bioevent	Top		Bottom		Average depth (mbsf)	Event number*	Comment
		Core, section, interval (cm)	Depth (mbsf)	Core, section, interval (cm)	Depth (mbsf)			
		204-1250C-		204-1250C-				
0.30	LO *Proboscia curvirostris*	4H-CC	30.42	5H-CC	41.30	35.86	1	Diatom
0.27	FO *Emiliania huxleyi*	5H-CC	41.30	6H-CC	51.34	46.32	2	Nannofossil
0.46	LO *Pseudoemiliania lacunosa*	5H-CC	41.30	6H-CC	51.34	46.32	3	Nannofossil
1.59	FO *Calcydiscus macintyrei*	8H-CC	71.23	10H-CC	81.89	76.56	4	Nannofossil

Notes: FO = first occurrence, LO = last occurrence. * = number in Figure **F15,** p. 45.

Table T3. Interstitial water data, Holes 1250C, 1250D, 1250E, and 1250F. (See table notes. Continued on next page.)

Core, section, interval (cm)	Depth (mbsf)	pH	Alkalinity (mM)	Salinity (g/kg)	Cl (mM)	SO_4 (mM)	NH_4 (mM)	PO_4 (µM)	Na (mM)	K (mM)	Mg (mM)	Ca (mM)	B (µM)	Ba (µM)	Fe (µM)	Li (µM)	Mn (µM)	Sr (µM)	DOC (mM)
204-1250C-																			
1H-1, 0–10	0.00	7.67	39.31	34	559	0.6	7.2	370	510	11.8	42.5	2.9	591	66.0	7.8	12.00	1.22	74.65	12.79
2H-CC, 1–10	5.07	7.71	64.10	39	598	0.9	10.4	355	537	13.5	53.0	3.0	721	82.7	9.9	16.04	1.19	94.28	—
3H-2, 140–150	16.90	7.41	68.48	38	592	0.5	12.1	364	543	13.9	50.4	3.5	835	108.1	15.3	20.22	1.15	93.13	14.17
3H-5, 140–150	21.40	7.51	68.02	37	581	0.0	11.5	367	537	13.6	48.4	3.3	882	106.2	9.0	20.94	1.05	91.02	—
4H-2, 140–150	26.40	7.81	68.85	36	574	0.1	12.2	346	530	13.3	47.0	3.1	874	108.1	39.0	21.50	1.04	92.17	14.49
4H-4, 140–150	29.00	7.40	68.85	35	578	0.2	12.4	363	495	13.2	47.8	5.6	920	110.6	35.1	22.27	1.47	91.46	—
5H-2, 140–150	35.88	7.43	68.92	35	565	0.3	14.2	327	486	13.8	44.9	3.3	890	115.9	13.4	22.06	2.22	87.67	17.43
5H-5, 133–143	40.31	7.53	69.91	36	564	0.5	14.2	350	481	14.1	44.0	3.1	892	112.4	17.2	22.84	2.29	90.93	—
6H-2, 57–67	44.57	7.62	57.70	32	503	2.9	12.2	298	405	11.3	36.8	2.9	687	82.6	25.0	19.18	0.96	73.72	14.74
6H-5, 118–128	48.95	7.54	70.45	36	564	0.4	14.8	323	525	13.9	43.0	3.0	844	109.9	16.3	23.45	0.81	91.66	—
7H-5, 130–140	58.00	7.76	70.50	35	562	0.4	13.9	299	490	14.2	40.4	3.0	747	114.1	7.9	26.13	0.69	93.36	18.10
8H-2, 140–150	64.40	7.44	69.36	35	547	0.5	15.3	354	473	14.1	39.9	3.2	848	114.1	6.9	26.54	0.64	92.97	17.69
8H-5, 140–150	68.90	7.44	68.23	35	547	0.1	15.0	350	475	13.2	39.6	3.2	824	122.4	12.0	28.84	0.69	95.56	—
10H-2, 81–96	75.31	7.44	62.74	34	524	0.9	14.4	355	453	12.6	38.1	3.1	794	111.5	7.9	30.84	0.58	89.30	22.77
10H-5, 135–150	79.81	7.58	78.98	36	559	0.1	16.0	382	490	13.4	41.7	4.1	908	135.6	10.0	35.90	1.28	101.52	18.03
11H-3, 95–110	86.36	7.46	61.89	33	485	1.7	13.8	303	428	12.1	34.0	3.4	680	101.5	3.8	30.13	0.58	80.66	—
11H-5, 130–145	89.31	7.54	68.10	36	554	0.7	16.2	367	480	13.5	40.2	3.7	858	128.8	6.0	37.77	0.74	98.29	—
12H-1, 50–65	92.50	7.45	67.36	35	543	0.7	15.6	356	466	13.0	39.6	3.8	848	113.1	13.3	37.85	1.04	96.91	—
12H-5, 140–155	98.43	7.61	68.38	36	552	0.1	15.5	284	479	13.9	38.5	3.0	823	130.3	4.5	39.49	0.57	95.88	—
13H-2, 130–150	103.19	7.36	66.33	34	517	0.5	16.2	371	450	11.7	36.8	4.0	814	125.8	10.1	35.22	0.88	97.52	—
13H-5, 130–150	107.69	7.51	68.29	35	543	0.4	15.7	319	473	12.9	37.8	4.1	826	135.4	5.7	37.19	0.88	102.86	21.39
14H-2, 130–150	113.80	7.63	66.72	35	544	1.0	16.1	267	472	13.2	37.0	4.5	710	134.3	4.1	35.56	0.56	100.48	—
14H-4, 40–60	115.33	7.46	66.28	35	545	0.8	17.1	379	473	12.0	38.6	4.6	784	140.5	7.5	35.48	0.67	103.79	18.45
15H-1, 106–126	121.56	7.55	61.94	35	542	1.7	15.7	257	373	9.5	36.7	4.7	784	127.2	3.6	37.16	0.63	96.90	—
15H-4, 100–120	125.86	7.45	64.61	35	543	0.3	16.8	259	473	12.0	35.1	4.6	783	188.3	4.9	39.72	0.76	101.27	17.63
16P-1, 64–84	130.64	—	—	—	—	1.4	—	—	—	—	—	—	—	—	—	—	—	—	—
17H-1, 130–150	133.30	7.49	60.68	34	543	0.8	16.4	133	469	11.9	35.7	4.6	748	200.7	9.5	47.71	1.09	96.95	—
17H-2, 140–150	134.90	—	—	—	541	—	—	—	—	—	—	—	—	—	—	—	—	—	—
17H-3, 130–150	136.30	7.76	58.29	34	551	1.7	17.1	124	471	12.5	34.4	4.5	680	156.7	5.6	49.47	1.12	91.41	12.45
19X-2, 130–150	141.30	7.40	58.53	34	552	0.5	16.0	129	474	11.3	35.9	4.4	743	203.0	9.3	56.86	1.12	94.27	—
19X-5, 130–150	145.75	7.46	58.47	35	551	0.0	15.9	117	471	11.4	34.0	4.5	701	204.0	7.2	61.95	1.27	92.02	14.47
204-1250D-																			
3H-4, 52–62	21.02	7.51	66.22	37	578	0.2	12.1	369	547	13.4	47.5	3.6	801	110.7	25.6	20.55	1.00	90.13	14.22
3H-7, 140–150	24.90	7.48	67.65	36	578	0.4	12.9	359	540	13.1	47.0	3.3	757	113.5	21.6	20.25	1.06	88.35	12.61
4H-5, 140–150	32.90	7.38	65.93	35	545	0.8	13.4	347	525	12.8	44.1	3.4	783	114.6	20.7	29.86	1.25	83.56	13.54
5P-1, 20–30	35.20	—	—	—	568	1.7	—	—	535	14.1	—	—	—	—	—	—	—	—	—
6H-2, 145–150	39.95	—	—	—	562	0.6	14.3	309	501	14.0	—	—	—	—	—	—	—	—	—
6H-5, 129–144	44.24	7.49	69.02	36	553	—	14.1	350	—	—	42.7	4.2	897	114.3	18.4	23.22	1.08	90.86	12.15
8H-5, 130–150	61.48	7.41	68.96	36	554	0.8	—	362	545	14.3	40.0	3.4	831	116.4	15.7	26.09	0.60	92.96	13.75
10H-5, 140–150	81.22	7.45	66.74	36	546	0.8	16.1	349	496	14.0	—	—	847	142.6	5.2	37.14	0.69	95.27	15.86
12H-5, 0–20	99.75	7.54	68.44	35	546	1.6	17.9	343	486	13.6	—	—	822	131.1	6.2	40.53	0.92	97.73	15.70
13P-1, 75–95	104.25	—	—	—	—	1.4	—	—	481	12.6	—	—	—	—	—	—	—	—	—
14H-4, 0–20	109.83	7.81	66.72	35	547	0.3	17.7	222	485	14.5	—	—	694	147.7	3.5	36.79	0.69	97.13	17.40
15X-5, 0–25	120.91	7.31	66.19	35	547	1.1	16.6	367	488	12.1	—	—	841	156.9	9.5	37.54	0.96	103.73	12.98
16X-4, 130–150	130.32	7.46	62.86	35	—	1.0	17.4	249	478	11.3	—	—	813	178.6	12.4	43.78	1.21	101.20	11.24
18P-1, 20–30	135.40	—	—	—	—	4.1	—	—	470	12.2	—	—	—	—	—	—	—	—	—
19X-5, 130–150	144.50	7.30	57.36	34	—	1.1	16.9	116	478	11.1	—	—	721	180.0	4.9	61.19	0.96	91.98	11.31

Table T3 (continued).

Core, section, interval (cm)	Depth (mbsf)	pH	Alkalinity (mM)	Salinity (g/kg)	Cl (mM)	SO_4 (mM)	NH_4 (mM)	PO_4 (µM)	Na (mM)	K (mM)	Mg (mM)	Ca (mM)	B (µM)	Ba (µM)	Fe (µM)	Li (µM)	Mn (µM)	Sr (µM)	DOC (mM)
204-1250E-																			
1H-1, 140–150	1.40	8.16	39.31	34	555	1.7	1.5	121	492	12.2	44.9	5.6	513	61.4	14.8	21.28	2.17	76.93	—
1H-2, 131–141	2.81	8.31	38.20	30	—	1.5	3.1	226	438	10.1	38.6	5.6	439	75.7	14.5	10.13	2.55	65.04	—
2H-5, 140–150	13.90	7.51	69.07	39	613	1.4	13.6	360	568	14.3	48.1	4.2	803	112.8	13.9	20.35	1.94	98.97	—
204-1250F-																			
1H-2, 122–142	101.55	7.14	63.35	35	528	0.5	15.1	333	454	12.1	37.0	3.7	810.5	126.3	7.9	37.72	—	95.35	—
1H-3, 130–150	103.05	7.18	67.27	35	550	0	16.0	358	475	12.7	37.9	4.0	841.8	135.5	11.4	38.02	—	96.66	—
1H-4, 130–150	104.55	7.10	68.44	36	552	0	16.7	346	481	12.6	38.3	3.9	852.4	140.3	10.2	37.72	—	101.33	—
1H-5, 130–150	106.05	7.18	66.59	35	542	0	16.5	349	474	12.5	37.4	3.7	827.6	131.1	9.6	37.72	—	96.45	—
1H-6, 130–150	107.55	7.25		35	538	0	16.5	336	473	12.5	37.4	3.9	793.8	132.2	7.6	36.09	—	95.53	—
2H-1, 130–150	110.80	7.47	66.54	34	546	0	16.8	354	474	12.5	36.3	4.2	806.5	141.8	8.7	35.92	—	97.87	—
2H-2, 130–150	112.30	7.18	66.76	35	545	0.4	16.3	321	470	12.1	37.4	4.2	756.9	132.5	10.0	35.24	—	97.18	—
2H-3, 69–89	113.19	7.23	66.35	35	545	0	16.6	356	480	12.2	37.4	4.3	781.9	145.9	7.5	36.45	—	102.14	—
3X-1, 130–150	114.80	7.17	68.47	36	544	0	16.7	362	475	12.0	37.0	4.4	838.3	163.7	17.7	37.88	—	103.24	—
3X-2, 130–150	116.30	7.26	66.90	35	547	0	17.3	336	472	11.8	37.4	4.6	756.9	162.3	5.8	35.89	—	101.74	—
3X-3, 130–150	117.80	7.38	66.46	35	542	0.1	17.3	302	376	9.7	35.6	4.3	709.2	150.3	5.6	35.83	—	96.43	—
4P-1, 10–20	119.20	—	—	—	—	—	—	—	—	—	—	—	—	—	—	—	—	—	—
5H-1, 130–150	122.30	7.21	64.36	35	545	0	17.4	286	460	11.6	32.9	4.2	756.6	172.7	8.0	37.86	—	95.44	—
5H-2, 130–150	123.80	7.41	64.85	35	544	0	18.1	141	482	12.7	34.5	4.4	679.6	184.2	4.7	40.21	—	95.53	—
6X-1, 130–150	128.60	7.14	64.56	35	546	0	17.4	265	478	11.2	34.3	4.7	808.1	187.8	6.3	42.42	—	97.96	—
6X-2, 100–120	129.80	7.13	64.36	35	547	0	17.6	201	467	11.0	34.8	4.5	728.1	198.4	16.4	42.79	—	95.65	—
7P-1, 20–30	130.20	—	—	—		0.5	—	—	—	—	—	—	—	—	—	—	—	—	—
9X-2, 130–150	136.80	7.19	62.26	35	545	0	17.9	163	—	—	34.4	4.4	766.2	218.5	9.1	50.39	—	93.90	—
9X-5, 130–150	141.30	7.01	61.06	35	546	0	17.6	166	—	—	35.1	4.4	796.2	213.6	10.5	56.12	—	92.18	—
10X-1, 130–150	144.90	7.06	58.42	35	546		17.5	136	—	—	35.4	4.4	785.4	214.2	12.9	64.45	—	89.63	—
10X-3, 130–150	147.90	7.51	56.03	34	543	0	17.6	94	—	—	35.6	4.4	737.9	185.6	4.2	66.09	—	87.78	—
11X-2, 98–123	155.68	7.13	50.61	34	541	0.6	17.0	150	—	—	33.1	3.8	798.6	152.3	6.8	57.88	—	84.51	—
12X-3, 125–150	167.05	7.20	45.91	34	545	0.2	16.3	131	—	—	31.2	3.4	702.9	128.4	13.2	49.06	—	83.22	—
13X-3, 125–150	176.65	7.16	40.77	33	543	0.4	16.0	137	—	—	28.6	3.0	689.5	113.6	11.4	43.77	—	82.55	—

Notes: DOC = dissolved organic carbon. — = no sample was available.

Table T4. Concentrations of methane, ethane, ethylene, and propane in headspace gas, Holes 1250C, 1250D, and 1250E.

Core, section, interval (cm)	Depth (mbsf)	C_1 (ppmv)	C_2 (ppmv)	$C_{2=}$ (ppmv)	C_3 (ppmv)	C_1/C_2	C_1 (mM)
204-1250C-							
1H-1, 120–125	1.20	12,019	13.7			880	2.3
2H-CC	5.06	7,271	9.3			782	1.9
3H-3, 0–5	17.00	16,942	10.3			1,638	3.5
4H-4, 0–5	27.60	34,893	5.9			5,944	9.3
5H-3, 0–5	35.98	13,115	2.1			6,367	2.6
6H-3, 0–5	44.77	9,654					1.5
7H-5, 0–5	56.70	10,442	1.5	0.5	5.2	7,201	1.9
8H-3, 0–5	64.50	8,964	1.1			8,076	2.1
10H-3, 0–5	75.46	15,818	3.3		3.4	4,793	2.5
11H-3, 0–5	85.41	13,918	2.4		6.7	5,728	2.1
12H-2, 0–5	92.65	12,874	2.7		6.0	4,716	1.9
13H-3, 0–5	103.39	17,293	25.4			681	2.7
14H-3, 0–5	114.00	13,276	36.1		5.9	368	1.8
15H-2, 0–5	121.86	12,111	27.6			439	2.0
17H-3, 0–5	135.00	12,894	30.0			430	2.4
19X-3, 0–5	141.50	11,271	18.7			603	1.9
204-1250D-							
1H-2, 0–5	1.19	4,710	8.4			559	1.4
2H-4, 0–5	10.26	10,539	8.1			1,295	2.0
3H-4, 0–5	20.50	13,511	5.2			2,588	2.9
4H-3, 0–5	28.50	5,001	1.3			4,001	1.2
6H-2, 0–5	38.50	16,917	1.5			11,587	2.4
8H-4, 0–5	58.71	19,284	1.4			13,974	3.0
10H-4, 0–5	78.32	16,422	1.7			9,492	2.8
14H-5, 0–5	111.33	2,668	21.3	4.1		125	0.4
15X-3, 0–5	118.00	10,232	38.6	8.0		265	1.4
16X-3, 0–5	127.60	7,209	15.7			459	1.6
19X-3, 0–5	140.20	8,330	11.9			698	1.8
204-1250E-							
2H-3, 0–5	9.50	12,038	11.97			1,006	2.0

Note: C_1 = methane, C_2 = ethane, $C_{2=}$ = ethylene, C_3 = propane.

Table T5. Concentration of light hydrocarbon and nonhydrocarbon gases in VAC samples of core gas void, Holes 1250B, 1250D, 1250E, and 1250F. (**See table notes.** Continued on next page.)

Core, section, interval (cm)	Depth (mbsf)	C_1 (ppmv)	C_2 (ppmv)	C_3 (ppmv)	*i*-C_4 (ppmv)	*n*-C_4 (ppmv)	*i*-C_5 (ppmv)	*n*-C_5 (ppmv)	*i*-C_6 (ppmv)	CO_2 (ppmv)	O_2 (ppmv)	N_2 (ppmv)	C_1/C_2
204-1250B-													
1H-1, 100	1.00	942,209	743	23.8	7.3	10.0	5.5			387,582	6,230	22,069	1,268
2H-1, 55	5.05	805,408	772	8.4						5,251	20,744	1,043	1,043
3H-1, 96	14.96	871,052	188							31,227	16,161	66,238	4,646
3H-6, 145	22.95	950,127	128	9.0						19,968	2,356	7,262	7,434
4H-2, 70	25.70	954,172	139	12.2						16,663	1,114	8,934	6,855
4H-4, 105	28.65	932,816	91.9	12.9						13,190	8,299	35,128	10,150
5H-1, 120	34.20	946,099	101	11.7						19,265	2,562	10,208	9,414
5H-5, 0	38.98	969,790	81.8	13.5						11,005	75	1,348	11,856
6H-6, 0	49.05	983,242	98.3	5.2						5,236	22	528	10,002
7H-5, 130	58.00	955,972	37.8	33.6	5.6					18,753	52	1,856	25,290
8H-1, 120	62.70	952,778	21.1	34.3	5.1					2,231	6,438	166,773	45,155
8H-6, 29	69.29	973,349	103	11.8						5,974	1,455	1,313	9,432
10H-3, 6	75.52	977,463	127	2.0						6,009	31	560	7,709
10H-3, 69	76.15	976,144	94.2	20.0									10,367
10H-3, 69	76.15	972,148	101	25.4						9,648	78	1,045	9,592
10H-6, 33	80.29	966,719	79.5	25.6	3.5					9,258	87	1,113	12,163
11H-2, 66	84.62	959,452	41.9	33.2	4.4								22,888
11H-6, 0	89.46	892,025	49.0	44.7	6.2					15,835	13,662	60,774	18,216
12H-2, 66	93.31	923,921	72.7	67.3	10.0	4.1				46,066	1,911	1,550	12,702
12H-5, 120	98.23	961,546	118	47.5	7.4					14,440	87	829	8,125
13H-2, 0	101.89	967,955	1,211	12.9						2,857	15,561	57,521	800
13H-6, 0	107.89	965,380	397	23.4	4.5					6,546	1,965	1,552	2,434
14H-1, 55	111.55	921,755	919	58.3	14.4		5.3						1,003
14H-3, 45	114.45	963,094	117	45.0						14,505	73	795	8,232
15H-4, 42	125.28	792,658	515	39.1	11.3					10,972	37,404	145,466	1,539
17H-4, 20	136.70	957,094	444	5.0						15,616	298	11,412	2,156
19H-4, 126	144.21	939,755	477	7.3						333	296	9,802	1,969
204-1250D-													
2H-1, 109	7.59	958,899	475.6	5.3						16,369	285	18,664	2,016
2H-5, 50	12.26	957,977	706.1	6.3						5,045	324	16,306	1,357
3H-1, 126	17.26	956,395	132.5	11.6	4.2					15,690	189	24,679	7,218
4H-1, 149	26.99	954,905	58.3	9.0						13,468	244	13,855	16,379
6H-2, 98	39.48	949,159	10.5	8.5	2.7					11,917	154	14,459	90,396
8H-7, 51	63.69	817,572	33.3	3.8						3,497	151	9,911	24,530
10H-7, 76	83.58	804,629	20.2	12.1	37.7					14,565	112	7,161	39,892
14H-2, 100	108.00	949,473	1,106.0	27.7	5.4					7,209	165	7,043	858
15X-3, 96	118.96	919,613	915.3	96.5	34.4					29,586	368	25,144	1,005
16X-3, 47	128.07	944,246	430.3	7.2						12,862	329	10,477	2,194
204-1250E-													
1H-1, 140	1.40	837,221	921.9	4.4						13,311	7,153	13,874	908
2H-1, 10	6.60	952,495	664.2	9.8						14,249	309	11,718	1,434
2H-1, 55	7.05	879,538	480.5	7.8						22,145	6,276	63,968	1,830
204-1250F-													
1H-2, 23	101.73	547,504	121.6	15.3									4,503
1H-2, 23	101.73	537,946	64.6							10,572	90,665	340,094	8,327
1H-2, 141	102.91	951,008	275	20.3									3,454
1H-2, 141	102.91	946,737	146							10,533	1,672	1,287	6,497
1H-3, 102	104.02	958,756	324	20.1									2,962
1H-3, 102	104.02	953,652	171							7,843	1,330	950	5,577
1H-4, 7	104.57	961,734	392	25.5						4,755	1,446	1,201	2,456
1H-4, 94	105.44	959,698	175	39.3						6,283	1,139	1,134	5,496
1H-5, 75	106.75	966,270	531	25.0						5,120	1,489	1,112	1,820
1H-6, 149	108.99	956,640	619	27.9		3.2	1.5	1.4		3,268	998	156	1,545
2H-1, 76	110.26	936,949	815	81.5	24.7	4.5	8.5			12,119	6,516	16,156	1,150
2H-2, 96	111.96	957,385	1,107	73.1									865
2H-3, 1	112.51	959,947	1,167	76.5	33.1	2.6	9.2			6,360	2,299	1,351	823
2H-3, 7	112.57	945,991	1,144	87.9	34.8	3.3	10.5			10,303	3,691	4,737	827
3X-2, 54	115.54	934,700	1,258	143.1	83.6	1.6	26.9			26,587	3,099	5,886	743
5H-1, 34	121.34	948,353	771	49.5									1,230
5H-1, 130	122.00	964,914	691	42.8	18.4	1.9	5.5			10,107	1,581	1,169	1,396
5H-2, 55	123.05	968,006	620	29.8	9.4	1.9	5.2			6,747	1,559	1,112	1,561
6X-1, 100	128.30	933,551	647	12.4		5.8	4.9			28,678	2,325	9,901	1,443
6X-2, 26	129.06	907,593	618	12.7		4.8	3.2			31,412	4,000	16,977	1,469
9X-1, 106	135.06	944,049	409	8.1			1.8			8,178	1,551	1,492	2,308
9X-2, 124	136.74	955,343	449	7.9			1.9						2,128

Table T5 (continued).

Core, section, interval (cm)	Depth (mbsf)	C_1 (ppmv)	C_2 (ppmv)	C_3 (ppmv)	*i*-C_4 (ppmv)	*n*-C_4 (ppmv)	*i*-C_5 (ppmv)	*n*-C_5 (ppmv)	*i*-C_6 (ppmv)	CO_2 (ppmv)	O_2 (ppmv)	N_2 (ppmv)	C_1/C_2
10X-3, 73	147.33	770,925	312										2,474
10X-3, 73	147.33	796,757	483	10.5			3.1			2,437	37,416	137,219	1,650
11X-2, 98	155.68	972,109	4,011	872	400	8.6	38.4			7,009	1,456	1,382	242
11X-3, 145	157.38	929,271	4,174	906	409	7.6	32.7			8,792	5,800	15,703	223
11X-5, 0	158.90	963,019	4,426	1,042	445	5.3	29.5			6,920	1,183	970	218
12X-1, 111	163.91	928,188	5,330	1,623	496	339	1.3			13,185	2,684	12,061	174
12X-2, 133	165.63	941,979	5,473	1,808	481	402	185	1.4		11,258	2,073	9,557	172
12X-4, 119	168.49	930,330	5,596	1,921	652	675	242	2.3		15,864	1,522	5,076	166
12X-5, 45	169.25	931,335	5,203	1,844	667	676	240	3.2		3,430	2,733	10,307	179
13X-2, 72	174.62	924,075	7,465	7,077	798	1,101	304	28.0	7.7	15,160	4,538	14,055	124
13X-5, 30	178.70	302,182	2,408	1,094	378	428	182	8.4	1.8	4,140	149,412	535,498	126

Notes: C_1 = methane, C_2 = ethane, C_3 = propane, *i*-C_4 = isobutane, *n*-C_4 = normal butane, *i*-C_5 = isopentane, *n*-C_5 = normal pentane, *i*-C_6 = isohexane, CO_2 = carbon dioxide, O_2 = oxygen, N_2 = nitrogen. Blank cells = below detection limit.

Table T6. Composition of gas from analyses of decomposed samples of gas hydrate, Holes 1250C, 1250D, and 1250F.

Core, section, interval (cm)	Depth (mbsf)	C_1 (ppmv)	C_2 (ppmv)	C_3 (ppmv)	*i*-C_4 (ppmv)	*n*-C_4 (ppmv)	*n*-C_5 (ppmv)	*i*-C_6 (ppmv)	H_2S (ppmv)	CO_2 (ppmv)	O_2 (ppmv)	N_2 (ppmv)	C_1/C_2
204-1250C-													
1H-CC	1.39	977,550	840	8.3					1,550	244	40	701	1,163
1H-CC	1.39	557,737	504	8.7					426	380	47,529	183,768	1,107
2H-CC, 0	5.06	944,819	624	11.0	4.2					4,360	10,505	17,404	1,513
11H-3, 94	86.35	916,522	40.3							5,328	11,754	41,594	22,742
204-1250D-													
1H-1, 100	1.00	829,572	624	17.1					1,198	628	24,874	118,566	1,329
1H-2, 14–17	1.33	731,754	633	4.5					456	1,007	34,866	153,405	1,156
1H-2, 14–17	1.33	553,749	538.4	9.8						1,678	30,220	137,375	1,029
1H-2, 14–17	1.33	796,716	673.4	7.5						2,871	201	7,644	1,183
10H-3, 53–84	78.01	795,474	17.5	97.2						4,013	452	12,298	45,456
204-1250F-													
1H-1, 23	100.23	903,894	27							2,554	17,393	61,192	33,981

Notes: C_1 = methane, C_2 = ethane, C_3 = propane, *i*-C_4 = isobutane, *n*-C_4 = normal butane, *n*-C_5 = normal pentane, *i*-C_6 = isohexane, H_2S = hydrogen sulfide, CO_2 = carbon dioxide, O_2 = oxygen, N_2 = nitrogen. Blank cells = below detection limit.

Table T7. Composition of gas from PCS experiments, Holes 1250C, 1250D, and 1250F.

Sample	Volume (mL)	C_1 (ppm)	C_2 (ppm)	C_3 (ppm)	*i*-C_4 (ppm)	*n*-C_4 (ppm)	*i*-C_5 (ppm)	*n*-C_5 (ppm)	*i*-C_6 (ppm)	*n*-C_6 (ppm)	O_2 (ppm)	N_2 (ppm)	CO_2 (ppm)	C_1/C_2
204-1250C-9P (71–72 mbsf)														
G1	60	501,446	31.0								83,713	385,007	897	17,581
G2	220	925,918	71.0								47,965	764	252	
G3	420	953,044	65.0	10.0							306	24,592	279	
G4	210	946,204	50.0	17.0							386	31,094	574	
G5	115													
G6	250	738,893	33.5	17.6							21,736	145,161	627	
G7	380	878,475	37.7	24.7							731	51,237	1,617	
G8	400													
G9	190	881,199	41.7	3.9	3.9						1,149	74,059	3,453	
G10	80	899,645.1	50.2	26.8	4.3						714	60,874	4,256	
G11	70	906,732.1	54.1	27.1	4.1						637	63,792	3,142	
G12	80	909,122.5	56.1	27.7	4.3						699	65,296	2,992	
204-1250D-5P (35–36 mbsf)														
G1	200	729,034	40.4	3.0							32,438	186,797	637	16,215
G2	200	921,658	55.6	1.7							850	41,984	440	
G3	260	946,660	63.1								305	17,797	18	
G4	510	791,860	48.0								207	19,455	223	
G5	400	826,747	51.5	5.0							22,865	129,255	363	
G6	330	941,295	54.8	4.4							549	37,521	390	
G7	320	928,858	53.8								829	46,505	308	
G8	360	898,650	54.3								1,362	68,884	390	
G9	380	890,531	54.0								1,516	77,276	775	
G10	430	894,101	55.9	4.2							1,081	75,986	1,452	
G11	320	863,349	53.2	4.3							1,304	99,615	1,476	
G12	250	911,154	58.3	4.9							389	63,135	2,742	
G13	150	905,232	56.3	5.4							687	66,506	3,344	
G14	90	901,936	57.7	5.7							666	68,273	3,337	
G15	110	875,187	58.4	6.8							882	84,718	3,267	
G16	150	682,214	52.1	6.3							41,645	226,215	4,399	
204-1250D-13P (103.5–104.5 mbsf)														
G1	170	852,437	285	7.9							12,775	104,464	1,396	3,230
G2	620	970,326	406	5.8							191	7,212	548	
G3	470	942,269	349	8.6							1,228	36,350	611	
G4	310	948,830	288	14.0							796	27,721	725	
G5	410	960,724	250	21.5		3.6					176	12,477	743	
G6	350	941,697	217	34.1	21.8	4.8					657	30,008	1,339	
G7	390	940,601	218	44.2	24.8	5.6					632	31,230	2,724	
G8	200	941,177	231	45.7	27.5	6.3					315	29,179	4,634	
G9	100	928,502	238	45.6	29.0	6.8					643	41,658	4,367	
G10	110	933,304	265	128	29.0	6.9					165	32,591	4,860	
204-1250D-18P (135.2–136.2 mbsf)														
G1	60	420,427	110			4.0					456,038	89,069	1,342	2,837
G2	300	875,444	247			5.0					552	33,710	510	
G3	290	937,555	322			7.3					791	32,140	829	
G4	280	921,366	334			8.8					1,138	47,069	609	
G5	180	907,174	350			9.2					1,355	60,289	1,194	
G6	100	938,554	373			9.1					209	32,260	1,426	
G7	175	918,267	385.1			6.8					678	45,691	1,637	
204-1250F-4P (119–120 mbsf)														
G1	130	669,285	770	69.0	41.2	1.3	10.0				52,333	271,494	619	885
G2	490	844,042	867	114	106	2.4	28.1				6,739	135,599	376	
G3	460	831,608	890	98.0	74.7		16.1	2.9			4,915	136,105	311	
G4	500	866,421	945	97.5	56.6		12.1	1.9			4,338	114,988	376	
G5	480	873,617	977	95.2	98.3	4.4	20.5	5.6			7,294	94,741	632	
G6	560	912,731	1,037	98.6	120	2.2	34.9				3,840	54,944	1,348	
G7	520	923,996	1,065	102	76.7		16.9	2.9			3,794	47,437	1,543	
G8	620	930,803	1,083	105	98.1		23.3				3,277	37,010	2,465	
G9	810	945,746	1,070	115	98.2		25.8				2,919	18,714	4,669	
G10	210	941,795	1,126	114	104	2.1	30.2	3.8			2,615	27,764	5,102	
G11	330	948,673	1,138	118	103	2.0	31.5	4.3			2,334	22,286	7,467	
G12	280	938,506	1,120	122	153	3.2	66.7	5.7			3,895	19,970	9,024	

Note: C_1 = methane, C_2 = ethane, C_3 = propane, *i*-C_4 = isobutane, *n*-C_4 = normal butane, *i*-C_5 = isopentane, *n*-C_5 = normal pentane, *i*-C_6 = isohexane, *n*-C_6 = normal hexane, O_2 = oxygen, N_2 = nitrogen, CO_2 = carbon dioxide. Blank cells = below detection limit.

Table T8. Carbonate carbon, calcium carbonate, total carbon, organic carbon, total nitrogen, and total sulfur contents and C/N ratios, Holes 1250C and 1250D.

Core, section, interval (cm)	Depth (mbsf)	Carbonate carbon (wt%)	$CaCO_3$ (wt%)	Total carbon (wt%)	Organic carbon (wt%)	Total nitrogen (wt%)	Total sulfur (wt%)	C/N
204-1250C-								
3H-5, 66–67	20.66	0.45	3.74	2.09	1.64	0.21	0.58	7.81
4H-5, 54–55	29.64	0.12	1.00	1.43	1.31	0.18	0.38	7.28
5H-5, 58–59	39.56	0.33	2.79	1.68	1.35	0.16	0.32	8.44
7H-1, 80–81	52.80	0.39	3.27	1.42	1.03	0.15	0.46	6.87
10H-1, 93–94	73.93	0.65	5.40	1.78	1.13	0.16	0.67	7.06
11H-1, 94–95	83.44	0.64	5.35	2.01	1.37	0.17	0.29	8.06
12H-1, 26–27	92.26	0.31	2.59	1.74	1.43	0.19	0.31	7.53
13H-3, 76–78	104.16	0.45	3.78	2.00	1.55	0.20	0.42	7.75
14H-1, 90–91	111.90	0.48	3.98	1.55	1.07	0.15	0.14	7.13
15H-1, 88–89	121.38	0.43	3.60	1.84	1.41	0.19	0.22	7.42
17H-1, 75–76	132.75	0.37	3.11	1.70	1.33	0.18	0.46	7.39
19X-5, 71–72	145.16	0.46	3.85	1.72	1.26	0.17	0.33	7.41
204-1250D-								
2H-1, 34–35	6.84	0.29	2.42	1.63	1.34	0.16	0.44	8.38

Table T9. Rock-Eval pyrolysis of samples, Hole 1250C.

Core, section, interval (cm)	Depth (mbsf)	Organic carbon (wt%)	S_1 (mg/g)	S_2 (mg/g)	Production index ($S_1/[S_1+S_2]$)	Hydrogen index (mg S_2/g C)	T_{max} (°C)
204-1250C-							
5H-5, 58–59	39.56	1.35	0.35	2.06	0.15	153	404
11H-1, 94–95	83.44	1.37	0.30	1.96	0.13	143	410
13H-3, 76–78	104.16	1.55	0.35	2.40	0.13	155	413
17H-1, 75–76	132.75	1.33	0.26	1.95	0.12	147	408
19X-5, 71–72	145.16	1.26	0.20	1.82	0.10	144	412

Note: S_1 and S_2 are as defined in **"Organic Matter Characterization,"** p. 18, in "Organic Geochemistry" in the "Explanatory Notes" chapter.

Table T10. Intervals sampled for microbiology, Holes 1250D and 1250E.

Core, section, interval (cm)	Depth (mbsf)
204-1250D-	
3H-2, 145–150	18.95
3H-7, 0–140	23.50
4H-2, 145–150	28.45
4H-5, 106–140	32.56
6H-5, 20–129	43.15
8H-5, 63–130	60.81
10H-5, 46–140	80.28
12H-5, 20–75	99.95
14H-4, 20–95	110.03
15X-5, 25–115	121.16
16X-4, 59–130	129.61
19X-5, 60–130	143.80
204-1250E-	
1H-1, 0–140	0.00
1H-2, 0–131	1.50
2H-1, 1–150	6.51
2H-5, 0–140	12.50

Table T11. Core quality indicators in intervals sampled for microbiology at Site 1250. Perfluorocarbon tracer samples were not taken at Site 1250.

Core, section, interval (cm)	Depth (mbsf)	Microspheres per g	
		Inside core	Outer edge
204-1250D-			
3H-7, 130–140	24.80	BDL	BDL
4H-5, 120–130	32.70	BDL	992
6H-5, 109–119	44.04	BDL	748
8H-5, 120–130	61.38	BDL	54,000
10H-5, 125–135	81.07	BDL	2,520
12H-5, 20–30	99.95	BDL	30,000
14H-4, 30–40	110.13	258	2,220
16X-4, 130–140	130.32	BDL	11,000
19X-5, 120–130	144.40	199	181
204-1250E-			
1H-1, 125–135	1.25	1,240	3,920
2H-1, 90–100	7.40	9,160	13,600

Note: BDL = below detection limit.

Table T12. Presence of gas hydrate based on infrared images of cores in liners, Holes 1250C and 1250D. (See table notes. Continued on next page.)

Core, section	ΔT (°C)	Gas hydrate texture*	Depth interval (mbsf)† Top	Depth interval (mbsf)† Bottom	Anomaly designation‡	Sampled interval Top (cm)	Sampled interval Bottom (cm)	Sampled interval Depth (mbsf)
204-1250C-								
1H-1			NA		NA	20	22	0.20
1H-1			NA		NA	122	125	1.22
2H-1			NA		NA	0	56	4.50
2H-CC			NA		NA	0	1	5.06
3H	–0.5	Disseminated	14.27	14.50	IR344			
4H	–0.6	Disseminated	23.68	24.19	IR345			
4H	–1.6	Disseminated; vein	24.65	24.85	IR346			
4H	–0.5	Disseminated	25.60	25.65	IR347			
4H-3	–4.3	Vein; nodular	28.28	28.65	IR348	100	110	27.50
5H	–2.2	Vein on steeply dipping fracture	33.90	34.10	IR349			
5H	–0.7	Disseminated; hint of fracture parallel to IR349	34.30	34.50	IR350			
5H	–1.7	Disseminated; nodular or vein	34.75	35.65	IR351			
5H	–4.9	Vein; steeply dipping	35.85	36.10	IR352			
5H	–0.6	Disseminated	36.30	36.70	IR353			
5H	–0.6	Disseminated	37.35	37.42	IR354			
5H	–0.8	Disseminated	38.97	39.00	IR355			
5H	–0.4	Disseminated; nodular	39.25	39.28	IR356			
5H	–0.7	Disseminated	40.18	40.23	IR357			
5H	–3.1	Vein parallel to bedding	41.86	41.90	IR358			
6H	–1.2	Disseminated; mottled	43.62	43.80	IR359			
6H	–1.6	Vein; moderate dip	44.25	44.37	IR360			
6H-2	–3.0	Nodular	44.70	44.76	IR361	67	77	44.67
6H	–1.7	Vein; slight dip	45.40	45.46	IR362			
6H	–0.4	Disseminated	46.22	46.30	IR363			
6H	–0.4	Disseminated	48.60	48.65	IR364			
8H	–0.5	Disseminated	62.40	62.50	IR365			
8H	–1.3	Vein; parallel to bedding	66.39	66.57	IR366			
8H	–4.2	Vein; parallel to bedding	67.45	67.64	IR367			
8H	–1.6	Vein; parallel to bedding	68.60	68.67	IR368			
8H	–1.6	Disseminated	69.41	69.44	IR369			
10H	–1.4	Disseminated	74.30	74.65	IR370			
10H	–1.1	Disseminated; vein	75.55	75.63	IR371			
10H	–1.0	Vein	75.78	75.80	IR372			
10H	–2.5	Disseminated	75.92	76.06	IR373			
10H	–1.6	Nodular	76.47	76.60	IR374			
10H	–1.4	Disseminated	77.05	77.16	IR375			
11H-3	–4.8	Nodular	87.10	87.20	IR376	94	95	86.35
12H-1	–1.5	Vein; nodular	92.90	92.95	IR377	50	51	92.50
12H	–3.6	Nodular	93.05	93.10	IR378			
13H	–1.0	Disseminated	101.50	101.59	IR379			
13H	–2.1	Disseminated; nodular	103.70	103.90	IR380			
13H	–1.0	Disseminated	104.25	104.90	IR381			
13H	–0.5	Disseminated	105.70	106.70	IR382			
13H	–0.3	Nodular	108.80	109.00	IR383			
13H	–0.7	Disseminated	109.20	109.30	IR384			
204-1250D-								
1H-1					NA	0	50	0.00
1H-2					NA	14	17	1.33
1H-3					NA	30	63	1.66
1H-4					NA	28	33	2.27
1H-CC					NA	0	1	2.57
1H-CC					NA	12	14	2.69
2H	–2.4	Disseminated; nodular	6.50	6.95	IR385			
2H	–0.6	Disseminated	13.20	13.32	IR386			
4H	–0.9	Disseminated	25.53	25.70	IR387			
4H	–0.5	Vein; parallel to bedding	27.80	27.90	IR388			
4H	–0.8	Disseminated	28.10	28.25	IR389			
4H	–0.5	Disseminated	28.75	28.80	IR390			
4H	–0.4	Disseminated; nodular	30.60	30.66	IR391			
4H	–1.5	Disseminated; 3 parts	32.80	33.40	IR392			
6H	–0.8	Disseminated	37.00	37.70	IR393			
6H	–0.6	Disseminated	39.55	39.69	IR394			
6H	–0.5	Disseminated	40.80	40.89	IR395			
6H	–1.5	Disseminated	42.55	42.70	IR396			
6H-5	–2.8	Nodular	43.10	43.14	IR397	0	20	42.95

Table T12 (continued).

Core, section	ΔT (°C)	Gas hydrate texture*	Depth interval (mbsf)† Top	Depth interval (mbsf)† Bottom	Anomaly designation‡	Sampled interval Top (cm)	Sampled interval Bottom (cm)	Sampled interval Depth (mbsf)
6H	–0.4	Disseminated	43.60	43.67	IR398			
6H-6	–1.9	Vein; parallel to bedding	43.74	43.93	IR399	0	20	44.39
6H	–1.6	Vein	44.15	44.20	IR400			
6H	–4.2	Vein parallel to bedding	44.50	44.56	IR401			
6H	–0.9	Vein	44.87	44.90	IR402			
6H	–0.5	Disseminated	45.18	45.21	IR403			
6H	–1.2	Disseminated	45.75	45.87	IR404			
6H	–1.0	Disseminated	46.75	46.80	IR405			
7H	–0.4	Disseminated	47.60	47.90	IR406			
7H-3	–3.6	Vein	50.95	51.00	IR407	133	143	50.83
7H	–0.8	Disseminated	51.95	52.22	IR408			
7H	–2.2	Nodular	52.20	52.41	IR409			
8H	–0.9	Disseminated	56.20	56.30	IR410			
8H	–0.9	Vein	56.65	56.70	IR411			
8H	–1.5	Nodular	57.22	57.30	IR412			
8H	–0.5	Disseminated	60.55	60.75	IR413			
8H	–0.6	Disseminated	62.00	62.04	IR414			
8H	–0.8	Vein; moderate dip	62.57	62.68	IR415			
8H	–2.6	Vein; disseminated	62.72	62.92	IR416			
8H	–2.7	Disseminated	65.00	65.15	IR417			
9H	–1.0	Vein; slight dip	65.70	65.80	IR418			
9H	–1.5	Nodular; vein slight dip	66.87	66.98	IR419			
9H	–0.8	Disseminated	68.60	68.69	IR420			
9H	–1.2	Disseminated	68.80	68.69	IR421			
9H	–0.9	Disseminated	72.00	72.05	IR422			
9H	–1.6	Disseminated	72.72	72.84	IR423			
9H	–0.8	Disseminated	74.19	74.60	IR424			
10H	–2.7	Nodular	75.30	75.40	IR425			
10H	–2.2	Disseminated	76.50	76.70	IR426			
10H	–0.8	Disseminated	78.80	79.15	IR427			
10H	–0.8	Disseminated	81.00	81.10	IR428			
10H-3	–1.1	Vein; dipping	82.87	83.00	IR429	53	84	78.01
10H	–0.9	Disseminated	84.10	84.21	IR430			
10H	–1.9	Nodular	84.50	84.68	IR431			
11H	–0.6	Disseminated	86.40	86.52	IR432			
11H	–0.9	Disseminated	89.75	90.00	IR433			
12H	–1.0	Nodular	94.05	94.15	IR434			
12H-2	–0.4	Disseminated	97.70	97.80	IR435	40	55	70.32
12H	–1.1	Vein	98.69	98.75	IR436			
12H-5	–0.4	Nodular	100.18	100.22	IR437	99	105	74.38
14H	–0.6	Disseminated	107.29	107.36	IR438			
14H	–0.7	Disseminated	111.72	111.80	IR439			
14H	–0.6	Vein; moderate dip	112.01	112.07	IR440			
14H	–0.8	Vein; disseminated	113.40	113.53	IR441			

Notes: * = from anomaly characteristics and core description, if available. ‡ = used for reference to specific anomalies in text and figures. † = from uncut core liner. The difference between these depth intervals and the equivalent curated section depth intervals is typically <1 m. NA = not available, no IR data for sampled interval.

Table T13. Moisture and density, Holes 1250C and 1250D.

Core, section, interval (cm)	Depth (mbsf)	Density (g/cm³) Bulk	Density (g/cm³) Grain	Porosity (%)
204-1250C-				
1H-1, 79–81	0.79	1.591	2.725	66.6
3H-1, 104–106	15.04	1.664	2.719	62.2
3H-3, 82–84	17.82	1.650	2.676	62.1
3H-4, 60–62	19.10	1.660	2.731	62.7
3H-5, 66–68	20.66	1.633	2.623	61.9
3H-6, 60–62	22.10	1.667	2.678	61.1
4H-1, 74–76	24.24	1.642	2.639	61.7
4H-3, 74–76	27.24	1.673	2.633	59.7
4H-5, 54–56	29.64	1.722	2.715	58.7
5H-1, 74–76	33.74	1.636	2.723	64.0
5H-3, 74–76	36.72	1.714	2.695	58.7
5H-5, 58–60	39.56	1.694	2.623	58.1
5H-6, 31–33	40.72	2.033	2.754	41.7
6H-1, 74–76	43.24	1.739	2.786	59.4
6H-1, 120–122	43.70	1.840	2.749	52.7
6H-3, 82–84	45.59	1.774	2.678	54.6
6H-4, 50–52	46.77	1.740	2.683	56.8
6H-5, 46–48	48.23	1.834	2.686	51.3
6H-5, 74–76	48.51	1.747	2.755	58.2
6H-7, 28–30	50.72	1.709	2.703	59.2
7H-1, 80–82	52.80	1.713	2.773	60.6
7H-3, 74–76	55.41	1.700	2.774	61.4
7H-5, 98–100	57.68	1.735	2.722	58.2
8H-1, 60–62	62.10	1.682	2.745	61.8
8H-1, 88–90	62.38	1.819	2.717	53.0
8H-3, 74–76	65.24	1.685	2.727	61.2
8H-5, 58–60	68.08	1.870	2.730	50.4
8H-6, 62–64	69.62	1.701	2.726	60.2
9P-1, 6–8	71.06	1.648	2.728	63.4
9P-1, 46–48	71.46	1.685	2.702	60.6
9P-1, 80–82	71.80	1.759	2.779	58.1
10H-1, 91–93	73.91	1.692	2.750	61.3
10H-3, 76–78	76.22	1.640	2.758	64.5
10H-5, 74–76	79.20	1.685	2.682	60.1
10H-6, 74–76	80.70	1.761	2.715	56.4
11H-1, 91–93	83.41	1.656	2.712	62.6
11H-3, 50–52	85.91	1.678	2.678	60.5
11H-5, 52–54	88.53	1.681	2.700	60.8
11H-6, 30–32	89.76	1.763	2.718	56.4
12H-1, 24–26	92.24	1.731	2.696	57.7
12H-3, 74–76	94.89	1.749	2.708	56.9
12H-5, 74–76	97.77	1.722	2.681	57.9
13H-1, 16–18	101.66	1.683	2.673	60.0
13H-3, 74–76	104.13	1.689	2.658	59.3
13H-5, 74–76	107.13	1.702	2.633	57.9
14H-1, 90–92	111.9	1.86	2.707	50.3
14H-3, 50–52	114.5	1.774	2.718	55.7
14H-5, 18–20	115.71	1.743	2.704	57.2
15H-1, 88–90	121.38	1.705	2.679	58.8
15H-3, 97–99	124.33	1.788	2.689	54.1
15H-5, 80–82	126.86	1.770	2.692	55.3
16P-1, 12–14	130.12	1.720	2.745	59.5
16P-1, 32–34	130.32	1.697	2.723	60.4
16P-1, 62–64	130.62	1.712	2.682	58.5
17H-1, 74–76	132.74	1.784	2.669	53.8
17H-2, 42–44	133.92	1.949	2.665	43.7
17H-3, 74–76	135.74	1.790	2.733	55.2
19X-1, 91–93	139.41	1.790	2.708	54.5
19X-3, 88–90	142.38	1.768	2.677	55.0
19X-5, 71–73	145.16	1.761	2.674	55.3
19X-7, 50–52	147.45	1.778	2.727	55.7
204-1250D-				
2H-1, 34–36	6.84	1.663	2.711	62.1
2H-3, 40–42	9.16	1.715	2.727	59.5
2H-5, 42–44	12.18	1.646	2.752	64.0
5P-1, 6–8	35.06	1.719	2.904	63.1
5P-1, 40–42	35.40	1.642	2.683	62.8
5P-1, 78–80	35.78	1.684	2.703	60.7
13P-1, 9–11	103.59	1.793	2.644	52.5
13P-1, 41–43	103.91	1.784	2.645	53.1
13P-1, 60–62	104.10	1.804	2.648	52.0
18P-1, 14–16	135.34	1.635	2.605	61.3
18P-1, 40–42	135.60	1.655	2.676	61.8
18P-1, 60–62	135.80	1.671	2.691	61.2
18P-1, 88–90	136.08	1.660	2.590	59.4

Table T14. Thermal conductivity, Holes 1250C, 1250D, 1250E, and 1250F.

Core, section, interval (cm)	Depth (mbsf)	Thermal conductivity (W/[m·K])	Individual measurements (W/[m·K])		
204-1250C-					
3H-3, 80	17.80	1.018	0.997	1.058	1.000
4H-1, 75	24.25	0.929	0.935	0.945	0.906
4H-3, 65	27.15	1.016	1.018	1.004	1.025
5H-3, 75	36.73	0.992	0.980	1.005	0.990
6H-1, 75	43.25	0.999	0.982	1.024	0.990
6H-3, 40	45.17	1.077	1.122	1.053	1.055
6H-5, 55	48.32	0.968	0.972	0.971	0.961
7H-5, 10	56.80	0.926	0.925	0.948	0.906
8H-1, 75	62.25	0.886	0.869	0.877	0.911
8H-3, 60	65.10	0.937	0.946	0.926	0.938
8H-5, 50	68.00	1.094	1.118	1.062	1.101
10H-1, 35	73.35	0.920	0.910	0.910	0.939
10H-3, 90	76.36	0.898	0.903	0.892	0.900
10H-5, 75	79.21	1.008	1.010	0.996	1.017
11H-1, 50	83.00	0.973	0.964	0.977	0.979
11H-4, 70	87.21	1.057	1.084	1.013	1.074
11H-6, 60	90.06	1.053	1.065	1.026	1.068
12H-3, 67	94.82	1.017	0.995	1.028	1.029
13H-3, 76	104.15	0.970	0.991	0.951	0.968
14H-3, 43	114.43	0.972	0.966	0.967	0.984
15H-3, 75	124.11	1.016	1.033	0.991	1.024
17H-3, 70	135.70	1.029	1.028	1.025	1.034
19X-3, 75	142.25	0.981	0.971	0.986	0.986
204-1250D-					
4H-1, 75	26.25	1.008	1.052	0.990	0.982
4H-3, 82	29.32	0.959	0.955	0.937	0.985
4H-5, 65	32.15	1.044	1.060	1.029	1.043
6H-2, 50	39.00	0.932	0.937	0.932	0.928
6H-4, 75	42.20	1.060	1.057	1.062	1.061
6H-7, 90	46.09	1.056	1.059	1.028	1.080
7H-4, 11	51.04	0.956	0.958	0.946	0.965
8H-3, 80	58.01	0.862	0.867	0.853	0.867
8H-6, 50	62.18	1.044	1.027	1.058	1.047
8H-7, 11	63.29	0.992	0.994	0.976	1.006
9H-3, 10	68.60	0.857	0.863	0.865	0.843
10H-6, 75	82.07	1.026	1.027	1.020	1.032
11H-3, 69	87.82	1.022	1.004	1.015	1.048
12H-2, 75	96.00	0.949	0.956	0.937	0.955
12H-3, 67	97.42	0.947	0.944	0.962	0.934
12H-5, 52	100.27	0.980	1.002	0.970	0.968
14H-1, 74	106.24	0.832	0.830	0.829	0.836
15X-3, 72	118.72	0.953	0.947	0.964	0.948
16X-1, 70	125.30	1.012	1.023	1.020	0.993
16X-3, 83	128.43	1.004	1.015	0.983	1.015
16X-5, 60	131.12	0.924	0.923	0.918	0.932
19X-2, 75	139.45	0.960	0.957	0.954	0.968
19X-3, 84	141.04	1.062	1.077	1.035	1.075
19X-6, 50	145.20	1.047	1.048	1.051	1.075
204-1250E-					
2H-3, 70	10.20	0.847	0.863	0.855	0.823
2H-3, 75	10.25	0.884	0.900	0.881	0.870
2H-4, 100	12.00	0.842	0.849	0.851	0.825
204-1250F-					
1H-3, 75	102.50	0.948	0.945	0.941	0.958
2H-2, 50	111.50	0.979	0.981	0.982	0.974
3X-3, 100	117.50	0.977	0.980	0.958	0.994
5H-2, 75	123.25	0.964	0.966	0.966	0.961
6X-2, 75	129.55	0.973	0.992	0.972	0.954
9X-3, 75	137.75	0.982	0.968	0.987	0.991
10X-3, 76	147.36	0.969	0.944	0.976	0.986
11X-3, 75	156.68	1.068	1.076	1.066	1.061
12X-3, 69	163.55	1.016	0.997	1.029	1.022
12X-5, 50	166.49	0.988	0.999	0.973	0.991
12X-1, 75	169.30	1.054	1.060	1.067	1.035
13X-3, 75	176.15	0.910	0.911	0.915	0.904

Table T15. Temperature measurements at Site 1250.

Core	Depth (mbsf)	Temperature (°C)	Thermal conductivity (W/[m·K])	Tool ID
204-1250C-				
4H	33.0	6.06	1.02	12
6H	52.0	7.00	0.97	12
8H	71.0	8.02	1.09	12
10H	82.5	8.41	1.01	12
10H–11H	82.5	9.15	—	2
11H	92.0	9.24	1.05	12
18Y–19X	138.5	—	—	2*
204-1250D-				
4H	35.0	5.91	1.04	12
6H	46.5	6.81	1.06	12
8H	65.5	7.70	0.98	12
12H	103.5	9.71	0.99	12
14H–15H	115.0	10.88	—	2
19X–BOH	145.0	12.50	—	2

Notes: Measurements for which two core numbers are given (e.g. 204-1250C-10H–11H) were made with the DVTPP between these two cores. APCT measurements were made at the core catcher of the core listed. For APCT measurements, thermal conductivity represents the average of the nine measurements taken in the adjacent core. A star in the last column indicates that this measurement was not used in the calculation of subsurface thermal gradient. BOH = bottom of hole. ID = identification of tool.

Table T16. Results from degassing experiments, Holes 1250C, 1250D, and 1250F.

Core	Depth (mbsf) Top	Depth (mbsf) Bottom	Run time (min)	Total volume (mL)*	Volume (mL)† $O_2 + N_2$	Volume (mL)† C_1	Volume (mL)† CO_2	Volume (mL)† C_{2+}	Concentration (%)‡ $O_2 + N_2$	Concentration (%)‡ C_1	Concentration (%)‡ CO_2	Concentration (%)‡ C_{2+}	Core length (m)	Porosity (%)	C_1 (mM)**
204-1250C-															
9P	71	72	1800	2570	187.0	2379.0	3.7	0.18	7.3	92.6	0.1	0.007	0.90–1.00	60	112.4–124.9
204-1250D-															
5P	35	36	1408	4460	372.0	4082.8	4.9	0.26	8.3	91.5	0.1	0.006	0.92–1.00	61	189.5–206.0
13P	103.5	104.5	1698	3130	95.4	3028.6	4.9	1.06	3.0	96.8	0.2	0.034	0.95–1.00	58	146.2–153.9
18P	135.2	136.2	1196	1385	92.0	1291.2	1.3	0.46	6.6	93.2	0.1	0.033	0.93–1.00	55	65.7–70.7
204-1250F-															
4P	119	120	579	5390	416.4	4952.6	14.2	6.86	7.7	91.9	0.3	0.127	0.88–1.00	57	244.9–278.3

Note: * = volume of gas released. † = volume of components released. ‡ = concentration of components released. ** = concentration in situ. Core length is reported as measured after the core was degassed and split (i.e., curated length). All cores had a nominal length of 1 m. The difference between the measured length and 1 m may be due to two factors: (1) incomplete recovery and (2) dissociation of gas hydrate during degassing. The lower concentration estimate corresponds to the assumption of 100% recovery; the higher estimate corresponds to the assumption that core length represented the percentage of recovery.

Table T17. Summary of the recovery percentages for each of the holes drilled, Holes 1250C, 1250D, 1250E, and 1250F.

Hole	Penetration (m)	Cored (m)	Recovered (m)	Total (%)	Unit I (%)	Unit II (%)	Subunit IIIA (%)	Subunit IIIB (%)
204-								
1250C	0–148.1	143.0	117.3	82.0	31.0	68.75	92.3	—
1250D	0–146.85	142.0	133.7	94.1	42.0	97.8	91.9	—
1250E	0–15.27	16.0	11.9	74.7	49.0	92	—	—
1250F	100–180	77.0	69.1	89.7	—	—	—	89.7

Note: — = not cored.

Table T18. HYACINTH pressure coring summary, Holes 1250C and 1250D.

Core	Deployment number	Date (Aug 2002)	Local time (hr)	Depth Water (mbsl)	Depth Core (mbsf)	BSR (mbsf)	Lithology	Core recovered (cm)	Pressure (bar)	Comments
204-1250C-										
18Y	FPC 4	3	1255	796	137	112	Lightly indurated silty clay	84	0	Cut good core; no retraction
204-1250D-										
17E	HRC 3	4	1345	796	134	112	Lightly indurated silty clay	28	80	Good core recovered under pressure; poor recovery in soft material.

Note: FPC = Fugro Pressure Corer, HRC = HYACE Rotary Corer, BSR = bottom simulating reflector.

Table T19. Conventional wireline logging operations summary, Hole 1250F.

Date (Aug 2002)	Local time (hr)	Tool depth (mbsf)	Remarks
25	1445		Last core on deck
25	1600–1800		Wiper trip up to 80 mbsf; back down to 180 mbsf
25	1800–1815		Hole displaced with sepiolite mud
25	1815–1900		Set back top drive; bottom of pipe put at 73 mbsf
25	1940		Start logging rig-up
25	2120		Start going down with the triple combination (TAP/DIT/HLDT/APS/HNGS/QSST) tool string
25	2145	0	Stop 5 min at mudline for temperature calibration
25	2200	179	Tool at TD; start logging-up pass at 900 ft/hr
25	2225	58	Tool back into pipe; speed up to 1500 ft/hr to log mudline
25	2230	0	End of pass 1
25	2255	179	Tool at TD; start logging-up pass 2 at 900 ft/hr
25	2316	58	Tool back to pipe; end of pass 2
25	2320	179	Tool at TD for QSST checkshot survey
25	2350	58	Tool back into pipe
26	0035		Tool back on rig floor
26	0150		Finish rig-down
26	0150		Start logging rig up
26	0245		Start going down with the FMS-sonic (FMS/DSI/SGT) tool string
26	0335	182	Tool at TD; start logging-up pass at 900 ft/hr
26	0350	58	High tension when top of tool enters pipe
26	0410	58	Tool worked into pipe
26	0425	58	Tool back into pipe; end of pass 1
26	0435	182	Tool at TD; start logging-up pass 2 at 900 ft/hr
26	0455	58	Tool back into pipe
26	0515		Tool back on rig floor
26	0605		Finish rig-down

Notes: TD = total depth. See Table **T8,** p. 102, in the "Explanatory Notes" chapter for definitions of acronyms.